Summer 2021

Regulation of Inflammatory Processes by Tryptamine, Cannabidiol and 2,3,7,8-Tetrachlorodibenzo-P-Dioxin

Nicholas Dopkins

REGULATION OF INFLAMMATORY PROCESSES BY TRYPTAMINE, CANNABIDIOL AND 2,3,7,8-TETRACHLORODIBENZO-P-DIOXIN

by

Nicholas Dopkins

Bachelor of Sciences
University of Central Florida, 2016

Submitted in Partial Fulfillment of the Requirements

For the Degree of Doctor of Philosophy in

Biomedical Sciences

School of Medicine

University of South Carolina

2021

Accepted by:

Mitzi Nagarkatti, Major Professor

Prakash Nagarkatti, Major Professor

Jason Kubinak, Committee Member

Michy Kelly, Committee Member

Saurabh Chatterjee, Committee Member

Tracey L. Weldon, Interim Vice Provost and Dean of the Graduate School

DEDICATION

This work is dedicated to the laboratory mice that have given their lives to make these studies possible.

ACKNOWLEDGEMENTS

With this space I would like to acknowledge all the individual members of the Nagarkatti laboratory and Pathology, Microbiology, and Immunology department at the University of South Carolina school of Medicine. None of this work would have been possible without the amazing environment supplied by the faculty members who compose the department working collectively with the graduate students, undergraduate students, and postdoctoral researchers to make such an enjoyable environment. I would like to individually thank the Dr. Mitzi Nagarkatti and Dr. Prakash Nagarkatti for their tutelage and support for me as a young scientist, as well as thank Dr. Kathryn Miranda and Dr. William Becker for being “older siblings” of a sort for me when I joined the lab with no background knowledge or expertise regarding the field of immunology. While there is not enough space in this acknowledgments section to properly thank every individual colleague or family member that aided me in this process, do know that this dissertation was as much a product of the magnificent people surrounding me throughout this process as it was due to myself.

ABSTRACT

Host immunity is a complicated system of pro-inflammatory and anti-inflammatory processes that respond to exogenous and endogenous threats to regulate host physiology, inhibit carcinogenesis, and protect from infections. Sustained deviance from normal immunological function occurs due to a variety of factors both endogenous and exogenous, with some factors that can dysregulate host immunity including: genetics, microbiota composition, toxin exposure, age, gender, and smoking. The etiology of inflammatory disorders is both convoluted and complex due to the sheer number of facets regulating host immunity. To better contribute to understanding how immunological dysregulation occurs we focused on how three anti-inflammatory compounds (tryptamine, CBD, and TCDD) suppress inflammation, primarily with a focus on autoimmune neuroinflammation in a murine model of MS. MS is an incurable neurodegenerative perpetuated by the host immune system inadvertently recognizing--and inflammatory cascades directed at--peptides present in the myelin sheathing within the CNS. The encephalitogenic immunity of MS is characterized by overabundances of pro-inflammatory immune cells, such as Th17 and macrophages, driving neurodegenerative inflammation in a normally immunologically privileged site. Simultaneous to this increase in inflammatory processes in the CNS is an anti-parallel reduction of the regulatory processes, carried out by Tregs and MDSCs, that fight to maintain an immunologically privileged CNS. Sustained neuroinflammation in MS results in paralytic symptoms and atrophy that no current medications can fully reverse,

therefore putting an emphasis on the need for potential therapeutics. Our main findings demonstrate that tryptamine and CBD are both capable of significantly ameliorating paralytic symptoms in murine model of MS known as EAE, and that acute TCDD exposure leads to metabolomic disbalance that can contribute to immunotoxicity following exposure. Namely, we demonstrated that tryptamine ameliorates EAE via inhibiting encephalitogenic CD4+ T cells in an AHR dependent manner, and that CBD ameliorates EAE by inhibiting IL-1β expression and subsequently the myeloid-mediated immune response. Our studies regarding TCDD exposure demonstrate that changes in the circulating and cecal metabolome likely contribute to the suppression of NFκB and ERK1/2 activity following exposure. Collectively, these studies contribute to the etiological understanding of the mechanisms that drive immunological dysfunction and suggest therapeutics for treating autoimmune neuroinflammation and the correcting of metabolomic disbalance following dioxin exposure.

TABLE OF CONTENTS

LIST OF TABLES

LIST OF FIGURES

LIST OF SYMBOLS

α	Greek letter denoting molecular subunits labeled “alpha”
β	Greek letter denoting molecular subunits labeled “beta”
γ	Greek letter denoting molecular subunits labeled “gamma”
κ	Greek letter denoting molecular subunits labeled “kappa”
μ	Metric prefix denoting 10^{-6} units

LIST OF ABBREVIATIONS

AA ..... Arachidonic Acid

AHR ..... Aryl Hydrocarbon Receptor

ALA ..... Alpha Linoleic Acid

ARF ..... Animal Resource Facility

BMM ..... Bone Marrow Derived Macrophages

BSTFA ..... N,O-Bis(trimethylsilyl)trifluoroacetamide

CB1 ..... Cannabinoid Receptor Type 1

CB2 ..... Cannabinoid Receptor Type 2

CBD ..... Cannabidiol

CNRO ..... Cannabinoid Receptor Type 1 and 2 Knockout

CNS ..... Central Nervous System

COX ..... Cyclo-Oxygenase

DHA ..... Docosohexanoic Acid

DNA ..... Deoxyribonucleic Acid

DRE ..... Dioxin Response Element

EAE ..... Experimental Autoimmune Encephalomyelitis

ELISA ..... Enzyme Linked Immunosorbent Assay

FBS ..... Fetal Bovine Serum

FC ..... Fold Change

FDR ..... False Discovery Rate

FOXP3 ..... Forkhead Box Protein 3

GALT ..... Gastrointestinal Associated Lymphoid Tissue

GI ..... Gastrointestinal

GSDM ..... Gasdermin

H&E ..... Hematoxylin and eosin

H37Ra ..... Heat Killed Mycobacterium Tuberculosis

HEPES ..... 4-(2-hydroxyethyl)-1-piperazineethanesulfonic acid

HRP ..... Horse Radish Peroxidase

IECs ..... Intestinal Epithelial Cells

IL ..... Interleukin

KO ..... Knockout

LA ..... Linoleic Acid

LEfSe ..... Linear Discrimination of Effect Size

LPS ..... Lipopolysaccharide

MDSC ..... Myeloid Derived Suppressor Cell

MOG ..... Myelin Oligodendrocyte Glycoprotein

MS ..... Multiple Sclerosis

MTBE ..... Methyl Tert-Butyl Ether

NIAID ..... National Institute of Allergy and Infectious Disease

OTU ..... Operational Taxon Unit

PBS ..... Phosphate Buffered Saline

PCA ..... Principal Component Analysis

PPARγ ..... Peroxisome Proliferator-Activated Receptor Gamma

PTX ..... Pertussis Toxin

PUFA ..... Polyunsaturated Fatty Acid

qPCR ..... Quantitative Polymerase Chain Reaction

RBC.....Red Blood Cell

RNA ..... Ribonucleic Acid

RORγT .....RAR-Related Orphan Receptor Gamma

ROS.....Reactive Oxygen Species

RT ..... Room Temperature

SCFA..... Short Chain Fatty Acid

SEM .....Standard Error of the Mean

SPM.....Specialized Pro-Resolving Mediators

Th17 ..... T Helper 17 T Cell

THC..... Delta-9 Tetrahydrocannabinol

TIC .....Total Ion Chromatogram

TLR .....Toll-Like Receptor

Tregs .....Regulatory T Cell

WT .....Wildtype

CHAPTER 1

INTRODUCTION

1.1 THE ROLE OF GUT MICROBIOME AND ASSOCIATED METABOLOME IN THE REGULATION OF NEUROINFLAMMATION IN MULTIPLE SCLEROSIS AND ITS IMPLICATIONS IN ATTENUATING CHRONIC INFLAMMATION IN OTHER INFLAMMATORY AND AUTOIMMUNE DISORDERS[1]

1.1.1 THE GUT MICROBIOME AND NEUROINFLAMMATION

MS is a neurodegenerative autoimmune disorder in which the host immune system recognizes the myelin sheath surrounding axon terminals to be immunogenic, resulting in breakdown of tolerance. This triggers chronic inflammation within the CNS, lesion formation, demyelination of axons, along with breakdown in the blood–brain barrier BBB, and gradual paralysis stemming from an inability to perpetuate action potentials over time[1]. MS has various forms with varying degrees of severity possessing distinct phenotypic characteristics; however, most cases share a common theme of varying symptoms at early stages followed by unrelenting neurodegeneration over time. The inflammation in the CNS in patients with MS is mediated primarily by the Th1

[1]Dopkins N, Nagarkatti PS, Nagarkatti M. The role of gut microbiome and associated metabolome in the regulation of neuroinflammation in multiple sclerosis and its implications in attenuating chronic inflammation in other inflammatory and autoimmune disorders. Immunology. 2018 Jun;154(2):178-185.
Reprinted here with permission of publisher.

and Th17 T-cell subsets producing pro-inflammatory cytokines, which leads to infiltrating monocytes and macrophages in the CNS following damage to the BBB. These infiltrating mononuclear cells carry out these inadvertent effector functions resulting in neurodegeneration[2]. EAE is a CD4+ T-cell-mediated autoimmune disease induced in model organisms (primarily mouse and rat) in the research setting[3,4]. EAE is widely accepted as a reference standard disease model for in vivo laboratory research geared towards studying the physiology and potential treatments of MS[5,6]. EAE is inducible in mice through administration of antigens from the myelin sheath along with an adjuvant, which leads to induction of inflammatory T helper cells that infiltrate the CNS. These cells typically include Th1 and Th17 subsets that produce cytokines and chemokines, IL-17, TNF-a, interferon-γ and CCL5, observed both locally in the CNS as well as systemically in circulation[2,7–9]. Along with the up-regulation of pro-inflammatory markers following induction of EAE, there is suppression of functionality of an anti-inflammatory T-cell subset known as Tregs[10]. Treg cells are CD4+ cells characterized primarily by their expression of the transcription factor Foxp3 and production of the inhibitory cytokines such as IL-10 and TGFβ[3]. The production of these suppressive cytokines inhibiting T helper cell proliferation and function is the key mechanism by which Treg cells accomplish their effector function of inducing immune tolerance[11]. In addition to producing inhibitory cytokines, Treg cells accomplish their functions through cell–cell contact[11]. Treg cells have garnered great interest as a potential focal point for MS treatment due to their induction of tolerance displaying protective effects against demyelination[12]. The microbiota is a microbial collective composed of commensal organisms and opportunistic pathogens alike that reside along barrier sites of the host

organism. The microbial diversity along these barrier sites plays a regulatory role in digestion, immune system activation, protection from development of opportunistic pathogens, and various other physiological processes[13,14]. The importance of a tightly regulated microbiota on host physiology has gained a greater appreciation over recent years due largely to novel technologies giving a previously unavailable ability to culture fastidious organisms, rapidly sequence various macromolecules, and characterize microbe–host interactions with greater detail. The commensal relationship between host and microbial community possesses a highly complicated web of modulatory crosstalk among organisms and has been recognized as an undeniable factor affecting host response in disease states[15]. The count of living microbial cells, as well as genes expressed by those cells, possesses a towering presence over the host it resides within. The relative parity between these numbers is disputed due to difficulties in calculating definitive quantities in an ever-changing microbiota; however, the ratio is believed to be at the very least a 10-fold difference favoring the microbial flora[16].

1.1.2 GUT-BRAIN AXIS IN MS AND EAE

Interactions between the host microbiota and the GALT help shape the immune system both locally and systemically throughout the host[17]. The GALT has become a focal point in research targeting autoimmune disorders because of Treg activation by bacterial strains inducing immune tolerance within host organisms[18]. The gut–brain axis is a term used to describe the interactions between host and microbiota residing within the gut and the lingering effects between these interactions that take effect within the CNS. The biodiversity present within the gastrointestinal tract has a collective metabolome very different from that of the human host that regulates the availability of

nutrients for the host[19]. The result of bacterial metabolism under dysbiotic conditions can either prevent nutrients from reaching the host through bacterial sequestering or provide an excess of unwanted xenobiotic metabolites with detrimental effects. The study of outward products of bacterial metabolism in the gut–brain axis is relatively new but rapidly expanding. In combination with microbial metabolism, the interactions between bacteria and the immune cells are an important aspect of the gut– brain axis and are often dependent on the products of bacterial metabolism. Interventional therapies focusing on regulation of microbial diversity as well as the metabolic traits of the microbiome have started showing progress in the treatment of MS, including the use of established non-pathogenic probiotic regimens in the treatment of EAE[20]. Although there are numerous reviews on the immune mechanisms that regulate the pathogenesis of EAE and the role of the microbiome in shaping the immune response in the gut, there is a paucity of reviews that help to understand the effects of microbiota in the gut–brain axis. It was therefore the primary objective of the current review to elucidate the complex interactions between the microbial metabolome found in the gut and how it can regulate immune response in the CNS in EAE and MS.

1.1.3 AMINO ACID METABOLISM

1.1.3.1 CYSTEINE METABOLISM

Desulfovibrionaceae are strictly anaerobic bacteria that desulfinate the amino acid 'cysteine' for downstream purposes as a primary carbon source[21]. The presence of *Desulfovibrionaceae* within the human gut has been shown in healthy colons; however, intestinal dysbiosis resulting from elevated levels of *Desulfovibrionaceae* has been shown in studies by sequencing the intestinal microbiota in both patients with MS and EAE-

induced mice[22,23]. An overabundance of *Desulfovibrionaceae* plays a vital role in the host metabolism due to its sequestering of the amino acid cysteine within the gastrointestinal tract. Abnormal availability of the amino acid cysteine can have widespread effects throughout the host body because it is a building block required for host production of sulfur-containing bioactive compounds, such as glutathione. The rate-limiting step of glutathione production, which is a tripeptide antioxidant, is the condensation reaction of cysteine with glutamate to form c-glutamylcysteine[24]. Glutathione levels are garnering focus due to their role as the primary countermeasure against ROS-related damage within the CNS. Currently, clinical studies are being performed to better understand the pathogenic role of underlying glutathione deficiencies in MS patients at different stages of the disease[25]. Damage related to ROS in glutathione-deficient patients has been shown to be reversible by the dietary supplementation of cysteine and glycine[26]. Supplementation of sulfur-containing precursor molecules was also shown to reduce oxidative stress in studies focusing on EAE-induced mice[9]. These studies suggest that the link between the bioavailability of these precursor molecules and the effector function of glutathione to eliminate elevated levels of ROS are directly related in both mice and humans. Elevated levels of reactive oxygen species within the CNS arise from residential microglia, infiltrating macrophages, and general mitochondrial activity in combination with faulty countermeasures to rid the tissues of free radicals. The multifaceted role of ROS in MS pathogenesis has been gaining a greater appreciation within the research community in recent years[27] due to elevated concentrations of ROS in CNS tissues playing potential roles in the initiation of lesions, recruitment of lymphocytes and the phagocytosis of myelin. High levels of superoxide in the CNS initiate lesions along the

BBB due to disruption of the tight cell–cell junctions within cerebral endothelial cells as well as instigating a chemotaxis of monocytes towards the BBB[28]. The phagocytosis of myelin results in the loss of action potentials being perpetuated throughout the nervous system (causing the symptoms of paralysis) and is carried out by infiltrating macrophages. This phagocytosis of myelin sheathing has been shown to be dependent on the concentration of ROS present in the surrounding microenvironment[29]. In addition to an elevated ROS production, there is an increased expression of genes involved in the detoxification of ROS in an effort to alleviate self-inflicted damage caused by inflammation targeting the CNS[30]. This increased demand for antioxidant molecules locally within the CNS exposes and further exacerbates a potential susceptibility if substantial levels of antioxidant precursor molecules are not readily available. Collectively, the above studies suggest that pathological symptoms directly caused by accumulation of ROS during an inflammatory response in the CNS can be attributed at least in part to a lack of sulfur-containing precursor molecules related to either diet or bacterial dysbiosis. Dysbiosis arising from an overabundance of *Desulfovibrionaceae* within the host gut, provides a linkable mechanism of cysteine sequestering inducing a host deficiency of the sulfur-containing bioactive antioxidant glutathione. This glutathione deficiency aids in an abundance of ROS, which degrade the BBB, aid in the recruitment of immune cells to the CNS and are required for myelin phagocytosis.

1.1.3.2 TRYPTOPHAN METABOLISM

Bacterial metabolism of tryptophan can be linked to the modulation of inflammation through the production of indole-based compounds[31]. The enzyme tryptophanase, unique to bacteria, breaks down the amino acid residues into indole,

ammonia, and pyruvate for further bacterial use as an energy source or building block[32]. The outward indole by-products of this reaction can come with a variety of side chains attached to the third carbon. Some of the known side-chain functional groups include, but are not limited to, acetate, aldehyde and propionate[31]. These indole-based by-products have the capability to bind as well as activate the AHR present in host lymphocytes, similar to plant-derived indoles[33]. The AHR is a cytosolic receptor that upon activation undergoes conformational changes, binds a carrier protein to import it into the nucleus, and carries out an effector function within the nucleus as a transcription factor[34]. The ligands for AHR are primarily planar hydrophobic molecules. Each of the mentioned indole by-products containing unique side chains possesses a unique binding efficiency to the AHR ligand binding site. AHR ligands come from both endogenous and exogenous sources. Endogenous molecules produced by the host add a layer of complexity to the biological activity of ligands as environmental products and can either work as agonists activating the receptor, or as antagonists occupying the binding site with low efficacy to defer the basal levels of endogenous ligand activation[35]. This contribution of various indole-based compounds from the microbiome, which then compete with endogenous ligands produced by the host, results in disruption of balance between commensal organisms and host immune tissue. Modulation of AHR activity through ligand binding by environmental pollutants such as 2,3,7,8-tetrachlorodibenzodioxin to dietary indoles has been shown primarily to lead to induction of Treg cells[36–38]. However, some endogenous ligands such as 6-formylindolo[3,2-b]carbazole have also been shown to induce Th17 cells[33,39,40]. The ability of AHR ligands to induce Treg cells versus Th17 cells may depend on their capacity to cause epigenetic changes including microRNA[38],

and clearly more research is needed to understand the complexity of the receptor. Studies focusing on AHR activation and inhibition in EAE have resulted in polarized effects of either amelioration or perpetuation of symptoms, through induction of Treg cells and Th17 cells, respectively[41–43].

It has become apparent that AHR activation via bacterial derivatives of tryptophan metabolism has a net positive effect on symptomatic outcomes of EAE. It was shown in one study that using a tryptophan-depleted diet worsened the overall disease state of EAE in mice, whereas tryptophan supplementation resulted in an amelioration of symptoms. This alleviation of symptoms within the CNS was found to be mediated in part by repressing the expression of Nos2 and Ccl2 in astrocytes[42]. An up-regulation of Nos2 and Ccl2 expression within astrocytes aggravated EAE symptoms due to a localized pro-inflammatory phenotype. Ccl2 is a cytokine involved in chemotaxis of memory T cells and monocytes to peripheral tissue sites, helping to initiate local inflammatory responses[44]. Nos2, commonly known as nitric oxide synthase, produces the reactive molecule NO, which contributes to vasodilatation and is used as a ROS in targeted killing[45]. There does appear to be promise in the protective nature of tryptophan by-products against autoimmune inflammation in the CNS through the gut–brain axis. However, this area of research is relatively new and will require much more focus in the coming years to pinpoint the exact roles of these dynamic processes in EAE.

1.1.4 CARBOHYDRATE METABOLISM

The gut microbiota also plays a key role in the production of SCFAs through the fermentation of carbohydrates that are indigestible to the host organism. These SCFAs direct inflammatory responses throughout the body by modulating the chromatin

structure within the nuclei of lymphocytes favoring gene products that result in the proliferation of anti-inflammatory Foxp3+ Treg cells[46,47]. SCFAs regulate T-cell populations through the inhibition and activation of histone-modifying enzymes that either up-regulate (through acetylation) or down-regulate (through deacetylation) transcription at proximal promoter regions. Treg induction by SCFA is accomplished through the inhibition of histone deacetylase activity near the Foxp3 promoter region while simultaneously promoting acetylation of histone 3 at the Foxp3 promoter region[48]. The actual SCFA binding sites among CD4+ T cells for inhibition of histone deacetylase enzymes are currently disputed and could occur through either intracellular binding affecting the mTOR pathway[49], or through the cell surface G-protein-coupled receptors such as GPR41 and GPR43, specific for SCFAs[50]. The SCFA ligand binding site on CD4+ T cells is currently debated due to GPR41 and GPR43 double knockouts having seemingly no effect on Treg cell proliferation as well as SCFAs being entirely permeable through the plasma membrane requiring no need for active transport[51].

Butyrate production stems from prokaryotic fermentation of acetyl CoA precursors originating from dietary fiber catalysis. A diverse collection of species within the gastrointestinal tract have shown capabilities to ferment acetyl CoA into butyrate within the colon, however there is a primary focus on the *Clostridium* clusters XIVa and IV and the phylum *Bacteroidetes*, which both produce large quantities of butyrate[52,53]. Clinical studies focusing on sequencing the microbiome have shown a relative depletion of *Bacteroidete*s as well as the *Clostridium* clusters XIVa and IV in human samples from patients with MS when compared with healthy individuals[54]. The direct effect of butyrate induction within the colon has been tested through both high-fiber diet supplementation

as well as direct oral butyrate treatments. Observed in both routes of butyrate supplementation was an amelioration of clinical symptoms of EAE using in vivo scoring algorithms combined with an increase in the numbers of Foxp3+ CD4+ T cells[46].

Propionic acid is another SCFA produced from bacterial fermentation of indigestible fibers that could play a role in the prevention and relief of symptoms in inflammatory disorders. Propionic acid is produced by fermentation within the succinate pathway and modulates histone modifications at the Foxp3 promoter region in a manner like butyrate[47,53]. A large portion of the intestinal flora has been linked to the production of propionic acid, including the Gram-negative phylum *Bacteroidetes* and the gram-positive phylum *Firmicutes*, which contains the genus *Clostridium*. Studies have shown that fecal transplants high in propionic acid in combination with propionic acid-producing bacterial species have been beneficial in ameliorating the clinical symptoms of EAE in mice[55].

Short-chain fatty acids are found within the body in staggering concentrations for biologically active compounds, relatively ~150 mM when pooled as a collective within the large intestine of healthy individuals, making changes in compositional and collective abundance more than sufficient to have changes in the phenotypic properties of lymphocytes within the GALT[53].

1.1.5 LIPID METABOLISM

1.1.5.1 POLYUNSATURATED FATTY ACIDS

Another mechanism modulating the inflammatory response throughout the host is perpetuated by the metabolism of polyunsaturated fatty acids, namely omega-6 and omega-3 fatty acids, from host cells as well as bacterial cells within the gut. These long

hydrocarbon chains are directly involved in the regulation of metabolic endotoxemia, a disorder in which an overabundance of lipopolysaccharide LPS-producing gut bacteria leads to activation of TLR4, producing widespread chronic low-grade inflammation[56]. Omega-3 fatty acids display an anti-inflammatory phenotype when ingested in higher proportions than omega-6 fatty acids due to the activation of intestinal alkaline phosphatase, an antimicrobial peptide that targets Gram-negative organisms while simultaneously promoting the growth of Gram-positive organisms[57]. In addition to reducing gram-negative abundance, intestinal alkaline phosphatase exhibits anti-toxic effects by hydrolyzing phosphate groups coupled to Lipid-A present on degraded LPS, reducing its binding efficiency to the TLR4 100-fold[57]. TLR4 activation leads to cryopyrin inflammasome activation releasing subsequent amounts of pro-inflammatory cytokines, TNF-a, IL-1 and IL-6 circulating in host organisms[58]. This chronic low-grade systemic inflammation connects the effects of microbial dysbiosis instigated by host diet to perpetual worsening of autoimmune disorders. This potential explanation coincides with the geographic distribution of diets high or low in omega-3 fatty acids. Regions of the world with diets rich in omega-3 fatty acids tend to have fewer instances of MS in comparison with those of the world that have a lower ratio of omega-3 fatty acids to omega-6 fatty acids[59], adding a potential geographical proof to polyunsaturated fatty acids as a contributing factor. With focus on polyunsaturated fatty acids as a non-invasive intervention in the treatment of MS, clinical trials have tested the effects of supplementation of unsaturated fatty acids and found that there was a positive trend in the attenuation of symptoms, although it did not produce statistically significant results[60].

1.1.5.2 SATURATED LONG-CHAIN FATTY ACIDS

Saturated long-chain fatty acids, such as lauric acid, have been shown to have antimicrobial properties in high concentrations[61]. These lipid molecules tend to primarily target Gram-positive microbes. They have even been implicated recently as a potential topical therapy for inflammatory skin conditions caused by Gram-positive organisms such as Propionibacterium acnes[61]. Because saturated fatty acids form an increasingly substantial portion of energy-supplying molecules in westernized diets, there has been growing interest in the role of lauric acid in EAE due to shaping the microbiota with antimicrobial properties as well as shaping the GALT with TLR4 agonist properties like that of LPS[62].

In vitro experiments supplementing media with saturated long-chain fatty acids, namely lauric acid, showed an up-regulation of Th17 cells and Th1 cells alongside a down-regulation of Treg cells[63]. In depth analysis of the transcriptome from these experiments showed an increase in pro-inflammatory markers (TNF-a, interferon-γ and Csf2) as well as a decrease in the anti-inflammatory marker Foxp3. Interestingly, these differential cytokine levels coincided with an up-regulation of the AHR, which shows a potential increased susceptibility to both endogenous and microbiota-produced compounds to compete as antagonists/agonists to drive further T-cell proliferation towards either an inflammatory or anti-inflammatory phenotype.

To focus on the effects of microbial by-products, researchers included fecal filtrates from saturated long chain fatty acid-fed mice to cell cultures in Th17 cell polarizing conditions, which resulted in higher proportions of activated Th17 cells than that of control groups when compared with media that were supplemented with the fecal

filtrates of mice fed a normal diet[63]. Sequencing analysis from these experiments showed decreased abundance of Bacteroidetes families as well as of *Prevotellaceae*. Both these bacterial populations have previously been implicated in having protective roles against the progression of EAE symptoms through production of the SCFA butyrate[52,53], which in turn up-regulates Treg cell proliferation.

1.1.6 PASSAGE THROUGH THE BBB

Passage of compounds from the peripheral blood supply into the CNS through the vascular endothelium composing the BBB is dependent on characteristics such as lipid solubility, tertiary structure, concentration, molecular weight, and charge of the compound[64]. Generally, compounds that can freely pass through the endothelium are low-molecular-weight lipid-soluble molecules with little to no charge. Majority of the bioactive compounds previously covered in this review are either theorized to be BBB permeable due to possessing key characteristics of BBB-positive compounds or have been proven to be BBB permeable through previous experimentation. Cytokines, generally hydrophilic in nature, present in the peripheral blood can modulate immunological functions within the CNS due to transporter-protein-mediated passage through the BBB and deposition into the CNS[65–67]. The passage of cytokines produced by peripheral lymphatic tissue through the BBB endothelium presents a bridge for BBB-negative compounds to have lasting effects on the physiology of the CNS through the modulation of peripheral lymphocytes. Intravenously injected indole compounds similar in structure to those produced by bacterial tryptophan metabolism have been shown to be able to freely pass through the BBB when present in the peripheral blood in high enough concentrations[68]. While structurally similar to many BBB-positive compounds the indole-

based microbial by-products of tryptophan metabolism have not been characterized as BBB-negative or -positive in vivo. The antioxidant glutathione is known to be BBB-positive due to well-defined transport proteins along the BBB that permit the deposition of glutathione in the non-oxidized state into the CNS[69]. LPS has been shown to be minimally invasive through the BBB endothelium of mice in vivo[70]. The neuroinflammatory effects of LPS can be accomplished by TLR activation in peripheral tissues inducing secondary effects within the CNS through BBB-positive mediators such as pro-inflammatory cytokines. SCFAs are BBB-positive, used by the CNS, and are integral in the development of proper permeability within the BBB[71,72].It is currently unknown how much of the protective effects displayed by SCFAs in EAE are the result of direct interaction with the CNS versus interactions in the periphery.

1.1.7 CONCLUSIONS REGARDING MICROBIAL METABOLITES AND MS

Multiple sclerosis is a debilitating autoimmune disease and like other autoimmune disorders, has no cure and limited treatment options aimed at reducing the clinical symptoms. Although there is increasing evidence suggesting that gut microbiota may play a critical role in the development or progression of MS, the precise mechanisms through which the gut microbiome can influence immune functions in the CNS despite the presence of BBB is unclear. This review systematically analyzed the role of microbial metabolites and how they may regulate the immune functions of the host both within and outside the CNS, thereby providing evidence to support the hypothesis on the gut–brain axis (Figure 1). So far, research on the role of microbiota in MS has been fruitful in developing a better understanding of the pathogenesis of MS, but much more research is clearly needed in this field. Specifically, whether MS results from alterations in the

microbiota caused by environmental factors and whether the microbiota influence the severity of the disease through regulation of immunological tolerance, needs additional research. Focusing research on probiotic organisms that produce beneficial metabolites or introducing changes in diet or other environmental factors to induce dysbiosis that is associated with induction of Treg cells or other immunosuppressive cytokines to attenuate chronic inflammation, can offer novel preventive and therapeutic modalities against a wide array of inflammatory and autoimmune diseases. Additionally, identification of specific deleterious microbiota triggering or promoting MS, and approaches to replace them with those that dampen chronic inflammation, can yield microbially based therapies that can help patients with minimally invasive procedures as well as cutting down on the costs of expensive long-term medications and their associated toxicity.

1.2 THE ROLE OF CANNABINOIDS IN THE REGULATION OF NEUROINFLAMMATION IN MULTIPLE SCLEROSIS AND ITS IMPLICATIONS IN ATTENUATING CHRONIC INFLAMMATION IN OTHER INFLAMMATORY AND AUTOIMMUNE DISORDERS

Cannabinoids are compounds isolated from the plant *Cannabis sativa*, which have garnered extensive attention by biomedical researchers for decades due to many cannabinoids possessing potent non-toxic immunosuppression and psychoactive side-effects[73–75]. Most studies have focused on the two major cannabinoids isolated from Cannabis known as THC and CBD. The receptors responsible for mediating the effects of cannabinoids isolated from Cannabis, as well as mediating the functions of similarly structured endogenous molecules that mediate host physiology known as

"endocannabinoids", are expressed in a diverse array of cell types and organ systems throughout the host[76,77]. Namely, the classical cannabinoid receptors known as CB1 and CB2 are found primarily in the CNS or the cells of the immune system, respectively[78,79]. Other non-classical receptors known to mediate the physiological changes observed following Cannabinoid exposure include FAAH, TRPV1, Adenosine A_{2A}, PPARγ, 5-HT1a, and GPR55[80]. Previous studies have demonstrated that THC works primarily as a partial agonist of CB1 and CB2 to induce potent immunosuppression in combination with the psychoactive side effects[81]. CBD has worked via more controversial interactions with due to weaker binding to the classical cannabinoid receptors, with various studies demonstrating both agonistic and antagonistic properties depending on the context, and some effects occurring entirely independent of the classical cannabinoid receptors[80–82].

Cannabinoids have been extensively postulated to be attractive therapeutics for the treatment of immunological and neurological disorders that lack treatments deemed sufficient and economically feasible by afflicted individuals[75,83]. Primarily, the application of Cannabinoids in immunological disorders has been deemed beneficial due to their innate ability to exploit the receptors of the endocannabinoid system to induce shifts in host immunity from a pro-inflammatory immune cell dominated landscape, towards an immunotolerant anti-inflammatory immune cell dominated landscape[75]. These results have been demonstrated by both the major cannabinoids isolated from Cannabis when given either alone or in combination. The psychoactive component THC has been demonstrated to alleviate symptoms of pathogenic inflammation in murine models of colitis, acute respiratory distress syndrome, and MS[84–87]; the non-psychoactive

counterpart CBD has been demonstrated to alleviate pathogenic inflammation in murine models of colitis, hepatitis, MS, and diabetes[80].

Collectively, the relatively novel aspect of studying cannabinoids and their potential in limiting autoimmune neuroinflammation is relatively poorly understood, however rapidly expanding due to expansions in omics-based technologies and interest from practitioners and patients alike. There is an imminent need for in-depth studies that demonstrate the mechanisms that these compounds exploit to alleviate these disorders to expediate, modify to minimize side-effects, and personalize their applications for patients that have interests or needs regarding these therapeutics. To address these concerns and contribute to the existing literature regarding the anti-inflammatory effects of cannabinoids, we demonstrate the benefits of CBD supplementation in a model of MS by taking an unprecedented look into the changes observed at sites of inflammation using various sequencing techniques.

1.3 DIOXIN EXPOSURE AND IMMUNITY

Dioxins are incredibly persistent organic pollutants derived primarily as byproducts by industrial processes. Human contact and exposure to dioxins, as well as dioxin contamination of agricultural products, pose as severe potential health risks to the public of industrialized regions. Dioxin exposure is related to negative health effects including, but not limited to: immunotoxicity, hormonal dysregulation, cancer, chloracne, cardiovascular dysfunction, and metabolic dysregulation[88]. Dioxin exposure posing as an increasing threat stemming from global expanses in industrialization has placed pressure on the biomedical community to further define the results stemming from exposure, as well as potential interventions to correct the associated pathology. Amongst all identified

dioxins, the most studied is TCDD due to its historical significance and significant threat to human help. TCDD is a particularly potent dioxin notorious for possessing and exceptionally high binding affinity towards the AHR, which mediates most of the contaminants toxic effects[89]. The downstream toxic effects of TCDD exposure are mediated via regulations in gene expression close to promoter regions affected by AHR activation known as DREs[90].

The long and short term results of TCDD exposure are poorly understood due to convoluted patient populations, only being properly identified in the 20th century, and having only brief insight into the mechanisms of action that drive pathogenesis[91]. While dioxin intake is quite rare, it is a notable concern due to the expanse of industrialization in global societies when combined with the bioaccumulation of toxic byproducts with long half-lives, such as TCDD[92]. In order to contribute to understanding the uncertainties that contribute to TCDD toxicity following exposure, we aimed to demonstrate the previously unidentified effects in the metabolomic profile following acute exposure. Identifying the immediate changes observed in individual organisms following exposure can aid researchers and clinicians alike in identifying exposure early to increase prognostic outcomes, help us understand how to potentially reverse processes that contribute to toxicity, and better understand how exogenous compounds can regulate host immunity or physiology via metabolomic shifts.

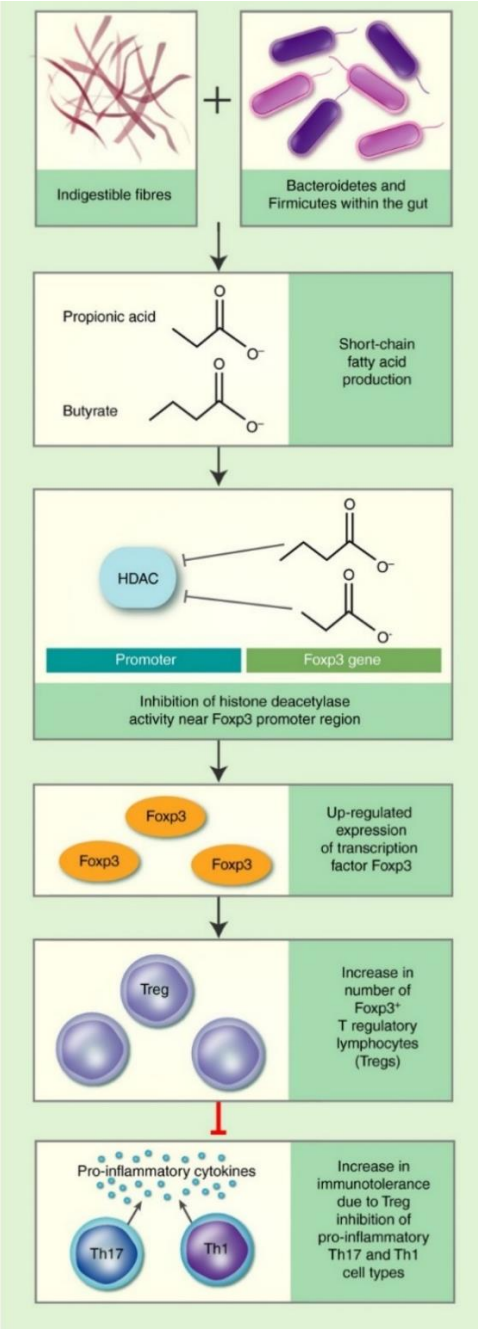

Figure 1.1. ***Graphical summary of immune tolerance induction through the production of short chain fatty acids by gut microbes.*** Gut bacterium are capable of inducing immunotolerance.

CHAPTER 2

TRYPTAMINE ATTENUATES EXPERIMENTAL MULTIPLE SCLEROSIS THROUGH ACTIVATION OF ARYL HYDROCARBON RECEPTOR[2]

2.1 ABSTRACT

Tryptamine is a naturally occurring monoamine alkaloid which has been shown to act as an AHR agonist. It is produced in large quantities from the catabolism of the essential amino acid tryptophan by commensal microorganisms within the GI tract of homeothermic organisms. Previous studies have established microbiota derived AHR ligands as potent regulators of neuroinflammation, further defining the role the gut-brain axis plays in the complex etiology in MS progression. In the current study, we tested the ability of tryptamine to ameliorate symptoms of EAE, a murine model of MS. We found that tryptamine administration attenuated clinical signs of paralysis in EAE mice, decreased the number of infiltrating CD4+ T cells in the CNS, Th17 cells, and RORγT cells while increasing FoxP3+Tregs. To test if tryptamine acts through AHR, MOG-sensitized T cells from wild-type or Lck-Cre $AHR^{flox/flox}$ mice that lacked AHR expression in T cells, and cultured with tryptamine, were transferred into wild-type mice

---

[2]Dopkins N, Becker W, Miranda K, Walla M, Nagarkatti P, Nagarkatti M. Tryptamine Attenuates Experimental Multiple Sclerosis Through Activation of Aryl Hydrocarbon Receptor. Front Pharmacol. 2021 Jan 25;11:619265
Reprinted here with permission of publisher.

to induce passive EAE. It was noted that in these experiments, while cells from wild-type mice treated with tryptamine caused marked decrease in paralysis and attenuated neuroinflammation in passive EAE, similar cells from Lck-Cre AHR$^{flox/flox}$ mice treated with tryptamine, induced significant paralysis symptoms, and heightened neuroinflammation. Tryptamine treatment also caused alterations in the gut microbiota and promoted butyrate production. Together, the current study demonstrates for the first time that tryptamine administration attenuates EAE by activating AHR and suppressing neuroinflammation.

2.2 INTRODUCTION

MS is an incurable autoimmune disorder in which the immune system recognizes the myelin sheath surrounding neurons, instigating an inadvertent cascade of pathogenic inflammation within the CNS. Inflammatory cascades in advanced MS accumulate to form plaques and lesions composed of demyelinated tissue in the CNS that hinder nervous tissue function. Symptoms arising from an advanced MS state include general discomfort, wasting, cognitive decline and paralysis due to hindered ability to produce action potentials in the CNS regions that innervate homeostatic, intellectual and sensory processes[93]. The aforementioned inflammatory cascade is characterized by a T lymphocyte landscape defined primarily by a disproportionate abundance of inflammatory Th17 cells infiltrating the CNS and further perpetuating the pro-inflammatory adaptive immune response[94]. Antiparallel to the overabundance of the Th17 cells driving neuroinflammation is an absence of activity by Tregs that suppress inflammation, and confer neuroprotection by the direct inhibition of adaptive immunity[95,96].

While the precise mechanisms of etiology of MS and autoimmune disorders is unclear, there is a growing body of evidence which suggests that environmental factors contribute significantly to the outcome and onset of autoimmune disease states[97,98]. One of these external factors that plays a critical role in regulating autoimmunity is the microorganisms residing within the GI tract referred to as the "gut microbiota". The gut microbiota has been established by previous studies to be an important external factor that influences the Treg/Th17 balance and regulates T cell immunity within the context of autoimmune disorders[99]. Advances in sequencing technologies, mass spectrometry and germ-free facilities have expedited the ability of researchers to better define the potential of the microbiota in limiting excessive inflammation in autoimmune disorders, including MS[100–104]. In particular, previous studies have demonstrated that a healthy microbiota limits excessive inflammation and alleviates inflammatory disorder pathology by inducing Tregs via the excretion of SCFAs and immunomodulatory AHR ligands[105,106]. However, the potential of the microbiome in inflammatory disorders serves as a double-edged sword due to chronic intestinal dysbiosis being demonstrated to worsen and instigate inflammatory disorders[56,107–110]. These previous studies have established that disparity in the microbial composition along barrier sites is directly involved with the clinical outcome of inflammatory disorders afflicting the host organism, and therefore suggest further studies focused on the etiological role of the microbiome in inflammatory diseases to develop novel therapeutics and identify biomarkers for early detection.

For this purpose, in the current study, we investigated the anti-inflammatory potential of an AHR agonist produced by the gut microbiota, tryptamine, in the limiting of autoimmune neuroinflammation in experimental MS. There is little known about the

effects of tryptamine on host immunity and GI tract function despite tryptamine being produced in large quantities by the gut microbiota of >10% of the population[31,111,112]. In this study, we found that tryptamine suppresses neuroinflammation and attenuates EAE by acting through AHR. To the authors knowledge this is the first report demonstrating any in vivo immunosuppressive properties of tryptamine in a state of acute or chronic autoimmunity.

2.3 MATERIALS AND METHODS

2.3.1 MICE

6-8-week-old female C57BL/6 mice were purchased from Jackson Laboratories (Bar Harbor, ME) and housed within the ARF at the University of South Carolina School of Medicine. Mice were cohoused for a period of 2 weeks prior to experimentation. On day 0, mice were randomly divided into either vehicle or treatment groups prior to the induction of EAE. Lck-Cre $AHR^{flox/flox}$ mice on C57Bl/6 background were bred in house using $AHR^{tm3.1Bra}$/J (Jackson stock number 006203) and dLCK-$hcre^{3779}$/J (Jackson stock number 012837) mice purchased from Jackson Laboratories. The resulting Lck-Cre $AHR^{flox/flox}$ are a cell-specific knockout that lack expression of a functional AHR in all T Cells. All donor Lck-Cre $AHR^{flox/flox}$ were age matched with WT donor mice prior to immunization for all passive EAE experiments. All animal work was conducted in accordance with protocols that follow the National Institute of Health guidelines and were approved by the Institutional Animal Care and Use Committee of the University of South Carolina.

2.3.2 REAGENTS

The following reagents were used during the course of the experiments and were purchased as following: RBC lysis buffer was purchased from Millipore Sigma (Burlington, MA); Percoll from GE Healthcare Life Sciences (Pittsburgh, PA); MOG35-55 from PolyPeptide Laboratories (San Diego, CA); PTX from List Biological Laboratories (Campbell, CA); H37Ra from Difco (Detroit, MI); β-mercaptoethanol, Freund's Adjuvant, propionic acid, n-butyric acid, isovaleric acid, 2-ethylbutyric acid, sulfuric acid and Tween-80 from Sigma-Aldrich (St. Louis, MO); absolute ethanol, acetic acid, lithium carbonate and tryptamine were purchased from Fisher Scientific (Hampton, NH); RPMI 1640, FBS, L- glutamine, PBS, luxol fast blue, cresyl violet, eosin, hematoxylin, and HEPES were purchased from VWR (West Chester, PA; fluorophore conjugated antibodies and ELISA kits from Biolegend (San Diego, CA); Illumina MiSeq reagents from Illumina Inc (San Diego, CA); QIAamp Stool Mini Kits from Qiagen (Germantown, MD); 10% formalin from Azer Scientific (Morgantown, PA).

2.3.3 INDUCTION OF CHRONIC PROGRESSIVE EAE AND TREATMENT WITH TRYPTAMINE

Chronic progressive EAE was induced in C57BL/6 mice according to previously published protocols[5,113]. Briefly, mice were immunized on day 0 with subcutaneous injections containing 150µg of MOG35-55 and 600mg heat killed *Mycobacterium tuberculosis* (H37Ra) suspended within an emulsion of PBS and Freund's complete adjuvant. On day 0 and 2, mice received a single intraperitoneal injection containing 200ng and 400ng of PTX, respectively. Beginning on day 1, mice received a 50µL intraperitoneal injection containing either a vehicle (sterile corn oil with 2% DMSO v/v)

or a treatment suspension (12.5mg/kg tryptamine in sterile CO with 2% DMSO v/v) every 48 hours. This dose of 12.5mg/kg was chosen in accordance with previous studies that have demonstrated it to be a safe dose that will not induce short term behavioral changes in mice[114]. This dose was also deemed to be safe and clinically relevant when converted to a human equivalent dose of 1mg/kg[115,116].

2.3.4 EAE SCORING OF PARALYSIS SYMPTOMS

The weight and paralysis symptoms were recorded within EAE mice daily. The scoring of paralysis symptoms was done according to the following key: 0 = no symptoms, 1 = inability to curl the distal end of tail, 2 = complete tail atony/impaired movement, 3 = partial hind limb paralysis, 4 = complete hind limb paralysis, 5 = tetraplegia/moribund state.

2.3.5 CELL ISOLATION

Single cell suspensions were prepared using neural tissue dissociation kits purchased from Miltenyi according to manufacturer instructions[117]. After dissociation of CNS tissue, myelin was removed from the single cell suspensions using two washes in 30% percoll. Remaining cells were then subjected to RBC lysis buffer, washed, and suspended in RPMI supplemented with FBS and penicillin/streptomycin for downstream use. Immune cells were isolated from the spleens and lymph nodes by use of mechanical dissociation followed by RBC lysis and filtration using 70μm filters. After washing, the remaining mononuclear fractions were suspended in RPMI for downstream use.

2.3.6 ELISA QUANTIFICATION OF SECRETED CYTOKINES

Media was collected from primary cultures of mononuclear cells isolated from the CNS and spleen plated at $10x10^6$ cells/mL under unstimulated conditions from EAE mice

treated in vivo and MOG35-55 (20µg/mL) stimulated conditions from MOG35-55 immunized mice treated in vitro for ELISA quantification of IL-10 and IL-17. ELISAs were performed according to Biolegend protocols. Briefly, high affinity protein-binding plates were coated by incubating a 100µL suspension of capture antibody overnight at 4°C.The plates were then washed 3 times using wash solution of (PBS+0.05% Tween80). The plates were then incubated with blocking solution for one hour at RT. After incubation, the plate was washed 3 times using wash solution and incubated for 2 hours at RT with 100µL of standards prepared using serial dilutions according to manufacturer instructions and 100µL of supernatant collected from overnight cell cultures. Plates were again washed three times with wash solution before incubating with 100µL of a biotinylated detection antibody solution diluted according to the manufacture's instruction in blocking solution at RT for 1 hour. After incubation with the detection antibody, plates were washed three times with solution and incubated with HRP conjugated avidin antibody for 30 minutes at RT. After incubation with HRP-avidin, the ELISA plates were washed five times with wash solution and incubated with TMB substrate for fast color development. After color development, the reaction was stopped simultaneously in all wells using 1N hydrosulfuric acid. The concentration of captured protein content was calculated by comparing relative absorbance of variable samples at a wavelength of 450nm to the standard curve calculated from standards of known concentration. Plates were analyzed with a PerkinElmer Victor^2 plate reader.

2.3.7 FLOW CYTOMETRY FOR QUANTIFICATION OF IMMUNE CELL PHENOTYPES

Suspensions of single mononuclear cells isolated from splenic and CNS tissue using previously described methods were phenotyped using a BD FACSCelesta flow cytometer. Single cell suspensions were tagged with fluorescently labeled monoclonal antibodies purchases from Biolegend (APC conjugated anti-RORγT, BV786 conjugated anti-CD4, FITC conjugated anti-CD3, BV421 conjugated anti-Foxp3, PE conjugated and BV605 conjugated anti-CD45). Analysis of .fcs files was conducted using FlowJo software.

2.3.8 STIMULATION OF MOG35-55 REACTIVE MONONUCLEAR CELLS IN VITRO

C57BL/6 mice were immunized with subcutaneous injections of 150µg of MOG35-55 and 600mg H37Ra suspended within an emulsion of sterile PBS and Freund's adjuvant. After 7 days, the mice were euthanized using isoflurane. Spleens were excised from the mice and cells were isolated via mechanical dissociation, RBC lysis and 70µm filtration. Live cells were plated at $10x10^6$ cells/mL in complete cRPMI activated with 20µg/ml MOG35-55. Cells were activated in the presence or absence of 100µM tryptamine in the medium and cultured for 48 hours. Statistical analysis was performed using paired t-tests to compare changes across donor samples in the presence or absence of tryptamine.

2.3.9 INDUCTION OF PASSIVE POLYCLONAL EAE

Passive polyclonal EAE was induced as previously described[118]. Briefly, C57BL/6 (wild-type) and Lck-Cre $AHR^{flox/flox}$ mice were immunized with subcutaneous

injections of 150µg of MOG35-55 and 600mg H37Ra suspended within an emulsion of sterile PBS and Freund's complete adjuvant. After 7 days, the mice were humanely euthanized. Cells were isolated from the spleens and inguinal lymph nodes of these donor mice as previously described. Live cells were incubated at a concentration of $4x10^6$ cells/mL in cRPMI medium supplemented with MOG35-55 (10µg/mL), rIL-2 (10U/mL), rIL-12 (25ng/mL) and rIL-18 (25ng/mL) in the presence or absence of tryptamine (100µM). After 48 hours, the cells were washed and plated in cRPMI medium supplemented with MOG35-55 (10µg/mL), rIL-2 (20U/mL), rIL-12 (25ng/mL) and rIL-18 (25ng/mL) in the presence or absence of tryptamine (100µM). After 24 hours, the cells were washed, counted, and brought to a final concentration of $4x10^6$ live cells/100µL within sterile PBS. $4x10^6$ live cells were given via retro-orbital injection to recipient C57BL/6 (wild-type) mice. After 2 hours, mice received an intraperitoneal injection containing 200ng of PTX suspended within sterile PBS. After 48 hours, the mice received a second intraperitoneal injection containing 400ng of PTX suspended in sterile PBS. Paralysis symptoms were recorded daily as previously described.

2.3.10 HISTOLOGICAL ANALYSIS

Euthanized mice were perfused with 10mL of heparinized PBS followed by 10mL of 10% formalin. After isolation, whole brains were held in 70% EtOH and embedded in paraffin blocks. 7 µm sections were cut using a microtome and placed onto microscope slides using a water bath. Slides were deparaffinized with washes of xylene and ethanol prior to staining with Luxol Fast Blue and H&E according to previously published protocols[119,120].

2.3.11 BACTERIAL PHYLOGENETIC PROFILING BY 16S ANALYSIS

Phylogenetic profiling of the cecal microbiota was conducted by use of 16s rDNA sequencing of DNA isolated from cecal contents of vehicle and tryptamine treated mice. Briefly, DNA was isolated from cecal contents using the QIAamp Stool Mini Kit according to the manufacturer instructions. Sequencing was performed using the Illumina MiSeq platform. Downstream analysis of .fastq files was conducted using the Nephele platform provided via the NIAID[121]. Further downstream analysis of Nephele OTU outputs was conducted using LEfSe analysis[122].

2.3.12 QUANTIFICATION OF SCFAS

SCFA content was quantified from cecal content using methods previously described[123,124]. Briefly, 100mg of cecal content was homogenized in 400µL deionized H20. After homogenization, samples were acidified by adding 1:4 of the total volume of 25% metaphosphoric acid. After 30 minutes of incubation, samples were centrifuged (12,000g for 15 minutes), with the supernatant being collected and filtered using Ultra-free MC Columns (ThermoFisher). Ethyl butyric acid was added to each sample at a final concentration of 0.0375mM for use as an internal standard to accurately calculate experimental concentrations. Samples then received 400µL of methyl tert-butyl ether (MTBE) and were vortexed vigorously. Samples were then spun at 400g for 5 minutes. Lastly, 100µL of the upper organic layer was transferred to a fresh glass tube. Samples were then analyzed with an HP 5890 gas chromatograph configured with flame-ionized detection,

2.3.13 STATISTICAL ANALYSIS

Statistical analysis was conducted using GraphPad Prism software version 8.4.3. Unpaired t tests were used to compare experimental groups separated by a single variable. Paired t tests were used to compare changes in experimental groups that shared a single subject prior to subjection to a variable. Samples from a shared donor are annotated by a solid line connecting individual values across groups. Statistical analysis on changes in paralysis symptoms and weight over time were calculated using unpaired t tests at each time point with significance values corrected for a desired FDR of 1% using a Benjamini, Krieger, and Yekutieli test. Statistical analysis of experiments with multiple variables was conducted using a 2-way ANOVA tests to determine significant interactions. Post hoc analysis to determine the degree of significance was conducted using Bonferroni's test. To test the efficacy of tryptamine in EAE, we used 4 experiments containing 5 mice per group equating to a total of 20 mice. The number of animals used in other experiments have been shown in Figure legends. All graphs show individual values with the mean ± SEM. Samples were considered statistically significant if $p < 0.05$. Degree of significance was demonstrated using the following key: $*p<0.05$, $**p<0.01$, $***p<0.001$.

2.4 RESULTS

2.4.1 TRYPTAMINE AMELIORATES EAE SEVERITY

To investigate the immunosuppressive potential of tryptamine, we administered tryptamine (12.5mg/kg) via i.p. injection every 48 hours in a murine model of chronic progressive EAE. We analyzed mice daily to observe paralysis symptoms and body weight until any individual mice displayed a severity of symptoms that reflected a

moribund state and required euthanasia. At this point, observed at day 13, all mice were humanely euthanized for uniform sample collection. Tryptamine treated mice demonstrated a significant reduction in paralysis symptoms beginning from day 8 that persisted for the remaining duration of the study (Figure 2.1A). The sum of paralysis scores per mouse further demonstrates a significant reduction in observed paralysis symptoms experienced between tryptamine vs vehicle treatment groups (Figure 2.1B). The average weight of mice was also measured throughout the time course of chronic progressive EAE, and the data expressed as percent of starting body weight, clearly showed that while the vehicle-treated group started losing weight, especially on days 11-13, the tryptamine-treated mice showed a substantial retention of weight when compared to the vehicle controls (Figure 2.1C). These results together demonstrated that tryptamine treatment of EAE mice ameliorates the clinical symptoms of paralysis and weight loss associated with EAE.

2.4.2 TRYPTAMINE TREATMENT ALTERS NEUROINFLAMMATION IN EAE MICE

To understand if the attenuation of clinical symptoms by tryptamine results from decreased neuroinflammation, we next investigated the T cell responses in the CNS of these mice. A representative flow plot demonstrated the reduction in CD4+ T cells found within the CNS of tryptamine treated mice (Figure 2.2A). When CNS infiltrating CD4+ T cells were analyzed using flow cytometry amongst the CD45+ population (Figure 2.5A), we noted that while the percentage of CD4+ T cells did not significantly decrease in comparison to the vehicle group (Figure 2.2B), there was significant reduction in the total number of infiltrating CD4+ T cells present in the CNS (Figure 2.2C). Analysis of

anti-inflammatory (IL-10) and pro-inflammatory (IL-17) cytokines secreted by cultured mononuclear cells isolated from the CNS revealed that tryptamine treated mice displayed no significant change in IL-10 secretion (Figure 2.2D) while significantly suppressing IL-17 secretion in comparison to the vehicle group (Figure 2.2E). Because the MOG antigen is injected peripherally, we also tested the spleens of the tryptamine for Tregs vs Th-17 cells to test if tryptamine also altered the immune response in the periphery. CD4+ T Cells were identified from the spleens as being CD3+CD4+CD8- prior to looking at transcription factor expression (Figure 2.5B). This increase in the Treg population of tryptamine treated mice is represented with overlaying histograms demonstrating Foxp3 expression amongst CD4+ T cells between the groups (Figure 2.2F). We found that tryptamine treated mice displayed a higher proportion (Figure 2.2G) as well as total number (Figure 2.2H) of anti-inflammatory Tregs in comparison to the spleens of vehicle treated mice. After discovering an increase in the anti-inflammatory Treg subset, we then studied the pro-inflammatory counterpart of RORγT+ T cells. The spleens of tryptamine treated mice demonstrated a reduction in the percentage of RORγT+ T cells as shown by a representative histogram (Figure 2.2K). Tryptamine treatment significantly reduced the proportion of the pro-inflammatory RORγT T cell subset within the spleens in comparison to the vehicle group (Figure 2.2I) while displaying a trend in the total number of Th17 lymphocytes, however this trend was not statistically significant (Figure 2.2J). Collectively these results showed that treatment with tryptamine suppresses inflammation in both the periphery and in the CNS.

2.4.3 TRYPTAMINE INHIBITS THE INFLAMMATORY CAPACITY OF MOG35-55 SPECIFIC CD4+ T CELLS AND AMELIORATES THEIR ENCEPHALITOGENIC ACTIVITY IN AN ARYL HYDROCARBON RECEPTOR DEPENDENT MANNER

In order to better demonstrate that tryptamine ameliorates EAE by regulating CD4+ T cell reactivity in an AHR-dependent manner we tested the immunosuppressive capacity of tryptamine on MOG35-55 reactive T cells donated from wild WT and Lck-Cre $AHR^{flox/flox}$ mice prior to the induction of CD4+ T cell mediated passive polyclonal EAE. Briefly, C57BL/6 wild-type and Lck-Cre $AHR^{flox/flox}$ mice were immunized with MOG35-55 antigen and immune cells from the spleens and lymph nodes were further activated with a combination of MOG35-55 and pro-inflammatory cytokines IL-2, IL-12 and IL-18 in vitro, in the presence or absence of tryptamine (100µM). Following a 72h incubation the cell suspensions were then transferred into naïve wild-type mice via retroorbital injection. The development of EAE symptoms were studied daily as described in Methods.

The mice which received transfer of cells from wildtype+Vehicle, Lck-Cre $AHR^{flox/flox}$ +Vehicle and Lck-Cre $AHR^{flox/flox}$ +Tryptamine demonstrated significant paralysis symptoms, while those that received transfer of cells from wildtype + tryptamine group developed only mild paralysis symptoms (Figure 2.3A). These results are further corroborated by the cumulative scores of paralysis scores per mouse (Figure 2.3B). Flow cytometry analysis of the spleen (Figure. 3C) and CNS (Figure. 3D) revealed that mice which received a transfer of tryptamine treated encephalitogenic T cells from wildtype mice displayed increased Treg abundance when compared to similar cells that were treated with vehicle. Measurement of IL-10 in in-vivo sensitized cells with MOG

that were activated in vitro with MOG in the presence of tryptamine showed an increase in IL-10 secretion when compared to vehicle controls, but it was not statistically significant (Figure 2.3E). Histological analysis of brain in passive EAE experiments showed a retention of myelin indicated by a deeper intensity of Luxol fast blue staining in the areas surrounding the dark blue stained neuronal cell bodies and a reduction of immune cell infiltration denoted by a lack of dark colored H&E-stained infiltrates in the mice that received cells treated with tryptamine in vitro when compared to mice that received similar cells treated with vehicle (Figure 2.3F).

Because culture of MOG-sensitized T cells in vitro with tryptamine and adoptive transfer led to decreased EAE when compared to vehicle-treated cells, we next investigated the mechanisms involved. Representative flow plots demonstrated the percentage of CD4+ and PCNA+ cells amongst all lymphocytes collected from immunized mice stimulated in vitro with MOG35-55 in the presence or absence of tryptamine demonstrated a reduction in proliferative activity (Figure 2.3G). Tryptamine treatment in vitro reduced the percentage of proliferating CD4+ T cells as demonstrated by PCNA+ cells (Figure 2.3H). Also, tryptamine treatment in vitro significantly reduced the percentage of CD4+ RORγT as shown in a representative flow cytometric analysis (Figure 2.3I) and the percentage of such cells from multiple samples (Figure 2.3J).

2.4.4 TRYPTAMINE TREATMENT IN EAE PROMOTES BUTYRATE PRODUCTION BY THE GUT MICROBIOTA

Previous literature has demonstrated that AHR ligands exert their anti-inflammatory properties by a combination of direct interactions on the immune system and indirect interactions mediated by the GI microbiota[124–126]. For this purpose, we

studied the effects of tryptamine treatment in-vivo on the composition of the cecal microbiota in EAE mice. The chao1 index (Figure 2.4A) and Shannon index (Figure 2.4B) of 16s sequencing reads indicated there were slight increases in the alpha diversity of the cecal microbiome composition in tryptamine treated mice. PCoA plotting demonstrated that the cecal microbiota of treated mice was distinctly clustered from the vehicle group (Figure 2.4C). LEfSe analysis was conducted on the 16s sequencing outputs to distinguish differentially regulated bacterial phylogenies (Figure 2.4D). 3 LEfSe identified phylogenies in *Dehalobacterium* (Figure 2.4E), *Bacteroides* (Figure 2.4F) and *Peptostreptococcaceae* (Figure 2.4G) to be significantly altered in tryptamine-treated groups when compared to the vehicle controls. When Short Chain Fatty Acids (SCFAs) were quantified using mass spec the data revealed a significant increase in n-Butyric Acid following tryptamine treatment when compared to vehicle controls (Figure 2.4H). These results suggested that tryptamine treatment alters the microbiota in the gut and promotes the induction of n-Butyric Acid.

2.5 DISCUSSION

MS is an incurable autoimmune disorder that is perpetuated by a complex etiology contributing to excessive inflammation occurring within the CNS. Previous studies have established that the gut microbiota shapes the host immunity in neuroinflammatory disorders and, when there is dysbiosis, it can trigger autoimmune encephalomyelitis [100,127–130]. Due to the critical role played by the microbiota in the etiology of inflammatory disorders, we studied the immunomodulatory potential of tryptamine, a microbial metabolite that is produced in large quantities within the GI tract. Tryptamine production within the gut has been characterized within two known

commensal microorganisms that inhabit the GI tract of homeothermic organisms, *Clostridium sporogenes* and *Ruminococcus gnavus*[111]. Clinical studies have demonstrated that Clostridium species are decreased in MS patients in comparison to healthy controls, while there are conflicting reports that demonstrate primarily increased abundance of Ruminococcus species in MS patients with one specific cohort of adolescent MS patients showing decreased Ruminococcaceae abundance[131,132]. These studies did not identify the bacterial composition of *Ruminococcus gnavus* or *Clostridium sporogenes* at the species level and do not definitively state that these tryptamine producing species specifically are regulated in MS patients. However, these studies in combination with our work strengthen the suggestion that hindered tryptamine production within the GI tract may affect the clinical severity of MS due to the upper-level phylogenies of these bacterial species being significantly regulated in MS patients when compared to healthy controls. Further studies are clearly needed to determine if tryptamine deficiency is associated with susceptibility to MS. This may involve measuring the concentrations of tryptamine within the intestinal tracts of patients, as well as quantifying the relative abundance of tryptamine producing bacterial species and the tryptophan decarboxylase enzyme.

Previous studies have demonstrated the strong association between exogenous AHR ligands regulating autoimmune neuroinflammation in an AHR-dependent manner[133–135].Our study demonstrates that tryptamine possesses a potent neuroprotective role in the context of EAE by limiting excessive neuroinflammation and ameliorating the associated paralysis symptoms by directly inhibiting encephalitogenic T cell activity in an AHR-dependent manner. With these data we suggest that interactions between host immunity and exogenously produced tryptamine exerts significant suppression of

neuroinflammation by preventing and inhibiting encephalitogenic T cell activity. We confirmed this by showing that transfer of WT encephalitogenic T cells treated with tryptamine ex-vivo into wild-type mice caused the induction of very mild form of EAE and significant attenuation of neuroinflammation when compared to similar cells treated with the vehicle which induced robust EAE and inflammation in the CNS. Interestingly, transfer of encephalitogenic T cells lacking a functional AHR, treated with tryptamine ex-vivo, displayed no reduction in encephalitogenic capacity in comparison to control groups. These data confirmed that tryptamine acts through AHR. Mechanistically, we found that treatment of encephalitogenic cells with tryptamine in vitro, inhibited the proliferation of CD4+ T cells and inhibited RORγT cells, and furthermore, when such cells were transferred into wild-type mice, they induced more Tregs than similar cells treated with the vehicle. The fact that encephalitogenic T cells lacking a functional AHR when treated with the vehicle ex-vivo, were able to induce the same levels of EAE as wild-type T cells treated with the vehicle also suggested that AHR expression on T cells per se may not play a role in the induction of EAE in the adoptive transfer model of EAE tested in the current investigation. Confirmation that the immunosuppressive effects of tryptamine are dependent on AHR expression coincides with previous literature demonstrating that a variety of AHR ligands promote an immunotolerant phenotype in T cell subsets[136].

Previous literature has demonstrated that a primary mechanism by which AHR ligands limit excessive immune responses in autoimmune disorders is by regulating a dysbiotic microbiota and promoting the production of the SCFAs[124,137]. Additionally, it has been suggested by previous studies that microbially produced tryptamine affects

intestinal motility and the enteric nervous system in a manner that may have effects regulating the GI flora[111,112,138]. For these purposes, we investigated the changes observed within the cecal contents of EAE mice that received tryptamine treatment in comparison with vehicle controls by use of 16s sequencing and mass spectrometry. Within the cecal contents of tryptamine treated mice, there was a significant increase in the abundance of *Peptostreptococcaceae,* a family of gram-positive bacteria which was shown to be downregulated in patients suffering from the autoimmune demyelinating disease, Neuromyelitis Optica[139]. While any potential mechanisms with which *Peptostreptococcaceae* species directly limit autoimmune neuroinflammation are not currently defined, *Peptostreptococcaceae* is normal constituent of a healthy gastrointestinal microbiota that contributes to maintaining intestinal homeostasis and has been shown to be significantly depleted under dysbiotic conditions[140,141]. Mass spectrometry analysis revealed that the tryptamine treatment significantly increased the concentration of the anti-inflammatory bacterial metabolite butyrate within the cecal contents of EAE mice. Cecal butyrate content has been established to induce the immunosuppressive Treg lymphocytes, which have been correlated with a positive outcome in autoimmune disorders and EAE[46,48]. Here we suggest that tryptamine treatment in inflammatory disorders promotes an anti-inflammatory metabolomic profile within the gut through promoting the production of butyrate. The translational impact of tryptamine enacting on the immune system, enteric nervous system and intestinal epithelium to further promote an anti-inflammatory gut microbiota is pivotal due to tryptamine's potential role as a novel messenger enabling crosstalk between the microbiota and host immunity at barrier sites. This promotion of butyrate suggests that

the production of tryptamine within a healthy gastric flora may play an important role in further influencing the immune system to maintain a healthy gastric flora and prevent excessive inflammation. Therefore, normal tryptamine production may be a negative regulator of inflammation involved in maintaining homeostatic conditions between the GI microbiota and host immunity by promoting Tregs, and when absent, leaves inflammation and bacterial dysbiosis unregulated as is observed in inflammatory disorders[19,52,53].

In summary, this study demonstrates for the first time that administration of tryptamine attenuates a murine model of MS by suppressing neuroinflammation and adds to the growing dataset demonstrating that microbial metabolism within the GI tract plays an important role in regulating neuroinflammation through the production of AHR ligands. Our study has demonstrated that tryptamine under inflammatory conditions shifts the T cell landscape towards an immunosuppressive state and directly interacts with myelin-reactive T cells to inhibit neuroinflammation in an AHR dependent manner. In combination with directly suppressing the immune response, tryptamine results in anti-inflammatory shifts in the metabolome of the GI microbiota suggesting that tryptamine may play an important role in the crosstalk between host and flora required to maintain intestinal homeostasis. In the long term, characterizing the immunomodulatory capacity of tryptamine and other AHR ligands produced by normal flora will help further define the complex etiology of autoimmune disorders and potentially translate into clinical applications such microbiome-based therapies.

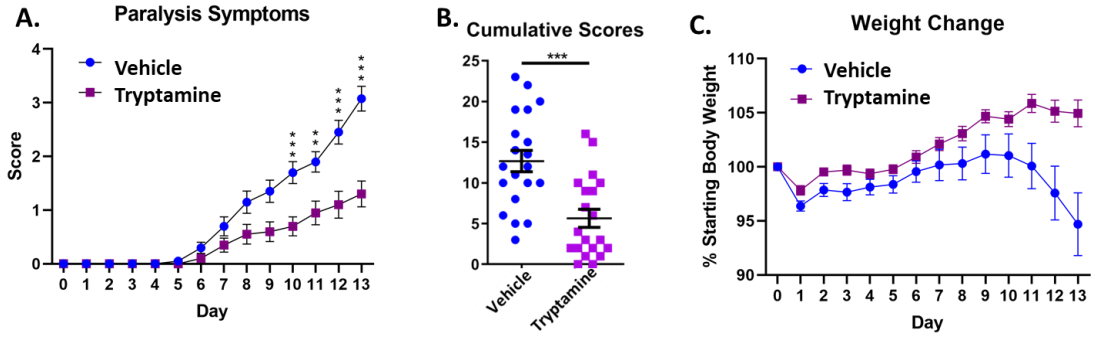

Figure 2.1 ***Tryptamine ameliorates EAE severity***. (**A)** Paralysis symptoms of vehicle treated (2% DMSO in corn oil) and tryptamine (12.5mg/kg every 48 hours) treated chronic progressive EAE mice (n=20 per group. Multiple t tests performed to compare daily means across groups with a desired FDR of 1% via a Benjamini, Kieger, and Yekutieli test. Day 11 FDR-P=0.002; Day 10, 12, and 13 FDR-P<0.0001). **(B)** Cumulative score per each mouse of vehicle treated (2% DMSO in corn oil) and tryptamine (12.5mg/kg every 48 hours) treated chronic progressive EAE mice (n=20 per group. $t(38)=4.197$, $p<0.001$). **(C)** Percentage of starting body weight vehicle treated (2% DMSO in corn oil) and tryptamine (12.5mg/kg every 48 hours) treated chronic progressive EAE mice (n=20 per group).

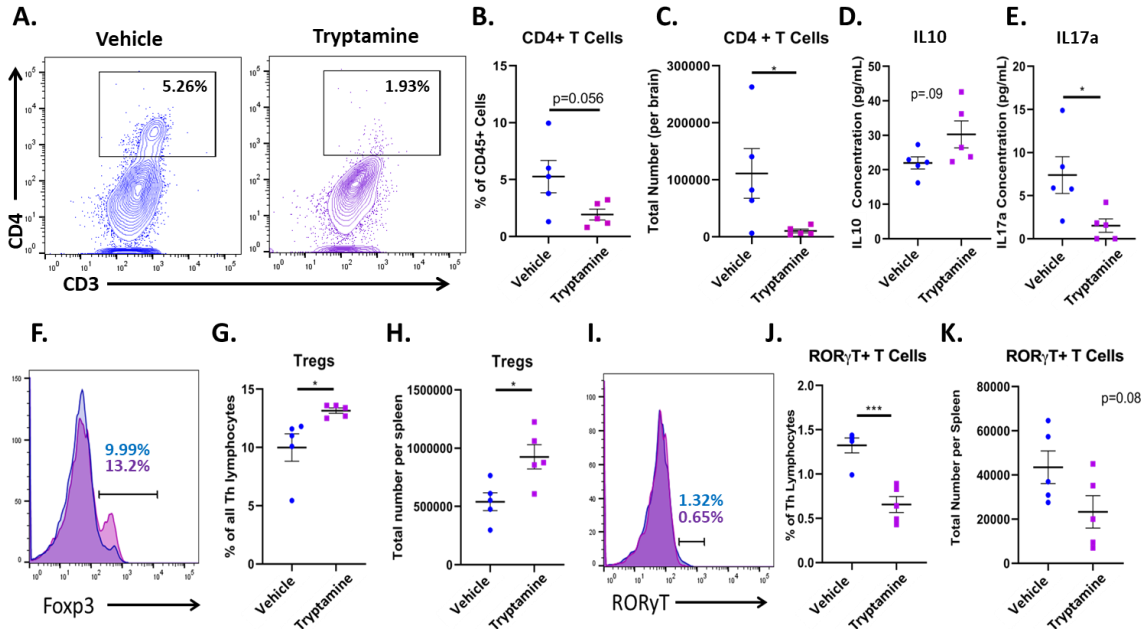

Figure 2.2 ***Tryptamine treatment alters neuroinflammation in EAE mice.*** **(A)** Representative flow plots of CD3 and CD4 expression in CD45+ cells in vehicle (blue) and tryptamine-treated (purple) mice. **(B)** CD4+ T Cells infiltrating the CNS of EAE mice represented as a percentage of all CD45+ cells (n=5 per group. t(8)=2.224, P=0.056). **(C)** Total number of CD4+ T Cells infiltrating the CNS of EAE mice (n=5 per group. t(8)=2.307, P=0.049). **(D)** Secreted IL10 concentration from cultured mononuclear cells ($10x10^6$ cells/mL in cRPMI for 24h isolated from the CNS of vehicle and tryptamine treated mice (n=5 per group. t(8)=1.928, P=0.09). **(E)** Secreted IL17a concentrations from cultured mononuclear cells ($10x10^6$ cells/mL in cRPMI for 24h) isolated from the CNS of vehicle and tryptamine treated mice (n=5 per group. t(8)=2.590, P=0.). **(F)** Representative flow plots of Foxp3 expression amongst CD4+ lymphocytes in vehicle (blue) and tryptamine-treated (purple) mice. **(G)** Percentage of Foxp3+ (assumed as Tregs) cells amongst all CD4+ lymphocytes isolated from the spleen of vehicle and tryptamine treated mice (n=5 per group. t(8)=3.091, P=0.014). **(H)** Total number of Tregs per spleen in vehicle and tryptamine treated mice (n=5 per group. t(8)=2.937, P=0.017). **(I)** Representative flow plots of RORγT expression amongst CD4+ lymphocytes in vehicle (blue) and tryptamine-treated (purple) mice. **(J)** Percentage of RORγT+ T cells amongst all CD4+ lymphocytes isolated from the spleen of vehicle and tryptamine treated mice (n=5 per group. t(8)=5.400, P<0.001). **(K)** Total number of RORγT+ T cells per spleen in vehicle and tryptamine treated mice (n=5 per group. t(8)=1.933, P=0.08).

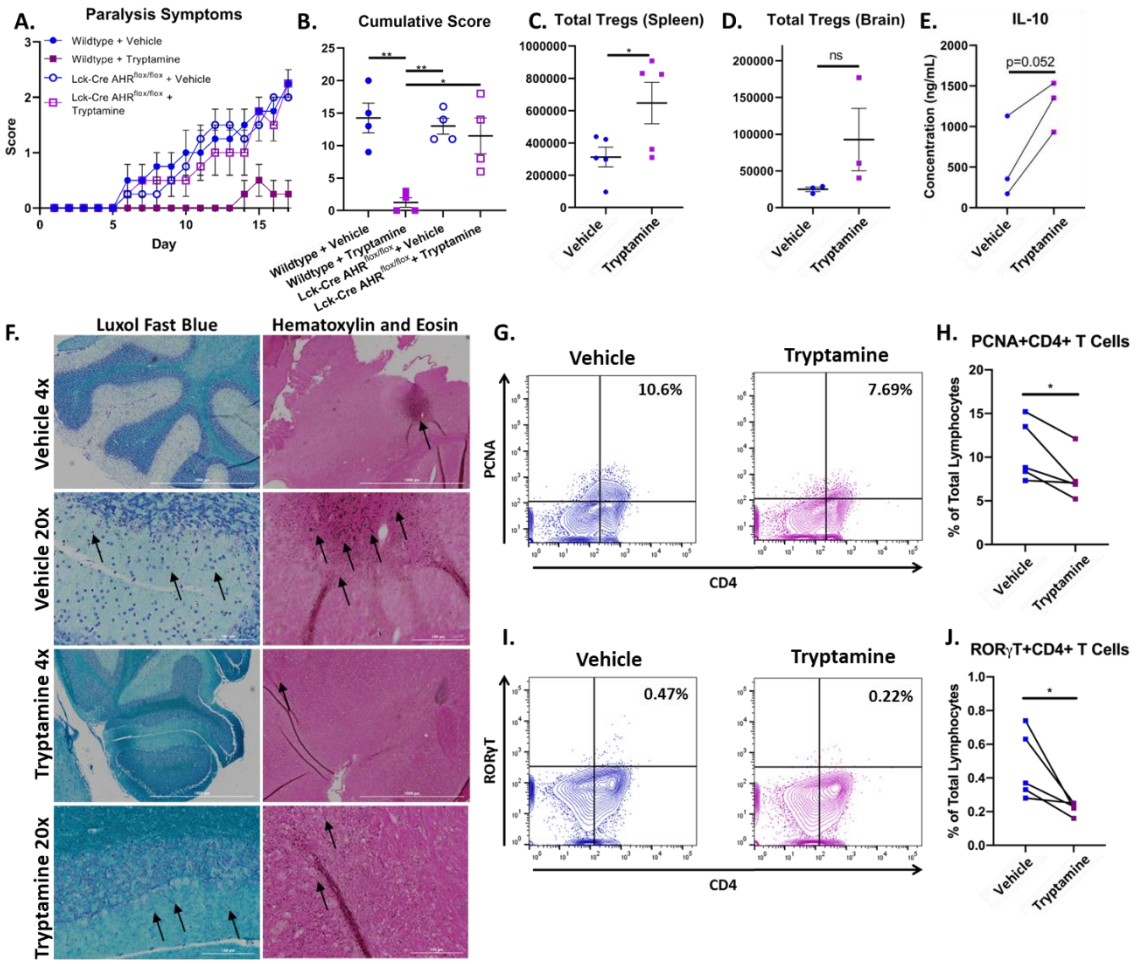

Figure 2.3 ***Tryptamine inhibits the inflammatory capacity of MOG35-55 specific CD4+ T Cells and ameliorates their encephalitogenic activity in an aryl hydrocarbon receptor dependent manner.*** (**A)** Paralysis symptoms of chronic progressive polyclonal passive EAE mice. Mice received a retro orbital injection of 4 million live cells that were cultured under stimulating conditions that promote the expansion of encephalitogenic CD4+ T cells. Donor cells were derived from WT and Lck-Cre AHR$^{flox/flox}$ mice and treated ex-vivo in the presence of vehicle (DMSO) or 100µM tryptamine prior to induction of disease and divided into 4 groups (wildtype + vehicle, wildtype + tryptamine treatment, Lck-Cre AHR$^{flox/flox}$ + vehicle, and Lck-Cre AHR$^{flox/flox}$ + tryptamine treatment; n=4 per group). **(B)** Cumulative score per each passive polyclonal EAE group (n=4 per group. 2-Way ANOVA with Bonferroni's multiple comparisons test, F (1, 12) = 8.891; Post hoc: Wildtype + Tryptamine vs. Wildtype + Vehicle p<0.0028, Wildtype + Tryptamine vs. Lck-Cre AHRflox/flox+ Tryptamine p=0.00164, Wildtype + Vehicle vs. Lck-Cre AHR$^{flox/flox}$+ Tryptamine p=0.0061). **(C)** Total number of Tregs per brain from

chronic progressive polyclonal passive EAE mice given cells treated ex vivo with either vehicle or tryptamine (n=5. t(8)=2.356, P=0.046). **(D)** Total number of Tregs per spleen from chronic progressive polyclonal passive EAE mice given cells treated with either vehicle or tryptamine (n=3. t(4)=1.586, P=0.18). **(E)** Production of IL-10 amongst mononuclear cells isolated from MOG immunized mice and stimulated with 20µg/ml MOG35-55 in vitro in the presence or absence of 100µM tryptamine ($10x10^6$ cells/mL in cRPMI with for 24h, n=3. t(2)=4.193, P=0.052). **(F)** Luxol Fast Blue and Hematoxylin and Eosin staining of the CNS from chronic progressive polyclonal EAE mice that received either tryptamine or vehicle treated encephalitogenic T Cells. Black arrows indicate neuronal bundles (Luxol Fast Blue) and areas with evidence of cellular infiltration (Hematoxylin and Eosin). **(G)** Representative flow plots of PCNA and CD4 expression amongst mononuclear cells isolated from MOG immunized mice and stimulated with MOG35-55 in vitro in the presence or absence of tryptamine. **(H)** Percentage of PCNA+CD4+ lymphocytes amongst all lymphocytes in mononuclear cells isolated from MOG immunized mice and stimulated with 20µg/ml MOG35-55 in vitro in the presence or absence of 100µM tryptamine ($10x10^6$ cells/mL in cRPMI with for 24h, n=5. t(4)=2.982, P=0.04). **(I)** Representative flow plots of RORγT and CD4 expression amongst mononuclear cells isolated from MOG immunized mice and stimulated with MOG35-55 in vitro in the presence or absence of tryptamine. **(J)** Percentage of RORγT+CD4+ lymphocytes amongst all lymphocytes in mononuclear cells isolated from MOG immunized mice and stimulated with 20µg/ml MOG35-55 in vitro in the presence or absence of 100µM tryptamine ($10x10^6$ cells/mL in cRPMI with for 24h, n=5. t(4)=2.802, P=0.048).

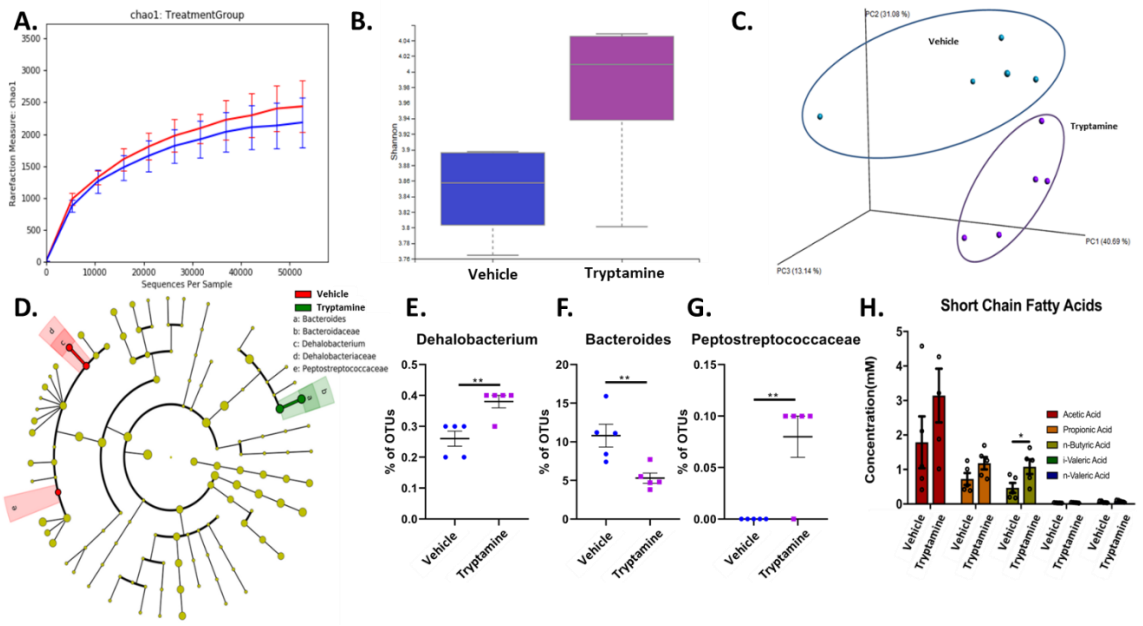

Figure 2.4 ***Tryptamine treatment in EAE promotes butyrate production by the gut microbiota*****. (A)** Sequenced reads were analyzed with Nephele software to plot the chao index indicating average number of unique 16s reads per sample of cecal content between vehicle and tryptamine treated mice (n=5 per group). **(B)** Sequenced reads were analyzed with Nephele software to plot the Shannon index between samples of cecal content between vehicle and tryptamine treated mice (n=5 per group). **(C)** PCoA plot displaying unique clustering of the cecal microbiota amongst mice treated with vehicle vs mice treated with tryptamine (n=5 per group). **(D)** LEfSe analysis indicating the observed changes within the cecal microbiota content. **(E)** Relative abundance of Dehalobacterium within the cecal content based on 16s sequencing reads (n=5 per group. t(8)=3.795, P=0.0053). **(F)** Relative abundance of Bacteroides within the cecal content based on 16s sequencing reads (n=5 per group. t(18)=3.403, P=0.0093). **(G)** Relative abundance of Peptostreptococcaceae within the cecal content based on 16s sequencing reads (n=5 per group. t(8)=4.000, P=0.0039). **(H)** SCFA concentration within the cecal content of vehicle vs tryptamine treaded mice (n=5 per group. n-butyric acid t(8)=2.400, P=0.043).

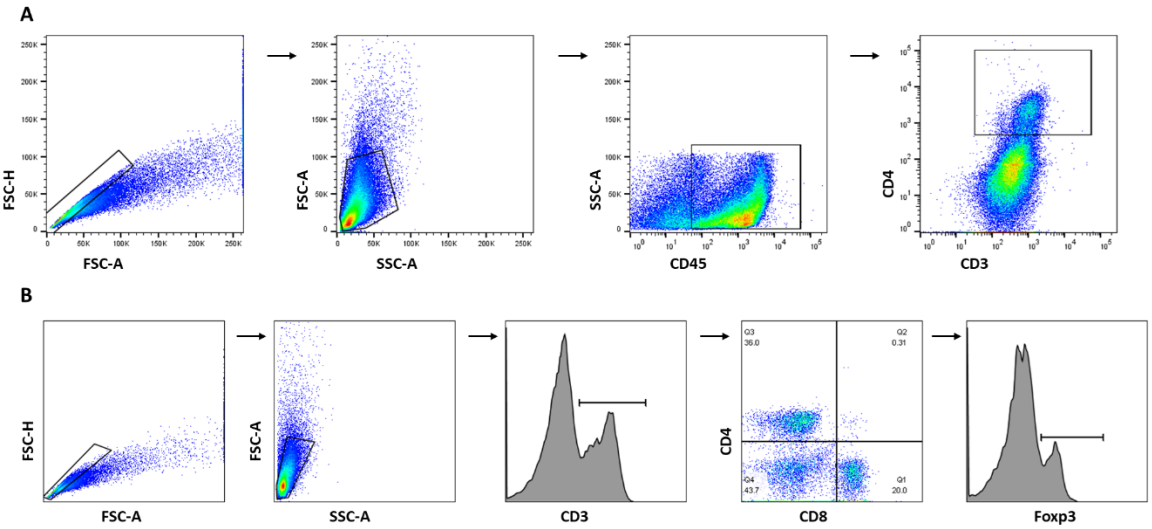

Figure 2.5 ***Gating strategies for CD4+ T cells*** **(A)** CD4+ T Cells isolated from the CNS were gated using forward scatter height by forward scatter area to first gate singlets. Cells were then gated for side scatter area by forward scatter area to identify an immune cell bubble. Cells were then gated on side scatter area by CD45 expression to further remove debris and focus on immune cells. CD45+ cells were then gated for CD3 and CD4 positivity to identify CD4+ T cells. **(B)** CD4+ T Cells isolated from the spleen were gated using forward scatter height by forward scatter area to first gate singlets. Cells were then gated for side scatter area by forward scatter area to identify an immune cell bubble. Cells were then gated for being CD3+ to identify lymphocytes present. Lymphocyte subsets were then gated on CD4 by CD8 positivity to identify T helper and cytotoxic T cells. CD4+ T cells were then gated using histograms to identify Foxp3+ and RORγT+ positivity amongst the CD4+ T cells.

CHAPTER 3

EFFECTS OF ORALLY ADMINISTERED CANNABIDIOL ON NEUROINFLAMMATION AND INTESTINAL INFLAMMATION IN THE ATTENUATION OF EXPERIMENTAL AUTOIMMUNE ENCEPHALOMYELITIS[3]

3.1 ABSTRACT

CBD is a bioactive compound isolated from Cannabis plants that has garnered attention within the medical community due to its potent anti-inflammatory properties. To better understand how CBD limits excessive neuroinflammation we administered CBD via oral gavage (20mg/kg) in a murine model of MS known as EAE. Using scRNA Seq and array-based transcriptomics we were able to delineate how CBD limits excessive inflammation within the CNS as well as within the intestinal lining in EAE. In-depth scRNA Seq analysis of CNS tissue demonstrated that CBD treatment resulted in a significant reduction in CXCL9, CXCL10 and IL-1β expression within the CNS, leading to inhibited infiltration of inflammatory macrophages. CBD inhibited IL-1β production independent of the classical cannabinoid receptors, CB1 and CB2. CBD treatment also

[3]Dopkins N, Miranda K, Wilson K, Holloman B, Nagarkatti PS, Nagarkatti M. Effects of orally administered cannabidiol on neuroinflammation and intestinal inflammation in experimental autoimmune encephalomyelitis.
Manuscript in preparation.

led to induction of MDSCs both in the CNS and periphery. Interestingly, CBD treatment of EAE mice revealed significant suppression of inflammation in the GI tract. The IECs of CBD treated mice demonstrated a transcriptional inhibition of a family of pyroptosis initiators that drive localized inflammation known as GSDMs. Further investigation into the GI tract via 16s sequencing of cecal and fecal contents demonstrated that oral administration of CBD resulted in no significant changes in the intestinal microbiota composition. These findings demonstrate the beneficial effect of CBD treatment on autoimmune neuroinflammation by ablating expression of pro-inflammatory chemoattractants, regulating inflammatory macrophage activity, promoting MDSC expansion, and limiting the systemic low-grade inflammation in the GI tract, culminating in the attenuation of EAE.

3.2 INTRODUCTION

MS is an incurable autoimmune disorder in which the host immune system inadvertently recognizes peptides deemed antigenic within the myelin sheath surrounding the axon terminals within the CNS[144]. The immunity-dependent pathology of MS is characterized by flairs of neuroinflammation within the CNS that drives neurodegenerative lesions, which manifest in paralytic symptoms, discomfort, impaired cognitive function, and atrophy[145]. Current immunosuppressant therapies aimed at slowing MS disease progression are often complicated by external factors that further worsen the quality of life for afflicted patients due to their exorbitant costs, lack of long-term efficacy, susceptibility to infections, and inadvertent toxicity[146,147].

Some of the most consumed and postulated alternative therapeutics hoped to combat inflammatory disorders include the major cannabinoids isolated from Cannabis

sativa, namely CBD and THC[75,148]. While clinical research pertaining to cannabinoids is still in its relative infancy, the treatment of animal models of inflammatory disorders with CBD and THC has yielded results that demonstrate their respective abilities to inhibit the excessive inflammatory processes that drive pathogenesis by promoting expansion anti-inflammatory regulatory immune cell subsets, and inhibiting pro-inflammatory effector immune cell activity[80,85–87,149,150]. Studies such as these have culminated into the adoption of cannabinoid-based treatments, such as Sativex®, consisting of a combination of THC and CBD from Cannabis plant, which has been shown to improve the quality of life in patients with MS without the associated psychoactive effects of THC due to the oromucosal consumption route yielding low plasma levels of soluble THC[151]. While THC exhibits psychotropic effects, CBD does not and thus, use of CBD alone to suppress inflammation looks clinically more promising. To that end, more research is needed to understand the mechanism of action of CBD to suppress inflammation.

To further understand the changes occurring in various inflammatory cells in the CNS of EAE mice treated with CBD, in the current study, we used scRNA Seq and array-based transcriptomics. Additionally, because of the crosstalk between the gut and the brain during autoimmune diseases such as MS/EAE [100], we also investigated immunological changes occurring in the peripheral immune system, including the mesenteric lymph nodes (MLN) and the gut.

The primary findings of our study demonstrate that CBD treatment regulates the pro-inflammatory phenotype of resident and infiltrating myeloid cells by inhibiting macrophage infiltration and inhibiting the production of soluble inflammatory mediators such as IL-1β, CXCL9 and CXCL10. Outside of the CNS, we saw an increase in anti-

inflammatory processes that combat the chronic low-grade inflammation observed systemically in EAE mice. Specifically, within the GI tract, we observed a reduction in the expression of a family of pyroptosis initiators known as GSDMs in the intestinal epithelium, and a reduction of neutrophils present within the mesenteric lymph nodes. Within the spleen, we observed an expansion of the anti-inflammatory immune cells, MDSCs. Collectively, these data further suggest that CBD treatment yields potent inhibition of neuroinflammation resulting in alleviated paralytic symptoms, while limiting the chronic low-grade inflammation in the periphery, including the GI tract.

3.3 MATERIALS AND METHODS

3.3.1. REAGENTS

The following reagents were used during the course of the experiments and were purchased as follows: CBD from Cayman Chemical (Ann Arbor, MI); red blood cell (RBC) lysis buffer and T007, from Millipore Sigma (Burlington, MA); Percoll from GE Healthcare Life Sciences (Pittsburgh, PA); Myelin oligodendrocyte glycoprotein peptide subunit 35-55 (MOG35-55) from PolyPeptide Laboratories (San Diego, CA); Pertussis Toxin (PTX) from List Biological Laboratories (Campbell, CA); Heat killed *Mycobacterium tuberculosis* (H37Ra) from Difco (Detroit, MI); β-mercaptoethanol, Freund's Adjuvant, toluene based mounting medium and Tween-80, from Sigma-Aldrich (St. Louis, MO); Absolute ethanol from Fisher Scientific (Hampton, NH); RPMI 1640, fetal bovine serum (FBS), L- glutamine, phosphate buffered saline (PBS) and HEPES, from VWR (West Chester, PA); SSO Advanced SYBR Green Supermix, from Bio-Rad (Hercules, CA); DNA oligos, from Integrated DNA Technologies (Coralville, IA); Bovine serum albumin (BSA), 4',6-Diamidino-2-Phenylindole (DAPI), Texas Red

conjugated-phalloidin, pHrodo™ green dextran, and GeneChip™ WT Pico Kits, from Thermo Fisher (Waltham, MA); macrophage-colony stimulating factor (M-CSF), fluorophore conjugated antibodies, from Biolegend (San Diego, CA); Chromium Next GEM Single Cell 5' Library Gel and Bead Kit v1.1, Chromium Single Cell 5' Library Construction Kit, Chromium Next GEM Chip Single Cell Kit and Chromium i7 Multiplex Kit, from 10x Genomics (Pleasanton, CA); Illumina MiSeq reagents and NextSeq 500/550 v2.5 kits, from Illumina Inc (San Diego, CA); HRP-conjugated anti-biotin and biotinylated protein ladder, from Cell Signaling (Danvers, MA).

3.3.2. MICE

Six-week-old female WT C57BL/6 were purchased from Jackson laboratories (Bar Harbor, ME) and housed in the Animal Resource Facility at University of South Carolina School of Medicine. Prior to the experiments, mice were cohoused during a 2-week period to acclimate to the facilities as well as a establish a baseline microbiota. All CB1KO, CB2KO, and CNRO mice were bread in-house, as describe previously[86]. All experiments were conducted in accordance with NIH guidelines. All protocols involving vertebrate animals were approved by the University of South Carolina Institutional Animal Care and Use Committee.

3.3.3 EAE INDUCTION AND CBD TREATMENT

Chronic progressive EAE was induced in C57BL/6 mice according to previously published protocols[5,152–154]. Briefly, on day 0 mice were given 150µg of MOG35-55 and 600mg H37Ra suspended within an emulsion of sterile PBS and Freund's adjuvant via 2 subcutaneous injections. This immunization was followed up by intra-peritoneal injections of PTX suspended within sterile PBS on day 0 (200ng) and day 2 (400ng). For

CBD treatment, EAE mice were randomly divided into groups receiving either CBD or vehicle gavages daily. The CBD group received a 200µl oral gavage composed of 20mg/kg of CBD suspended with 89.9% PBS, 10% ethanol and 0.1% Tween 80 daily, for 17 days. Control mice received vehicle treatments consisting of 200ul of 89.9% PBS, 10% ethanol and 0.1% Tween 80 via oral gavage daily. Mice were monitored, weighed, and scored for the onset of clinical symptoms associated with EAE severity daily.

3.3.4 EAE SCORING

The measurement for paralysis symptoms and EAE clinical scores were recorded as following according to previous studies[155]: 0 = no symptoms, 1 = inability to curl the distal portion of the tail, 2 = complete tail atony/impaired movement, 3 = partial hind/fore limb paralysis, 4 = complete hind limb paralysis, 5 = tetraplegia/moribund state.

3.3.5 FLOW CYTOMETRY

Spleens, whole CNS, and MLNs were isolated from mice for flow cytometry analysis of immune cells present. Whole spleens and MLNs were manually dissociated, incubated at room temp with RBC lysis buffer and filtered (70µm) to produce single cell suspension. CNS tissue was manually dissociated and washed twice in 30% percoll to remove excess myelin. Single cell suspensions were tagged with fluorescently labeled monoclonal antibodies (mAbs) purchased from Biolegend (APC labeled anti-CD45, PE labeled anti-CD45, BV421 labeled anti-MHCII, AF647 labeled anti-CD11b, FITC labeled anti-CD11b, AF700 labeled anti-CX3CR1, FITC labeled anti-CD45, BV510 labeled anti-Ly6C, V450 labeled anti-Ly6G, PerCP Cy5 labeled anti-CD3, BV786 labeled anti-CD4, BV421 labeled anti-Foxp3, PE labeled anti-RORγT). Flow cytometry of fluorescent-labeled mAb tagged samples was conducted using a BD FACs Celesta

flow cytometer. Analysis of FCS files was conducted using FlowJo software purchased from BD Biosciences (San Jose, CA).

3.3.6 PHYLOGENETIC CHARACTERIZATION OF BACTERIAL SPECIES BY 16S RDNA SEQUENCING

Microbiota analysis was conducted using 16s rDNA sequencing of the V3 and V4 region of rDNA isolated from cecal and stool contents of EAE mice belonging to vehicle and CBD-treated groups. Briefly, mice were cohoused for 2 weeks prior to EAE induction and randomly divided into groups that would receive either vehicle or CBD treatments daily. DNA was isolated from stool content collected on day 0 and cecal content collected on day 17 by using the QIAamp Stool Mini Kit according to manufacturer's instructions. Sequencing of samples was performed using the Illumina MiSeq platform. OTU tables were generated from fastq. files derived from the sequencing run by the Nephele pipeline provided by the National Institute of Allergy and Infectious Diseases[156,157]. OTU tables were formatted and analyzing in R Studio using the phyloseq, ape and ggplot2 packages[158–161].

3.3.7 PE SELECTION FOR ISOLATION OF F4/80+ AND CD326+ CELLS

Positive selection using PE conjugated anti-F4/80 and PE conjugated anti-CD326 was used to isolate and enrich for myeloid cells and intestinal epithelial cells (IECs) respectively. Briefly, single cell suspensions from the CNS tissue and intestinal tract were Fc Receptor blocked, and then stained for their respective differentiation marker. EasySep™ PE selection cocktail followed by EasySep™ magnetic nanoparticles were added to the cell suspensions. The cell suspensions were brought up to an appropriate volume of 2.5mLs and placed within an EasySep™ magnet for retention. This step was

repeated 4 times to ensure that primarily PE-tagged cells were retained. The remaining cell pellet was suspended in QIAzol™ lysis reagent for downstream RNA quantification.

3.3.8 ARRAY BASED QUANTIFICATION OF MRNA PRODUCTION WITHIN INTESTINAL EPITHELIAL CELLS

Transcriptomic analysis was conducted on RNA isolated from IECs from VEH and CBD-treated EAE mice according to the GeneChip™ WT Pico Reagent Kit. Briefly, cDNA with a specified adaptor sequence was produced from whole mRNA content of CD326 positive cells. cDNA was purified prior to in-vitro transcription to produce labeled cRNA. Twenty ng of cRNA was used for production of ss-cDNA. After production, ss-cDNA was isolated, fragmented, labeled, and hybridized to a mouse-specific Clariom™ D assay. Hybridized Clariom™ D assay chips were washed in accordance with manufacturer's recommended fluidics protocol FS450_0001 using GeneChip™ Fluidics Station 450. After completion of the fluidics protocol, the assay chips were analyzed using a GeneChip™ Scanner. Downstream transcriptomic analysis was conducted using Applied Biosystems™ Transcriptomic Analysis Console version 4.0.

3.3.9 SINGLE CELL RNA SEQUENCING OF CNS TISSUE

scRNA Seq was conducted as described previously[87], using the 10X Genomics Chromium Controller Instrument and Chromium single cell 5' library & gel bead kit according to manufacturer's instructions. Briefly, 3000 cells (>90% viability) were loaded onto the controller to generate single-cell gel bead emulsions. After cell-lysis, cDNA was generated via barcoded reverse transcription. cDNA was then amplified, fragmented, and indexed prior to being sequenced on the NextSeq 550. Cell Ranger

version 3.1.0 (10x Genomics) was used to process raw sequencing data. Seurat Suite version 3.0 was used to perform downstream analysis of the Cell Ranger outputs[162,163]. The data files of reads from CBD-treated and VEH-treated EAE mice were integrated within Seurat using anchor and integration function. Scaling and PCA was conducted on integrated data. Clusters were identified following PCA analysis with a granularity resolution of 0.15.

3.3.10 EX-VIVO TREATMENT OF BONE MARROW DERIVED MACROPHAGES

BMDMs were generated from the bone marrow cells isolated from the tibia and femur of 6-week-old naïve female WT, CB1KO, CB2KO, and CNRO mice. Cells after isolation were cultured in complete DMEM/F12 medium containing 10% FBS, 1% penicillin/streptomycin, 2mM L glutamine and 1U/ml of M-CSF for 7 days as previously described[164]. After 7 days, the BMDMs were activated with LPS at a concentration of 100ng/ml for 24 hours in DMEM/F12 supplemented with 10µg/mL CBD for experimental treatment groups. In studies aimed at blocking PPARγ, cells were incubated with 25µM T007, a concentration previously established to demonstrate the effects of PPARγ antagonism[165]. Cells were incubated with T007 for a period of 2 hours prior to incubation with CBD and LPS.

3.3.11 REAL-TIME QUANTITATIVE PCR FOR VALIDATION OF GENE EXPRESSION

qPCR was performed to determine the expression of genes of interest on cDNA synthesized from RNA isolated from whole tissue, bone marrow derived macrophages, and lymphocytes/myeloid cells. cDNA was synthesized according to manufacturer protocol for the generation of messenger RNA using the miScript II RT Kit supplied by

Qiagen (Germantown, MD). qPCR was conducted using the SSO Advanced qPCR master mix according to manufacturer's protocol supplied by Bio-Rad. Fold changes for mRNA expression were collected using the $^{\Delta\Delta}$Ct method, where Ct is the threshold cycle to detect fluorescence. qPCR was used to detect the expression levels of IL-1β relative to GAPDH. A detailed list of primer sequences can be found in Table 3.1.

3.3.12 FLUORESCENT MICROSCOPY

For conducting fluorescent microscopy, mice were euthanized with isoflurane and subsequently perfused with 10mL of heparinized PBS followed by 10mL of 10% formalin. Whole brains were isolated and embedded in paraffin blocks before being cut into 7µm sections placed on glass slides. Slides were then deparaffinized by being completely submerging into the following solutions in the listed order: Xylene for 6 minutes, 1:1 xylene and ethanol for 3 minutes, ethanol for 6 minutes, 95% ethanol for 3 minutes, 70% ethanol for 3 minutes, 50% ethanol for 3 minutes, and lastly held in tap water. Slides were then incubated with a blocking solution of filtered PBS with 1% BSA w/v for 10 minutes. Slides were then incubated with a primary FITC-conjugated antibody suspended in blocking solution at a concentration of 2.5µg/mL for 1 hour in the dark. Slides were then washed three times for 1 minute in PBS to remove excess antibody. Slides were then incubated with Texas Red-conjugated phalloidin antibodies at a concentration of 165nM in blocking solution for 20 minutes in the dark. Slides were then washed three times for 1 minute in PBS to remove excess phalloidin. The slides were then incubated with DAPI dye diluted to a final concentration of 200nM in PBS for 5 minutes in the dark. After incubation, the slides were washed 3 times for 1 minute in PBS to remove excess DAPI. The slides were then mounted using a toluene based medium

and sealed prior to being visualized on LAS X version 3.4.2.18368 software on a Leica DM 2500 instrument.

3.3.13 ENDOCYTOSIS ASSAY

Endocytosis was measured via the uptake of pHrodo™ greed dextran by macrophages isolated from the peritoneal cavity of naïve WT mice. Briefly, the mononuclear cells isolated from the peritoneal wash of naïve WT mice was plated in complete DMEM/F12 at 1 million cells/mL in the presence of DMSO, CBD (10µg/mL), and/or T007 (25µM) for 2 hours at 37 degrees Celsius. Cells were pelleted, washed in sterile PBS, and Fc blocked in sterile PBS for 15 minutes at room temperature. Cells were then pelleted and resuspended in a solution containing 20µg/mL pHrodo™ green dextran, BV605 conjugated anti-CD45, AF647 conjugated anti-CD11b, and PE conjugated anti-F4/80 for 10 minutes at room temperature. Cells were then pelleted, washed in PBS, and ran on the FACSCelesta flow machine. Endocytosis activity was measured as the mean fluorescent intensity of FITC amongst CD11b+CD45+F4/80+ cells.

3.3.14 STATISTICAL ANALYSIS

All data are presented as the mean ± standard error of the mean. The number of biological replicates per experiment are identified in the figure legends. Statistical analysis of changes in paralysis symptoms and weight over time were calculated using unpaired t tests at each time point with values corrected for a desired FDR of 1% using a Benjamini, Krieger, and Yekutieli test. Statistical analysis of experiments with multiple variables was conducted using a 2-way ANOVA tests to determine significant interactions. Post hoc analysis to determine the degree of significance was conducted

using Bonferroni's test. All statistical analysis was conducted by using unpaired t tests to compare 2 groups differing by one variable. Degree of significance was demonstrated using the following key: *p < 0.05, **p < 0.01, ***p < 0.001, ****p<0.0001.

3.4 RESULTS

3.4.1 CBD AMELIORATES EAE SYMPTOMOLOGY

Previous studies have shown that CBD and a variety of other phytocannabinoids possess potent anti-inflammatory properties that are capable of ameliorating symptoms in neuroinflammatory disorders[83,152,166–168]. To better understand the processes by which treatment with CBD regulates anti-inflammatory neuroprotection during encephalitis, we first confirmed that oral administration of CBD at a concentration of 20mg/kg results in a significant amelioration of paralysis-associated EAE symptoms (Figure 3.1A-B). Concurrent with the reduction in paralysis symptoms observed in the CBD treated group was a resistance to neuroinflammation-associated atrophy observed from day 11 onward (Figure 3.1C-D).

3.4.2 CBD TREATMENT RESULTS IN AN ANTI-INFLAMMATORY SHIFT IN THE TRANSCRIPTIONAL PROFILE OF INFILTRATING MACROPHAGES AND RESIDENT MICROGLIA WITHIN THE CNS

To better define how CBD accomplishes neuroprotective effects that combat autoimmune encephalomyelitis, scRNA Seq was conducted on a single cell suspension isolated from whole CNS tissue. Overlaying tSNE plots demonstrated transcriptional diversity between EAE mice treated with CBD or the Vehicle (Figure 3.2A). Clustering of sequenced cells was performed using Seurat package, which identified 8 unique clusters[162] (Figure 3.2B). CD11b expression signified that the identified clusters 0-1 and

3-5 belonged to a myeloid lineage (Figure 3.2C). Ly6G expression further signified cluster 1 to be either PMN MDSCs or neutrophils dependent on the relative expression of Ly6C2 per cell (Figure 3.2D). Ly6c2 (Figure 3.2E) and CCR2 (Figure 3.2F) expression further identified clusters 0 as being infiltrating inflammatory macrophages. CXCL9 (Figure 3.2G), CXCL10 (Figure 3.2H), and IL-1β (Figure 3.2I) expression revealed a distinct pro-inflammatory cytokine expression amongst the resident and infiltrating myeloid cells of the CNS of vehicle-treated mice when compared to CBD-treated group. Gsdmd expression revealed an increased expression of the inflammatory pyroptosis-initiator within the infiltrating myeloid cells of cluster 0, 4 and 5 (Figure 3.2J). CD40 expression signified that clusters 0, 3 and 4 within the vehicle group, shown to be Ly6C and CD11b+, were actively participating in antigen presentation, while cluster 7 within the treatment group was the only cluster participating in antigen presentation (Figure 3.2K). Expression of STAT1 amongst the clusters demonstrated that CBD treatment globally inhibited STAT1 activity amongst all cell types present in the CNS (Figure 3.2L), while demonstrating modest changes in STAT2 (Figure 3.2M) and STAT3 (Figure 3.2N). Collectively, these data demonstrated that CBD treatment limits immune cell infiltration and activity within the CNS of EAE mice, potentially through inhibited transcription of STAT1 and a variety of soluble mediators such as CXCL9, CXCL10, and IL-1β. The suppressed expression of these pro-inflammatory soluble mediators in the CBD group correlated with the observed attenuation of pro-inflammatory macrophage infiltration as signified by cluster 0, when compared to the vehicle group.

3.4.3 CBD TREATMENT INHIBITS MACROPHAGE DERIVED PRODUCTION OF IL-1B UNDER INFLAMMATORY CONDITIONS

To better define how CBD limits macrophage-mediated inflammation, we further investigated the effects of CBD on IL-1β production by inflammatory macrophages. First, we quantified the expression of IL-1β within cells enriched for F4/80 positivity via PE selection from the mononuclear cell fraction of CNS tissue from EAE mice. Quantified gene expression revealed that the F4/80+ cells from the CNS of CBD-treated EAE mice demonstrated a significant reduction in IL-1β expression when compared to vehicle- treated EAE mice (Figure 3.3A). To test if CBD directly inhibits the expression of IL-1β by macrophages under inflammatory conditions, we cultured BMDMs from naïve wild-type mice and stimulated them in the presence of LPS. IL-1β expression across these samples, as detected by qPCR, demonstrated that CBD treated BMDMs under LPS stimulating conditions contained an 85-fold reduction in IL-1β expression (Figure 3.3B). To ensure that this change in expression was represented by a change in IL-1β excretion, ELISA quantification of IL-1β present within supernatants from these cultures was conducted. These data revealed that LPS-stimulated samples contained high levels of soluble IL-1β, while all other samples, including the CBD-treated samples stimulated with LPS, had no detectable levels of IL-1β in the supernatant (Figure 3.3C). Next, we used scatter plots to demonstrate which immunologically relevant markers are demonstrating the largest reduction in IL-1β expression in the scRNA Seq data from the CNS tissue of EAE mice treated with CBD. Amongst CD45+ cells present in the CNS of EAE mice treated with CBD (green) compared to vehicle (pink), there was a reduction of IL-1β expression (Figure 3.3D), however there was a more drastic reduction in IL-1β

expression in the CCR2+ cells infiltrating the CNS (Figure 3.4E). Inasmuch as IL-1β has been demonstrated to be produced by as well as grant access to $CCR2^{high}$ infiltrates that drive neuroinflammation in EAE via a positive feedback loop, we used immunofluorescence to visualize CCR2 positive cells present within the CNS of vehicle- and CBD-treated mice [169]. Representative immunofluorescent images demonstrated that the CNS of vehicle treated EAE mice has sizable infiltration of CCR2+ cells that were absent in the CNS of CBD treated EAE mice (Figure 3.3F).

3.4.4 CBD REDUCES IL-1B EXPRESSION IN LPS-STIMULATED BMDMS INDEPENDENT OF CLASSICAL CANNABINOID RECEPTORS

To discern how CBD treatment was suppressing the production of the pro-inflammatory cytokine IL-1β, we investigated the likely receptors which were propagating this anti-inflammatory effect. Intuitively, we first investigated the potential roles of the classical cannabinoid receptors CB1 and CB2 by use of BMDMs derived from CB1KO, CB2KO and CNRO donor mice. Analysis of gene expression demonstrated that LPS-stimulated macrophages derived from CB1KO (Figure 3.4A), CB2KO (Figure 3.4B), and CNRO (Figure 3.4C) mice demonstrated a significant reduction in IL-1β production in the presence of CBD. These results demonstrated that CBD treatment of inflammatory macrophages results in a suppression of IL-1β production independent of the classical cannabinoid receptors. Next, to explore the role of PPARγ, we treated these WT BMDMs with the PPARγ antagonist T007 prior to incubation with CBD. Surprisingly, addition of PPARγ antagonist caused a significant reduction in IL-1β expression by BMDM cells stimulated with LPS that resembled the levels of suppression caused by CBD (Figure 3.4D). ELISA quantification of excreted

IL-1β from these samples also demonstrated that T007 treatment caused significant inhibition like CBD (Figure 3.4E). To ascertain if PPARγ antagonism is the primary manner by which CBD inhibits pro-inflammatory macrophage activity, we investigated the effects of T007 and CBD in combination on endocytosis of pHrodo^{TM} green dextran labeled beads by peritoneal macrophages isolated from naïve mice (3.9A-B). T007 treatment in vitro resulted in no changes in endocytosis activity, while CBD treatment significantly reduced endocytosis activity independent of PPARγ (Figure 3.4F). These data suggested that endocytosis function of macrophages that was reduced following CBD treatment was independent of PPARγ.

3.4.5 ORAL TREATMENT WITH CBD ALLEVIATES INFLAMMATION VIA THE PROMOTION OF MDSCS AND LIMITATION OF NEUTROPHILS IN A TISSUE SITE-SPECIFIC MANNER

Previous research has shown that CBD treatment in an inflamed state induces an expansion of immunosuppressive MDSCs [170], however, their presence in the secondary lymphoid organs has not been previously defined. Thus, when we tested the spleens for monocytic MDSCs with the phenotype of CD45+CD11b+Ly6C+Ly6G- (gating shown in (Figure 3.8A), we found that the percentage of this population was significantly increased in CBD group when compared to Vehicle controls (Figure 3.5A). Within the spleen, there were no further changes in the PMN MDSCs (Figure 3.5B) or neutrophils (Figure 3.5C). Representative flow plots demonstrating MDSC expansion in the splenic tissue of CBD treated EAE mice compared to Vehicle treated (Figure 3.5D). Within the inflamed CNS of EAE mice, CBD treatment caused no significant changes in the monocytic MDSCs (Figure 3.5E) or neutrophils (Figure 3.5G) but did result in an increase in the PMN

MDSCs having the phenotype CD45+CD11b+Ly6C+Ly6G+ (Figure 3.5F and Figure 3.8B). Representative flow plots demonstrating MDSC expansion in the CNS tissue of CBD treated EAE mice compared to Vehicle treated (Figure 3.5H). To better define how CBD may be suppressing the immune response against MOG peripherally, and because EAE is also regulated by the intestinal microbiota and inflammation [17,54,171,172] we analyzed the cellular composition of the MLNs which drain the intestinal tract. Within the MLNs of EAE mice, CBD treatment resulted in no significant changes in the monocytic MDSCs (Figure 3.5I) or PMN MDSCs (Figure 3.5J) but did result in a decrease in the percentage of neutrophils (Figure 3.5K) possessing the phenotype of CD45+CD11b+Ly6C-Ly6G+ (Figure 3.5L and Figure 3.8C). Collectively, these data demonstrate that CBD does increase MDSC subsets both in the periphery and in the CNS of EAE mice, while simultaneously limiting neutrophil abundance in the intestinal tract.

3.4.6 ORAL TREATMENT WITH CBD ALLEVIATES INTESTINAL INFLAMMATION VIA INHIBITION OF GSDM PRODUCTION WITHIN THE INTESTINAL TRACT OF EAE MICE

In order to better understand how CBD regulates intestinal immunity by suppressing neutrophil abundance in the MLN and define any potential effects on limiting autoimmune neuroinflammation, we analyzed transcriptomic changes observed in the IECs that encompass the barrier between the GI microbiota and host. Array based transcriptomic analysis of purified IECs isolated from the colonic epithelium revealed significant changes in the expression of 390 coding genes with as denoted by a fold change of >2 (Figure 3.6A) and $p<0.05$ (Figure 3.6B) when compared between the vehicle and CBD-treated EAE mice. PCA analysis revealed that the transcriptomic

profiles of the IECs displayed proximity between the CBD-treated samples that was functionally different from the vehicle-treated groups (Figure 3.6C). Heat maps were utilized to visualize the significantly regulated genes between the IECs of the vehicle treated and CBD treated mice groups (Figure 3.6D). The top 3 downregulated genes by fold change in the intestinal epithelium of CBD-treated mice, when compared to vehicle-treated mice, were all isoforms of the pyroptosis initiating gsdmc gene (Figure 3.6E). Examination of H&E-stained sections of the proximal colon revealed that the CBD-treated EAE mice had fewer infiltrating cells in the underlying colonic tissue in comparison to the vehicle-treated EAE mice (Figure 3.6F).

3.4.7 EFFECT OF CBD ON GUT MICROBIOTA

Because the cross-talk between neuronal inflammation in EAE and gut microbiota being increasingly appreciated as a major factor that regulates neuroinflammation severity [173,174], we tested if the oral administration of CBD had an impact on the composition of the gut microbiota in a murine model of experimental MS. 16s sequencing and subsequent analysis with Phyloseq software packages in R Studio demonstrated that oral administration of CBD at 20mg/kg to EAE mice resulted in no significant changes to the cecal microbiota when compared to that of the vehicle-treated EAE mice. To confirm these results, 16s sequencing was performed on material isolated from fecal contents of previously cohoused mice on day 0 (n=10 per group) and on the cecal contents taken at time of sacrifice on day 17(n=10 per group). Metrics measuring alpha diversity, such as Chao1 index (Figure 3.7A) and Shannon index (Figure 3.7B), demonstrated no discernable changes in the microbiota composition across groups at either timepoint. Next, we studied beta diversity by use of PCA plots which demonstrate

that the fecal content prior to disease induction, as well as the cecal content after sacrifice between vehicle-treated and CBD-treated EAE mice, showed no separation between the vehicle- and CBD-treated groups when analyzed at either timepoint (Figure 3.7C). Further investigation into the specific reads as demonstrated by stacked bar charts illustrating the phyla (Figure 3.7D), classes (Figure 3.7E), orders (Figure 3.7F), and families (Figure 3.7G) identified by 16s sequencing confirmed that there were no significant changes in bacterial composition between the genera at either time point. To discern if there was any potential change in bacterial metabolism affecting host immunity following CBD treatment, we analyzed the concentration of the well-defined anti-inflammatory metabolites namely the short chain fatty acids (SCFAs) within the cecal contents via mass spectrometry (n=10 per group). These data revealed that there were no significant changes in any of the detectable SCFAs between vehicle vs CBD treated mice (Figure 3.7H). These results collectively suggested that the anti-inflammatory effects of CBD on neuroinflammation and intestinal inflammation during EAE were not directly related to changes in the microbiota composition.

3.5 DISCUSSION

MS is a debilitating autoimmune disorder in which afflicted patients suffer chronic encephalomyelitis that manifests in symptoms of atrophy, discomfort and paralysis[93]. Current complications surrounding MS treatment include: complications arising from primary treatments, exorbitant treatment costs, lapses in medication, inefficient pharmaceuticals, and a complex etiology that makes early detection for proactive interventions associated with a beneficial prognosis incredibly difficult to accomplish[175–177]. MS pathology is exasperated by an inadvertent recognition of antigenic

peptides within the myelin sheath by encephalitogenic T cells that directly and indirectly drive inflammatory degradation of CNS tissue[178,179]. This antigen recognition triggers a variety of diverse inflammatory cascades that incorporate aspects of both adaptive and innate immunity; this underlying immunological diversity and variability that drives encephalomyelitis makes effective treatment of MS difficult to accomplish in the clinical setting. This multifactorial immunological diversity within encephalitic tissue is further contributed to by resident glia cells, recruited myeloid cells, and recruited lymphocytes all synergistically driving neuroinflammation[179–181]. Despite all the seemingly insurmountable barriers posed by such a convoluted and complex etiology driving disease progression, treatments that sway the balance of power in host immunity from a pro-inflammatory landscape towards an anti-inflammatory regulatory immune cell-dominated landscape, such as that associated with MDSC and Treg induced by cannabinoids, may provide novel therapeutic modalities[147].

The cannabinoid system has previously been established as an attractive candidate for the treatment of neurological and inflammatory disorders alike due to the safety of consumption, potent immunosuppressive potential, and low production costs of phytocannabinoids[182,183]. Our study demonstrates that treatment of EAE mice with the phytocannabinoids CBD results in potent anti-inflammatory effects within the CNS and GI tract of mice suffering from EAE, further validating the potential of CBD as a treatment of MS[80,170]. In the current study, we further defined the potential of CBD treatment on myeloid cell activity by use of scRNA seq on mononuclear cells isolated from the CNS tissue collected from EAE mice. Broadly, the results of this sequencing demonstrated that CBD reduces the abundance of infiltrating macrophages and inhibits

the production of CXCL9, CXCL10 and IL-1β by macrophages, monocytes, and resident microglia. ScRNA seq further revealed that CBD treatment resulted in a dramatic reduction in the total number of infiltrating macrophages while promoting microglia to adopt a less inflammatory transcription profile with decreased CXCL10 or IL-1β expression. Despite this specific change in the transcription profile, flow cytometric analysis revealed that there were insignificant changes in the proportion and total number of activated microglia, as denoted by a CD11b+CD45^{high}MHCII+CX3CR1+ phenotype (Figure 3.10A-D). Collectively, these results demonstrated that CBD limits macrophage infiltration into the CNS and inhibits the expression of IL-1β, CXCL9, and CXCL10 within the microglia and macrophage populations. This in-depth analysis technique was able to provide expansive results that demonstrated on a single-cellular level what is occurring in the CNS when CBD is consumed orally during encephalitogenic conditions. Our novel insights into how CBD alleviates neuroinflammation in a cell-specific manner at the site of inflammation in a murine model of experimental MS gives an unprecedented and timely insight into the mechanisms by which cannabinoids regulate myeloid-derived immune cell function and subsequently suppress the production of soluble mediators that contribute to the pathogenic autoimmune neuroinflammation.

Next, we tested the direct effects of CBD on IL-1β production by inflammatory macrophages. We tested this in vitro by use of BMDM cultures stimulated with LPS in the presence and absence of CBD. Our results demonstrated that supplementation of media with CBD resulted in ablated expression and excretion of IL-1β by BMDMs stimulated with LPS, while having no noticeable effect on unstimulated BMDMs, strengthening the hypothesis that CBD inhibits IL-1β production in activated

macrophages. Because IL-1β driven neuroinflammation has previously been shown to depend on the recruitment of bone marrow derived CCR2+ infiltrates[184], we used immunofluorescent imaging to test this possibility and found that CBD treatment resulted in the reduction of CCR2+ cells highlighted with a GFP- conjugated anti-CCR2 antibody. Collectively, these results demonstrated that CBD may attenuate IL-1β induction thereby preventing the recruitment of CCR2+ immune cells during EAE.

In the current study, in addition to the effect of CBD on inflammatory macrophages, we also tested the effect of CBD on MDSC abundance. CBD treatment resulted in an induction of monocytic MDSCs and PMN MDSCs in the spleen and CNS, respectively. Monocytic MDSCs possess previously defined immunosuppressive functions, primarily by inhibiting effector T cell function through the excretion of nitric oxide, in inflammatory disorders that include EAE[185,186]. PMN MDSCs however accomplish their immunosuppressive functions primarily via the inhibition of auto-antigen priming for presentation to encephalitogenic Th lymphocytes in EAE[186,187]. These results confirm previous studies which demonstrated that CBD treatment induces MDSCs in EAE [166], while further defining the phenotype of MDSCs induced in a site-specific manner. These data contribute to the literature established by previous studies which demonstrate the ability of CBD to directly induce anti-inflammatory MDSCs to alleviate inflammation-dependent symptomology and simultaneously promote immunotolerance in models of experimental autoimmunity [170,188].

While CBD is known not to directly activate CB1 or CB2 cannabinoid receptors, some studies have indicated that CBD may increase the levels of endocannabinoids such as anandamide[189], thereby activating CB receptors. To test this possibility, we isolated

BMDMs from CB1KO mice, CB2KO mice, and CNRO mice and activated them with LPS in the presence of CBD. Our data shows that BMDMs derived from classical cannabinoid receptor knockouts still demonstrate a significant reduction in IL-1β expression when stimulated LPS in the presence of CBD. These findings suggest that the inhibition of IL-1β expression by CBD occurs in a manner independent of the classical cannabinoid receptors CB1 and CB2.

Previous studies have shown that CBD may activate PPARγ, which in turn leads to suppression of inflammation[190–192]. To determine if PPARγ binding is required for CBD to inhibit IL-1β production in macrophages, we inhibited PPARγ activation by supplementation of the cell culture media with T007 prior to treatment with CBD. In these experiments, addition of T007 alone to antagonize PPARγ in LPS stimulated cultures caused a significant decrease in IL-1β production and moreover, combination of CBD and PPARγ inhibitor failed to have an additive or inhibitory effect when compared to T007 or CBD alone. While these data showed that CBD acted like T007, the precise role of PPARγ in the regulation of LPS-mediated IL-1β production by CBD is unclear. While the primary role of PPARγ in regulating inflammatory processes has been shown to be dependent on agonistic ligands perpetuating anti-inflammatory effects via activation of this receptor, a previous study has demonstrated that antagonism can also promote macrophages to develop an immunotolerant phenotype[193]. It has also been shown that PPARγ knockout macrophages, when stimulated with LPS, initially show a significant reduction in IL-1β production early on at 3 hours of culturing, followed by a significant increase in IL-1β expression at the 24 hour mark[194]. Thus, PPARγ may function both to suppress and enhance expression of the inflammatory cytokine IL-1β in a case and time-

dependent manner. Additionally, we tested if other anti-inflammatory effects of CBD on macrophages, such as the suppression of endocytosis, can potentially be attributed to the inhibition of PPARγ. To test this, we measured endocytosis of pHrodo^{TM} green dextran beads by CBD-treated peritoneal macrophages in the presence or absence of T007. Our results demonstrated that CBD significantly reduced the endocytosis activity of peritoneal macrophages, while T007 had no effect on suppressing endocytosis or reversing the effects of CBD on endocytosis, thereby showing that the inhibition of endocytosis activity by CBD was independent of PPARγ.

To further study how CBD exerts potent immunosuppression under encephalitic conditions when supplied orally, we investigated any changes in the GI tract by focusing on the draining MLNs of the GI tract and the IECs lining the colonic epithelium. Flow cytometry revealed that the MLNs of CBD treated EAE mice show a decrease in the proportions of neutrophils when compared to the MLNs from vehicle treated EAE mice, with no changes in the anti-inflammatory MDSCs being observed. To dissect what was occurring in the intestinal lining to potentially contribute to this reduction of neutrophils, we conducted transcriptome arrays that quantified the abundance of mRNA transcripts within the RNA content isolated from IECs. This array-based analysis demonstrated that the 3 most highly regulated genes between the vehicle- and CBD-treated mice (GSDMC2, GSDMC3, and GSDMC4) belong to a family of pyroptosis initiators known to instigate inflammatory processes in a variety of myeloid cells, and in neutrophils[195,196]. To confirm that CBD treatment alleviated the low-grade inflammation observed within the GI tract of EAE mice, we next investigated the morphology of the colonic epithelium and underlying tissue with H&E histology. This histology demonstrated that the CBD

treatment group contained fewer cellular infiltrates, demonstrating an alleviation of the state of intestinal inflammation that resembles low-grade neutrophil-driven cryptitis as observed in the underlying colonic tissue of vehicle treated mice[197,198]. Collectively, these results demonstrated that orally administered CBD alleviates the systemic low-grade intestinal inflammation that occurs in models of autoimmune neuroinflammation by inhibiting neutrophil activity and regulating the expression of GSDMC within the epithelium of the intestinal lining[199–201]. The relevance of intestinal inflammation following cannabinoid treatment in EAE has already been demonstrated, as the anti-inflammatory properties of cannabinoids are at least partially dependent on the control of the gut-brain axis by regulating intestinal immunity and regulating microbial dysbiosis[152,172].

Previous studies have shown that gut microbiota composition and associated metabolome regulates the severity of EAE and associated neuroinflammation[54,100]. To that end, we tested if oral administration of CBD would alter the gut microbiota to create an anti-inflammatory effect stemming from the gut microbiota. Our results demonstrated that the GI contents of mice that were treated with oral CBD administration during the entirety of the EAE model displayed no significant changes in the alpha diversity, beta diversity or phylogeny of the detected bacterial species within the fecal contents prior to EAE induction or within the cecal contents at day 17 post-induction of EAE. Collectively, these results demonstrated that there were no significant changes in the bacterial composition of the EAE mice treated with CBD down to the genus level (Figure 3.7). Additionally, to detect if the reduction of neuroinflammation driven paralysis was potentially due to changes in the metabolomic profile of the GI microbiota we quantified

the concentrations of SCFAs within the cecal contents of EAE mice, which also demonstrated no significant changes between the vehicle treated and CBD treated group. Collectively, these results suggested that oral CBD treatment during EAE induces an anti-inflammatory state in the CNS and the gut, but this occurs independent of inducing changes in the GI microbiota composition.

Collectively, the study demonstrates that CBD treatment in a murine model of experimental MS results in a significant amelioration of paralysis symptoms accredited to a reduction in inflammation within the CNS, as well as systemically within the secondary lymphoid organs and GI tract. Mechanistically, CBD may limit excessive neuroinflammation by suppressing the pathogenic infiltration of macrophages and inhibiting the expression of pro-inflammatory chemo-attractants such as CXCL9, CXCL10 and IL-1β. This specified regulation of excessive inflammation was identified in key tissues such as the CNS, lymph nodes, spleen, and intestinal lining. In addition to affecting the inflammatory macrophages, oral administration of CBD was also able to induce MDSCs.

Table 3.1 ***List of Primers***

Gene name	**F Primer Sequence**	**R Primer Sequence**
IL-1β	TGGACCTTCCAGGATGAGGACA	GTTCATCTCGGAGCCTGTAGTG
GAPDH	TGATGGGTGTGAACCACGAG	CAGGGATGATGTTCTGGGCA
TNFα	CTGAACTTCGGGGTGATCGG	GGCTTGTCACTCGAATTTTGAGA
IL-6	CCAAGAGGTGAGTGCTTCCC	CTGTTGTTCAGACTCTCTCCCT
IL-10	GCTCTTACTGACTGGCATGAG	CGCAGCTCTAGGAGCATGTG
IL-13	CCTGGCTCTTGCTTGCCTT	GGTCTTGTGTGATGTTGCTCA

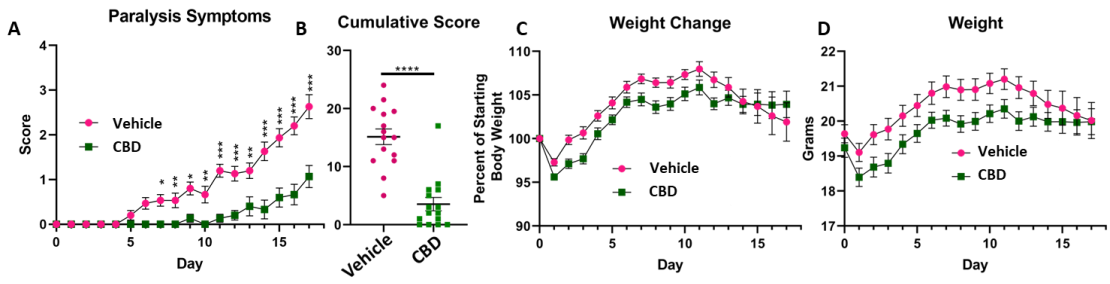

Figure 3.1 ***CBD Ameliorates EAE symptomology***. (**A**) Clinical scores, outlined in the Materials and Methods section, over time of EAE mice receiving either vehicle (n=15) or treatment (n=15) gavages containing 20mg/kg CBD (Multiple t tests performed to compare daily means across groups with a desired FDR of 1% via a Benjamini, Kieger, and Yekutieli test. Day 7 FDR-P=0.0016; Day 8 FDR-P=0.004; Day 9 FDR-P=0.003; Day 10 FDR-P=0.005; Day 14 FDR-P=0.007; Day 11, 12, 13, 15, 16, 17, and 18 FDR-P<0.001). (**B**) Composite score of paralysis symptoms per mouse (n=20. t(2)=6.548, P<0.0001) . (**C**) Change in body weight represented as a percentage of starting body weight. (**D**) Body weight over time.

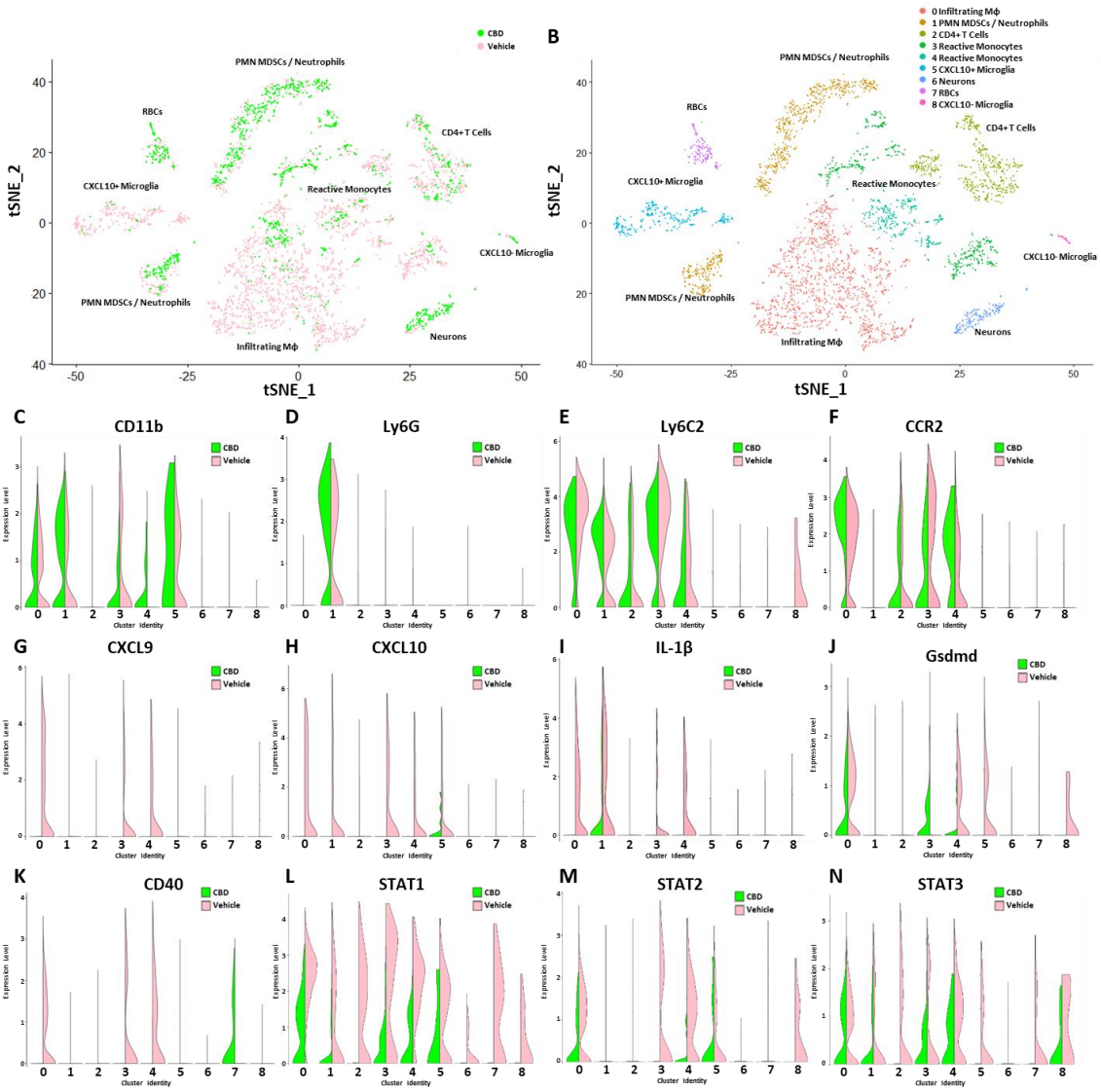

Figure 3.2 ***CBD treatment results in an anti-inflammatory shift in the transcriptional profile of infiltrating macrophages and resident microglia within the CNS*****.** (**A**) tSNE mapping of scRNA-seq reads from single cell suspensions of whole CNS tissue from vehicle (pink) and CBD (green) treated mice. Vehicle (3,011 Cells – 88,022,395 Reads – 29,233 Mean Reads per Cell) Treatment (1492 Cells – 103,253,015 Reads – 69,204 Mean Reads per Cell). (**B**) Clusters identified by Seurat based on a resolution of 0.15. Violin plots demonstrating relative expression levels of CD11b (**C**), Ly6G (**D**), Ly6C (**E**), CCR2 (**F**), CXCL9 (**G**), CXCL10 (**H**), IL-1β (**I**), GSDMD (**J**), CD40 (**K**), STAT1 (**L**), STAT2 (**M**), and STAT3 (**N**) amongst clusters identified by Seurat analysis of scRNA sequencing

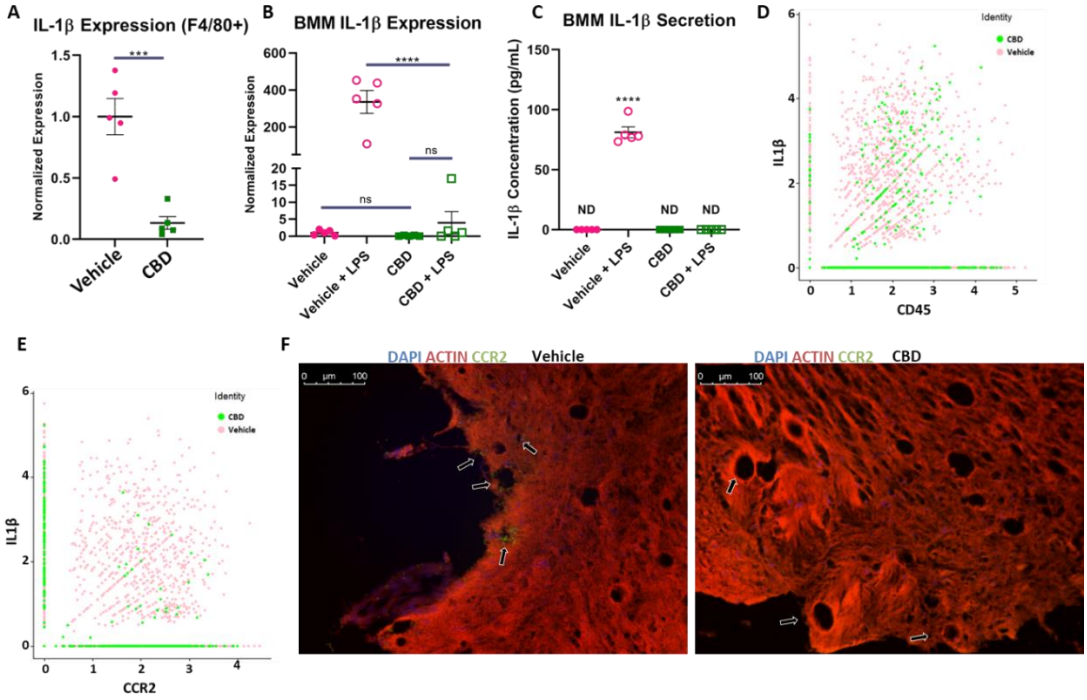

Figure 3.3. ***CBD treatment inhibits macrophage derived production of IL-1β under inflammatory conditions.*** (**A**) Expression of IL-1β is significantly reduced within in F4/80+ cells selected from the CNS of CBD treated mice in comparison with vehicle treated (n=5 per group, t(8)=5.512, P<0.001). (**B**) Bone marrow macrophages treated with CBD and stimulated with LPS displayed a significant decrease in IL-1β expression when compared to macrophages treated with DMSO and stimulated with LPS. Bone marrow macrophages treated with CBD and stimulated LPS show no significant change in the expression of IL-1β when compared to bone marrow macrophages treated with CBD alone (n=5, 2-Way ANOVA with Bonferroni's multiple comparisons test, F (1.000, 4.000) = 28.78. Vehicle + LPS vs CBD + LPS: p=0.0349). (**C**) Secreted IL-1β protein concentration in media collected from bone marrow macrophages treated with or without CBD under normal and LPS stimulated conditions (n=5, 2-Way ANOVA with Bonferroni's multiple comparisons test, Vehicle + LPS vs CBD + LPS: p<0001). (**D**) Scatter plot demonstrating co-expression of CD45 and IL-1β in CNS infiltrating cells as identified by scRNA Seq data. (**E**) Scatter plot demonstrating co-expression of CCR2 and IL-1β in CNS infiltrating cells as identified by scRNA Seq data. (**F**) Fluorescent microscopy shows CCR2 expression in 7µm sections of CNS tissue isolated from vehicle treated (left) and CBD treated (right) EAE mice.

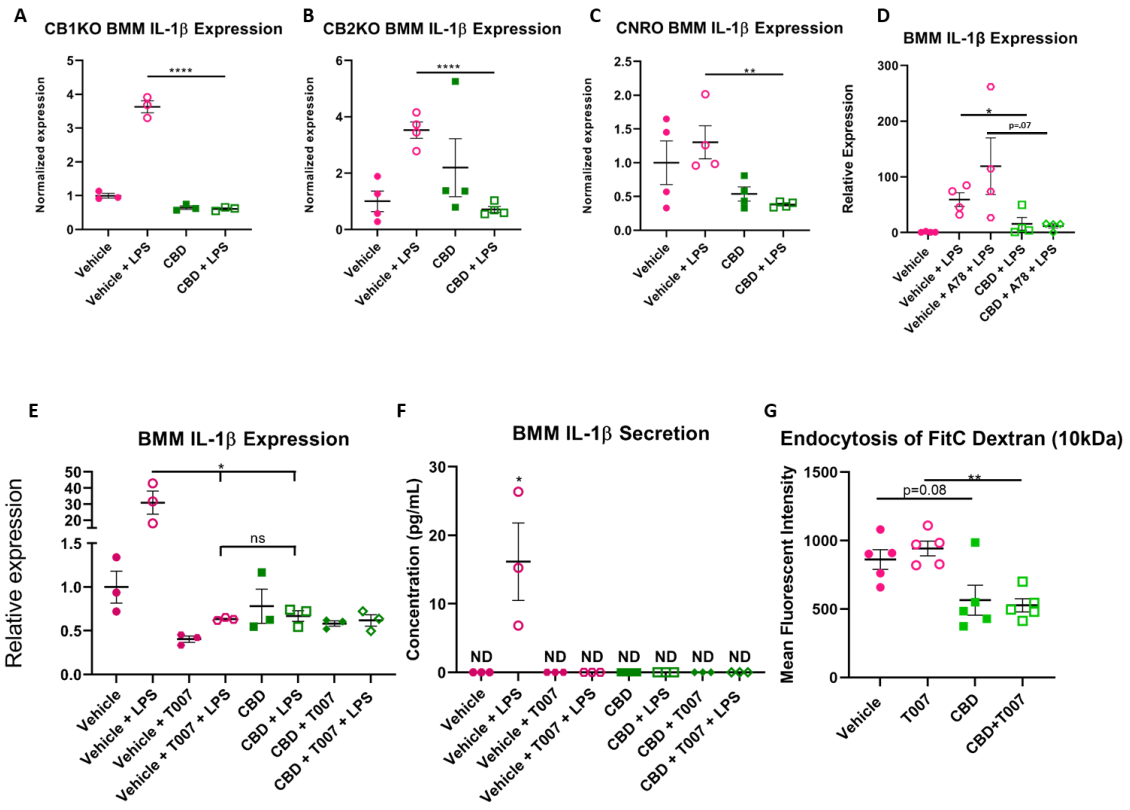

Figure 3.4 ***CBD reduces IL-1β expression in LPS-stimulated BMDMs independent of classical cannabinoid receptors*****.** (**A**) Bone marrow macrophages isolated from CB1KO mice treated with CBD and stimulated with LPS displayed a significant decrease in IL-1β expression when compared to macrophages treated with DMSO and stimulated with LPS (n=3, 2-Way ANOVA with Bonferroni's multiple comparisons test, F (1.000, 2.000) = 149.8; Post hoc: Vehicle + LPS vs CBD + LPS: p=0.0143). (**B**) Bone marrow macrophages isolated from CB2KO mice treated with CBD and stimulated with LPS displayed a significant decrease in IL-1β expression when compared to macrophages treated with DMSO and stimulated with LPS (n=4. 2-Way ANOVA with Bonferroni's multiple comparisons test, F (1.000, 3.000) = 14.03; Post hoc: Vehicle + LPS vs CBD + LPS: p=0.016). (**C**) Bone marrow macrophages isolated from CNRO mice treated with CBD and stimulated with LPS displayed a significant decrease in IL-1β expression when compared to macrophages treated with DMSO and stimulated with LPS (n=4. 2-Way ANOVA with Bonferroni's multiple comparisons test, F (1.000, 3.000) = 3.284; Post hoc: Vehicle + LPS vs CBD + LPS: p=0.22). (**D**) WT LPS stimulated BMDMs treated with PPARγ antagonist T007 (25μM) display decreased expression of IL-1β in a manner that is indistinguishable from CBD treatment. (n=3. 2-Way ANOVA with Bonferroni's multiple comparisons test, F (3, 6) = 17.25; Post Hoc: Vehicle + LPS vs T007 + LPS

p=0.0046, Vehicle + LPS vs CBD + LPS: p=0.0046). (**E**) WT LPS Stimulated BMDMs treated with PPARγ antagonist secrete no detectable levels of IL-1β (n=3. 2-Way ANOVA with Bonferroni's multiple comparisons test, F (3, 6) = 7.356; Post hoc: Vehicle + LPS p=0.036). (**F**) CBD significantly inhibits endocytosis activity in peritoneal macrophages while T007 has no effect (n=5. 2-Way ANOVA with Bonferroni's multiple comparisons test, F (1.000, 4.000) = 2.042; Post hoc Vehicle vs CBD p=0.0889; T007 vs CBD + T007 p=0.002).

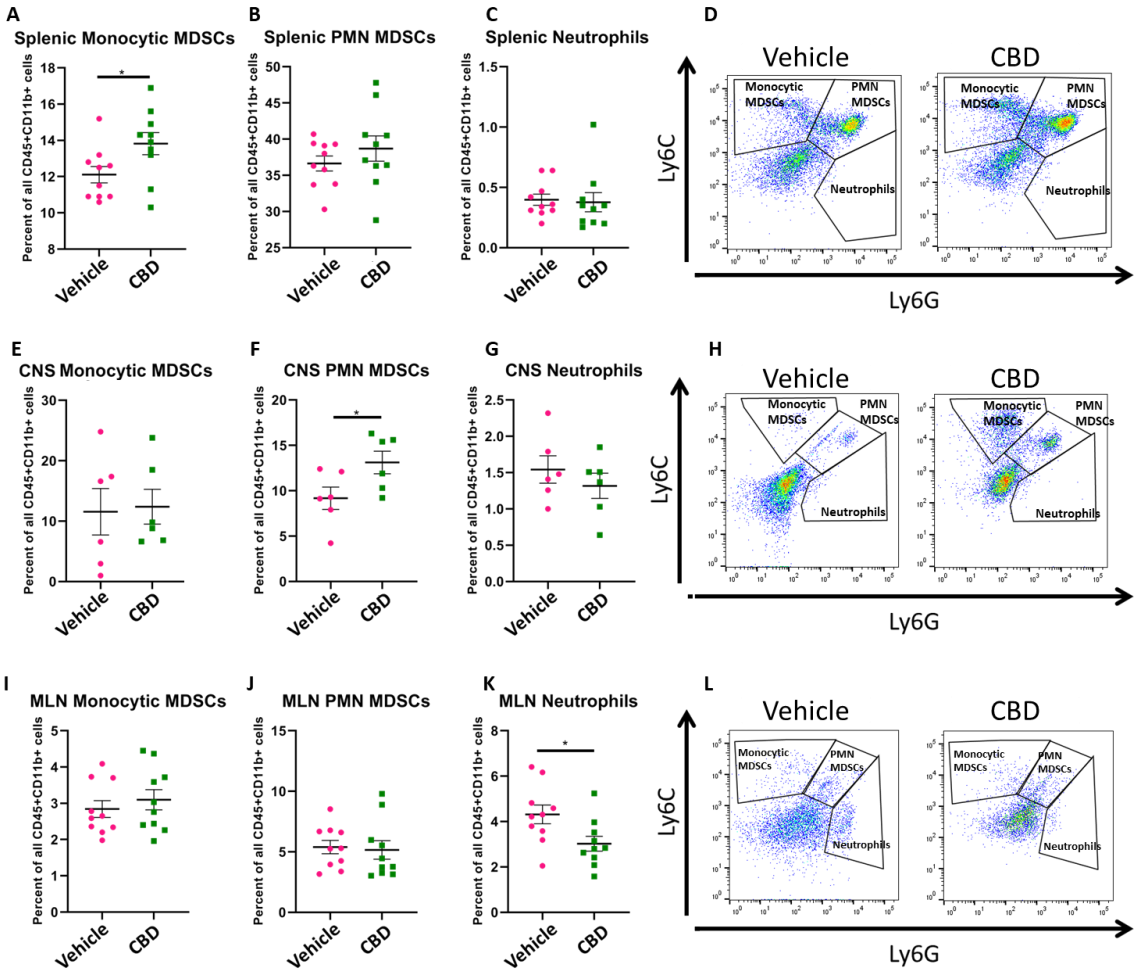

Figure 3.5 ***Oral Treatment with CBD Alleviates Inflammation via the Promotion of MDSCs and Limitation of Neutrophils in a Tissue Site-Specific Manner*****.** (A-C) Percentage of MDSCs and Neutrophils of all CD45+CD11b+ cells within the spleen in vehicle (n=10) vs treated (n=10) mice. (D) Representative flow plots for Figure 5A-C displaying Ly6C expression vs Ly6G expression on the vertical and horizontal axes, respectively (Figure 3.5A t(18)=2.246, P=0.037). (E-G) Percentage of MDSCs and Neutrophils of all CD45+CD11b+ cells within the CNS in vehicle (n=6) vs treated (n=6) mice (Figure 3.5F t(10)=2.259, P=0.047). (H) Representative flow plots for Figures 5E-G displaying Ly6C expression vs Ly6G expression on the vertical and horizontal axes, respectively. (I-K) Percentage of MDSCs and Neutrophils of all CD45+CD11b+ cells within the MLN in vehicle (n=10) vs treated (n=10) mice (Figure3.5K t(18)=2.249, P=0.02). (L) Representative flow plots for Figures 5I-K displaying Ly6C expression vs Ly6G expression on the vertical and horizontal axes, respectively.

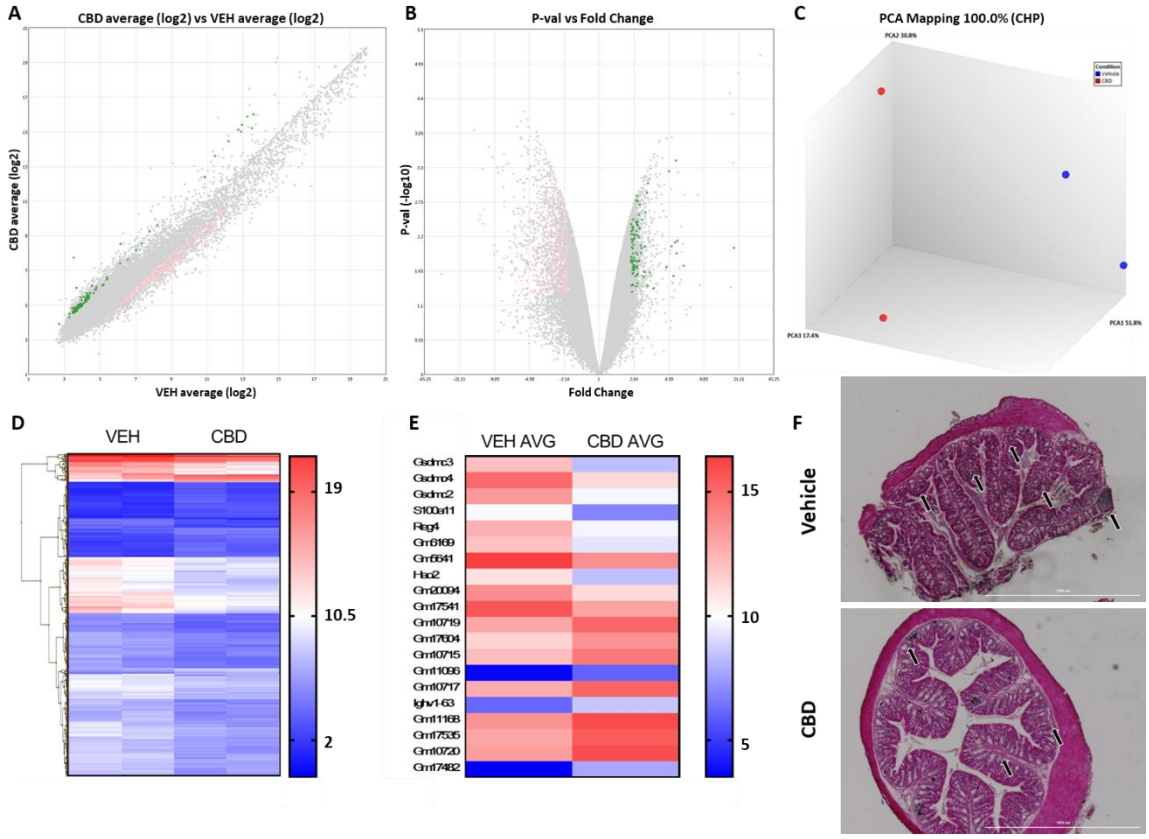

Figure 3.6 ***Oral Treatment with CBD alleviates intestinal inflammation via inhibition of GSDM production within the intestinal tract of EAE mice*****.** (A) log2 fold change between the mRNA content of IECs isolated from CBD vs VEH treated mice with coding genes significantly upregulated in the IECs of treatment mice (green) and vehicle mice (pink) highlighted (>=2 fold change; p<0.05). (B) lP-val vs fold change between the mRNA content of IECs isolated from CBD vs VEH treated mice with coding genes significantly upregulated in the IECs of treatment mice (green) and vehicle mice (pink) highlighted (>=2 fold change; p<0.05). (C) PCA Mapping of the transcriptome of vehicle treated (blue) vs CBD treated (red) IECs (n=2; 5 mice per sample). (D) Heat map of all 390 genes significantly regulated between vehicle and CBD treated groups(>=2 fold change; p<0.05). (E) Heat map of the 10 significantly regulated genes with the highest and 10 significantly regulated genes with the lowest fold change value between vehicle and treated mice (>=2 fold change; p<0.05). (F) Representative histology sections of the proximal colon of EAE mice.

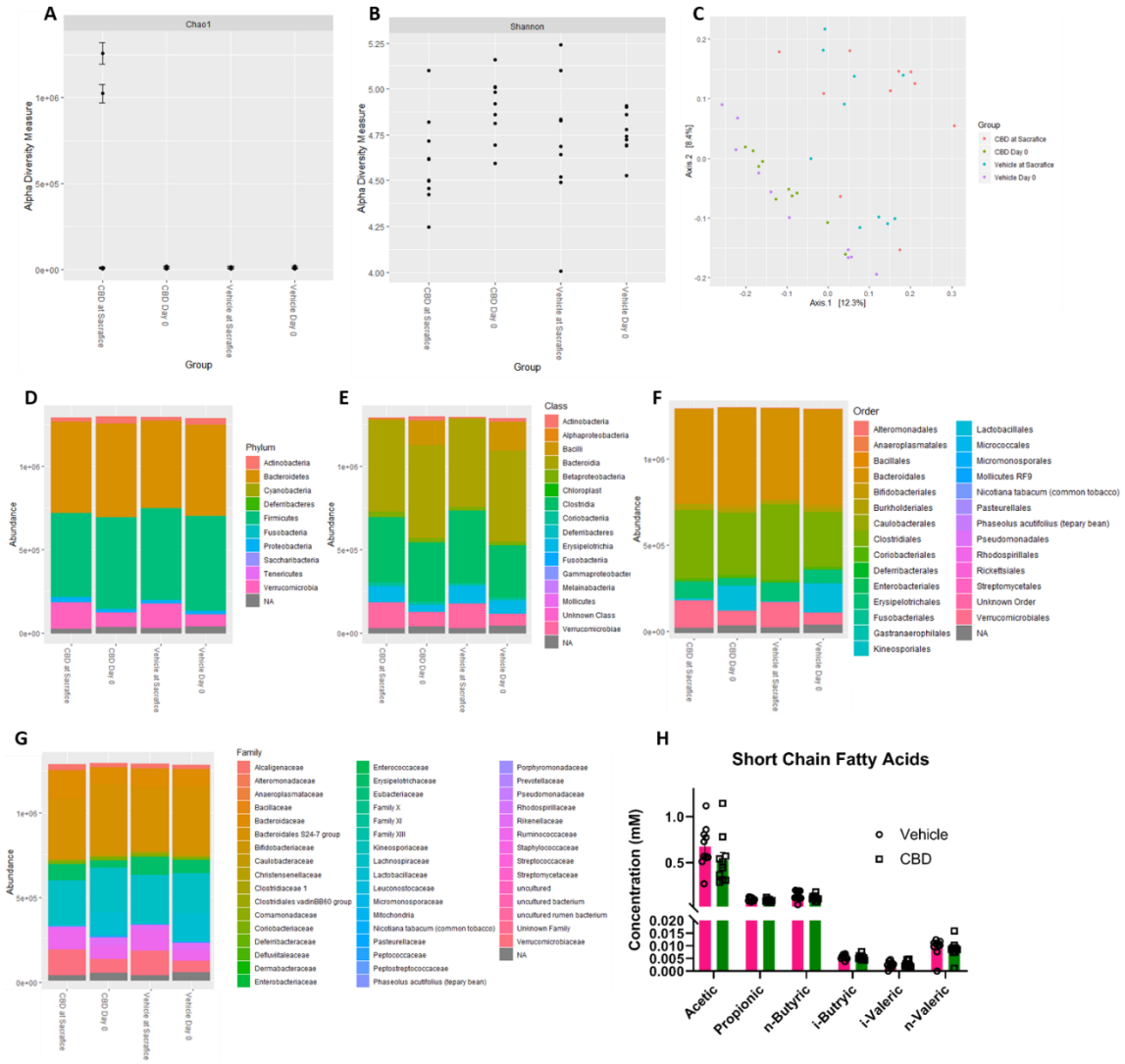

Figure 3.7 ***Effect of CBD on gut microbiota***. (**A**) Alpha diversity of 16s sequencing reads as measured by Chao1 index for cecal contents from vehicle and CBD treated mice at sacrifice and stool contents at day 0 (n=10 per group). (**B**) Alpha diversity as measured by Shannon index for cecal contents from vehicle and CBD treated mice at sacrifice and stool contents at day 0 (n=10 per group). (**C**) PCA plot demonstrating beta diversity of 16s sequencing reads as measured by Chao1 index for cecal contents from vehicle and CBD treated mice at sacrifice and stool contents at day 0 (n=10 per group). (**D**) Stacked bar charts demonstrating average abundance of identified bacterial phyla from 16s sequencing reads for cecal contents from vehicle and CBD treated mice at sacrifice and stool contents at day 0 (n=10 per group). (**E**) Stacked bar charts demonstrating average abundance of identified bacterial classes from 16s sequencing reads for cecal contents from vehicle and CBD treated mice at sacrifice and stool contents at day 0 (n=10 per

group). (**F**) Stacked bar charts demonstrating average abundance of identified bacterial orders from 16s sequencing reads for cecal contents from vehicle and CBD treated mice at sacrifice and stool contents at day 0 (n=10 per group). (**G**) Stacked bar charts demonstrating average abundance of identified bacterial families from 16s sequencing reads for cecal contents from vehicle and CBD treated mice at sacrifice and stool contents at day 0 (n=10 per group). (**H**) Concentration of detectable short chain fatty acids within the cecal contents of vehicle vs CBD treated EAE mice (n=10 per group).

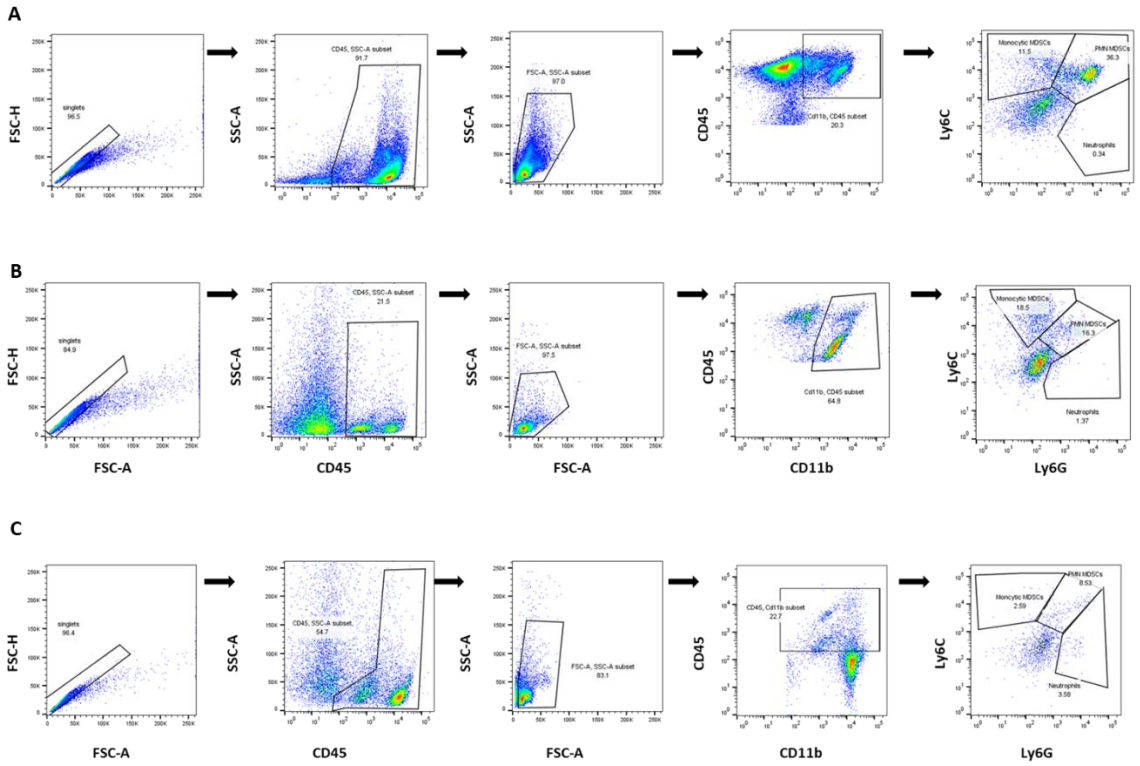

Figure 3.8 ***Gating Strategies for Flow Cytometry.*** Gating strategy for myeloid cells isolated from the **(A)** spleen, **(B)** CNS, and **(C)** MLN.

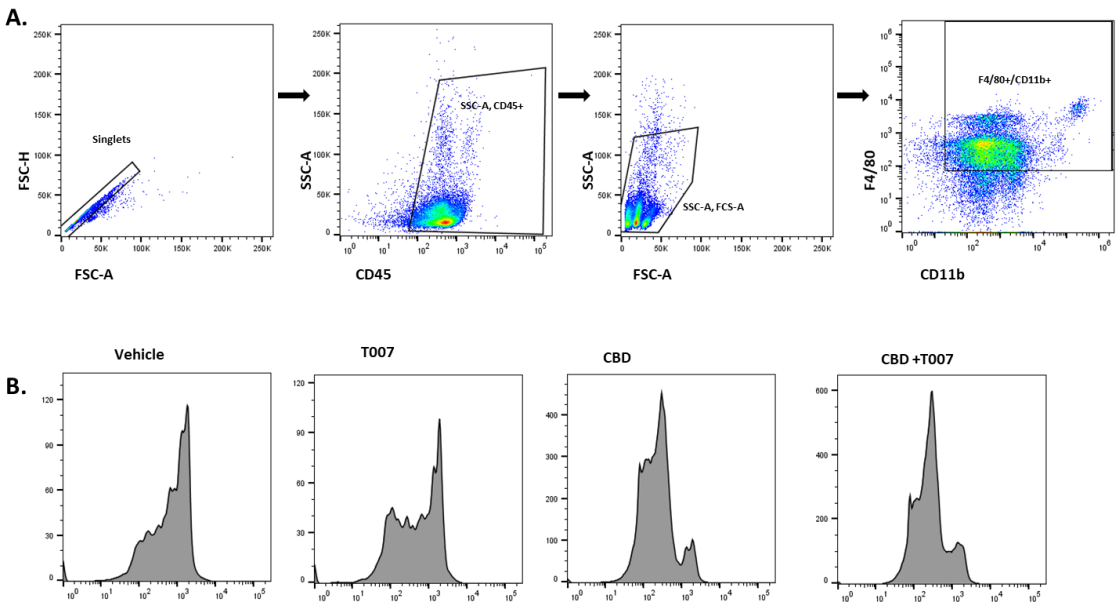

Figure 3.9 ***Endocytosis Assay of Peritoneal Macrophages.*** **(A)** Gating strategy to select for CD11b+CD45+F4/80+ macrophages. **(B)** Representative flow plots of FitC-Dextran engulfed by Vehicle, T007, CBD, and CBD+T007 treated macrophages**.**

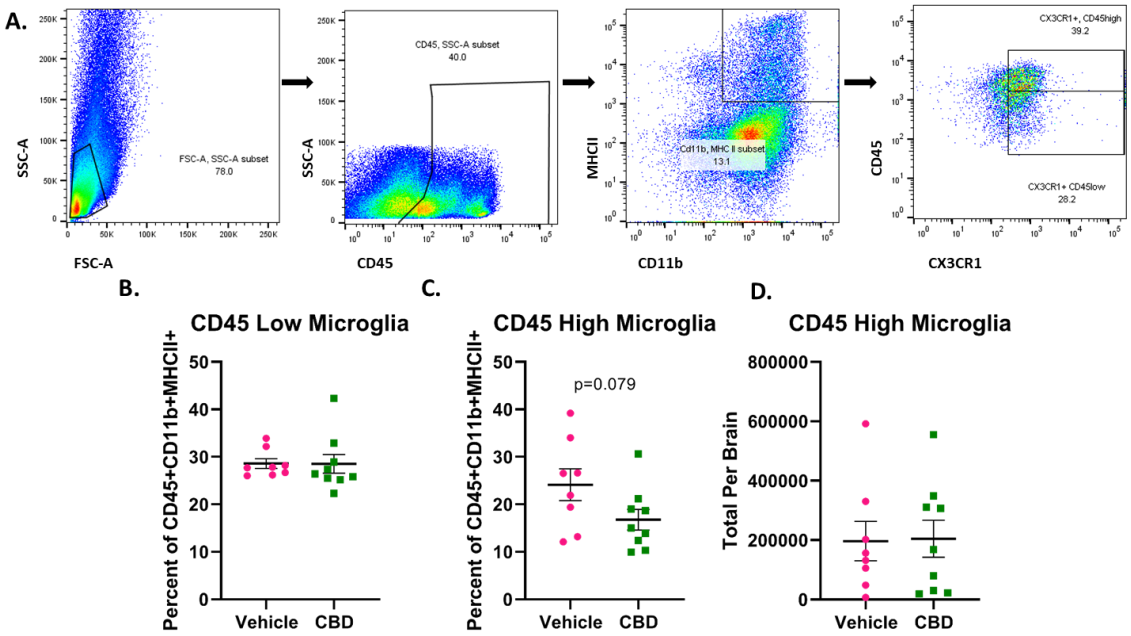

Figure 3.10 ***Cytometric Results of CXCR1+MHCII+ Microglia.*** **(A)** Gating strategy used for identification of CD45 high and low microglia populations. **(B)** $CD45^{low}$ microglia as a percentage of all CD45+MHCII+CD11b+ cells from the CNS. **(C)** $CD45^{high}$ microglia as a percentage of all CD45+MHCII+CD11b+ cells from the CNS. **(D)** Total number of $CD45^{high}$ per brain.

CHAPTER 4

EFFECTS OF ACUTE 2,3,7,8-TETRACHLORODIBENZO-P-DIOXIN EXPOSURE ON THE CIRCULATING AND CECAL METABOLOME PROFILE[4]

4.1 ABSTRACT

TCDD is a polyhalogenated planar hydrocarbon belonging to a group of highly toxic and persistent environmental contaminants known as “dioxins”. TCDD is an animal teratogen and carcinogen that is well characterized for causing immunosuppression through activation of AHR. In the current study, we investigated the effect of exposure of mice to an acute dose of TCDD on the metabolic profile within the serum and cecal contents to better define the effects of TCDD on host physiology. Our findings demonstrated that within the circulating metabolome following acute TCDD, there was significant dysregulation in the metabolism of bioactive lipids, amino acids, and carbohydrates when compared to the VEH treated mice. These wide-spread changes in metabolite abundance was identified to regulate host immunity via modulating NF-κB

[4]Dopkins N*, Neameh W*, Wilson K, Hall A, Lu K, Rutkovsky A, Gandy A, Nagarkatti PS, Nagarkatti M. Effects of Acute 2,3,7,8-Tetrachlorodibenzo-p-dioxin Exposure on the Circulating and Cecal Metabolome Profile.
*These authors contributed equally to this work.
Manuscript in preparation.

and ERK1/2 activity, and work as biomarkers for a variety of organ injuries and dysfunctions that follow TCDD exposure. Within the cecal content, of mice exposed to TCDD, we were able to detect changes in inflammatory markers that regulate NF-κB, markers of injury-related inflammation, and changes in lysine degradation, nicotinamide metabolism, and butanoate metabolism, which suggested an immediate suppression microbial metabolism. Collectively, these results demonstrate that acute TCDD exposure results in immediate irregularities in the circulating and intestinal metabolome which likely contributes to TCDD toxicity and can be used as biomarkers for the early detection of individual exposure.

4.2 INTRODUCTION

TCDD is a toxic and environmentally persistent contaminant which is produced as a by-product of industrial combustion processes, that garnered historical notoriety due to being a major component of the controversial herbicide used during the Vietnam War known as "Agent Orange"[202,203]. The pathology of TCDD exposure has been characterized by symptoms of immunotoxicity, hormonal dysregulation, developmental problems, increased cancer incidence and local skin irritation in the form of chloracne [88,204–208]. TCDD toxicity is carried out by activation of the cytosolic receptor and transcription factor known as the AHR, which then enhances transcription, proximal to DREs in the host genome[90,209]. Additionally, TCDD exposure leads to dysregulation of epigenetic regulators, such as the miRNA expression profile and microbiome composition, influencing downstream changes in phenotype[125,210–212]. Previous studies have demonstrated that the effects of TCDD are entirely dependent on the activation of the AHR, as AHR knockout mice are insensitive to majority of the toxic effects of TCDD

[213,214]. Experiments studying the effects AHR ligand binding have demonstrated the promiscuous role the receptor plays in regulating cell cycle progression, cellular metabolism and immunophenotype of cells[215]. TCDD exploits the AHR as a high-affinity ligand that when bound, results in dysregulations in metabolism, immunity, and normal cell cycle progression[216–219].

Unlike TCDD, other AHR ligands such as the endogenous, and those found in the diet, also activate AHR but are involved in normal immune system homeostasis and physiological functions. The precise mechanisms of such discrepancy in action mediated by AHR ligands is unclear but may be associated with degree of AHR affinity and the metabolism of the ligand[220]. A large portion of the uncertain changes in host physiology following TCDD exposure can be attributed to an absence of studies focusing on direct changes within the metabolomic profile immediately following TCDD exposure. In the current study, therefore, we investigated the metabolic activity within the GI tract and serum following acute TCDD exposure in naive mice. The timely importance of this study is derived from previous studies demonstrating that the effects of planar hydrocarbons on host physiology are often dependent on changes in the metabolomic profile of host organisms following AHR activation [221–225]. The goals of the current study were to identify key metabolites dysregulated immediately following acute TCDD exposure aimed at providing a comprehensive background for the mechanisms by which TCDD instigates pathogenic effects related to carcinogenesis, metabolic disorders and immunotoxicity. To the best of the authors knowledge, this is the first study focusing on the immediate changes in the metabolome following acute TCDD exposure.

4.3 MATERIALS AND METHODS

4.3.1 MICE

Six-week-old female WT C57BL/6 mice acquired from Jackson Laboratories (Bar Harbor, ME) were housed in an AAALAC-accredited specific-pathogen-free animal facility located at the grounds of the University of South Carolina School of Medicine for the entirety of all experiments. Mice within the facility were housed within polycarbonate cages containing cellulose fiber chips as bedding in a temperature and humidity-controlled environment. After a 2-week acclimatization period, the mice were divided randomly into two groups that would be administered a single 100µl intraperitoneal injection containing sterile corn oil (VEH group) or an intraperitoneal injection of 10µg/kg TCDD suspended within sterile corn oil (TCDD group). At the 72h time point following TCDD or VEH exposure, the mice were humanely euthanized by an overdose of inhaled isoflurane.

4.3.2 REAGENTS

The following reagents were used during the course of the experiments and were purchased as following: TCDD was provided by Dr. Steve Safe (Institute of Biosciences & Technology, Texas A&M Health Science Center, College Station, TX, United States); BSTFA and Methoxyamine HCl were purchased from Sigma-Aldrich (St. Louis, MO); Isoflurane was purchased from Henry Schein (Melville, NY); Corn oil, Methanol, Chloroform, and Ethanol were purchased from Fisher Scientific (Pittsburgh, PA).

4.3.3 CECAL CONTENT AND SERUM PROCESSING

Cecal content and serum samples were processed according to previously described protocols for the quantification of the metabolites present via Agilent GC-

MS[226,227]. Briefly, 20 mg of cecal content was vortexed with 1ml of a solution containing methanol, chloroform, and water (2:2:1). The samples were vortexed for 20 minutes followed by centrifugation at 1000g for 15 minutes. The aqueous and organic phase per each sample were aspirated into flat bottom HPLC vials and dried for a period of 4 hours in a SpeedVac. Samples were then derivatized with methoxyamine-HCl and BSTFA. For serum samples, 20µl of collected serum was vortexed with 80µl of cold ethanol for approximately 1 minute. The vortexed samples were then incubated at 4°C for 20 minutes and centrifuged for 10 minutes at 12,000rpm. The supernatant was aspirated, dried in a SpeedVac and derivatized using methoxyamine-HCL and BSTFA.

4.3.4 GAS CHROMATOGRAPHY-MASS SPECTROMETRY.

Peak alignment, integration, and filtering, as well as feature identification and calculation of cumulative peak intensity was performed with XCMS Online[228–230].

4.3.5. STATISTICAL ANALYSIS

PCA was conducted on resulting metabolites to produce scores plots visualizing separation between groups. Student's Two-tailed Unpaired T-test with an FDR rate of 0.05 for $\alpha = 0.05$, resulting metabolites were considered significant with $p \leq 0.05$ and FC ≥ 1.5. Metabolites that reached significance were used to conduct pathway analysis on the MetaboAnalyst 5.0 platform[231,232] using a hypergeometric test to determine metabolite enrichment and relative-betweenness centrality to visualize pathway topology. Due to limitations in available identification databases for measured metabolites- only those with KEGG and/or HMDB identifiers were able to be used for this pathway analysis. MetaMapp analysis was conducted on significantly altered metabolites for the purpose of identifying structural similarities between modulated metabolites to better

understand how acute TCDD exposure affects the composition of metabolite classes by chemical structure[233]. IPA was utilized for downstream effects on protein interactions and biochemical pathways based on significantly modulated metabolites[234].

The data shown in graphs is displaying the mean ± SEM. GraphPad Prism 8 was used for statistical analysis. Degree of significance was demonstrated using the following key: *p<0.05, **p<0.01, ***p<0.001.

4.4 RESULTS

4.4.1 CHARACTERIZATION OF ALTERATIONS IN THE METABOLIC PROFILE FOLLOWING ACUTE TCDD EXPOSURE

To study the metabolic profile after TCDD exposure, mice were injected i.p. with TCDD or vehicle and 72 hours later serum and cecal samples were analyzed. Within the serum of TCDD exposed mice, there were 1212 confirmed metabolites identified, and of these metabolites, 299 reached the previously defined threshold of significance (Figure 4.1A). PCA scores plot comparing normalized peak intensities revealed distinct clusters separating the serum metabolomes of the VEH and TCDD exposed groups (Figure 4.1B). Within the cecal content, 902 confirmed metabolites were identified, and of these, 107 were significantly different between groups (Figure 4.1C). PCA scores plot for cecal metabolites revealed distinct clusters separating the two groups with some overlap between the VEH and TCDD exposed groups (Figure 4.1D).

4.4.2 IDENTIFICATION OF METABOLIC PATHWAYS MOST IMPACTED FOLLOWING ACUTE TCDD EXPOSURE

MetaboAnalyst 5.0 revealed that within the serum, there were 404 KEGG metabolic pathways that contained one or more significant metabolites. Pathway

significance and impact were plotted on the Pathway Overview with larger, more intense red color circles indicating those overarching pathways were most meaningfully altered between groups (Figure 4.2A). Of these pathways, overlapping and incomplete pathways were identified, consolidated, and filtered, respectively, yielding 15 pathways with significant differences between TCDD and controls groups. In no significant order, these pathways within the serum involved the biosynthesis of the unsaturated FAs (Figure 4.3A-D), phenylalanine, tyrosine, and tryptophan biosynthesis (Figure 4.4A-D), purine metabolism (Figure 4.5A-G), lysine degradation (Figure 4.6A-E), valine, leucine, and isoleucine metabolism (Figure 4.7A-E), arginine biosynthesis (Figure 4.8A-E), and sphingolipid metabolism (Figure 4.9A-E). Cecal content pathway analysis yielded 9 pathways containing one or more significantly modulated metabolites, although both significance and impact of these pathways were reduced relative to serum pathway analysis (Figure 4.2B). In no significant order, these pathways within the cecal contents involved purine metabolism (Figure 4.10A-D), lysine degradation (Figure 4.11A-B), nicotinate and nicotinamide metabolism (Figure 4.12A-B), and butanoate metabolism (Figure 4.13A-B).

4.4.3 METAMAPP NETWORK VIEW OF SIGNIFICANTLY ALTERED SERUM METABOLITES IN TCDD-TREATED MICE WHEN COMPARED TO VEHICLE CONTROL GROUP

To further identify the mechanisms behind these metabolic shifts in the serum, metabolite enrichment based on structural homology was conducted using MetaMapp. MetaMapp analysis of the serum metabolites revealed that prostaglandins, sphingolipids,

ethanolamines and vitamin E analogs were selectively overabundant following TCDD exposure when compared to controls (Figure 4.14).

4.4.4 PATHWAY ANALYSIS OF PATHOLOGICALLY RELEVANT METABOLITES IN THE SERUM

IPA analysis was conducted to better understand the physiological importance of significantly altered metabolites within the serum and cecal content. In the serum, there were 7 metabolites that showed increased presence following TCDD exposure when compared to control group that either indirectly or directly showed associations with immunologically relevant proteins such as NF-κB, TGF-β, and FOXP3. Additionally, there were 9 direct and indirect interactions between metabolites that regulate the activity of ERK1/2, a master regulator of cell proliferation and cell death. (Figure 4.15A). Heat map demonstrating metabolites with significantly modulated abundance in VEH vs TCDD treated mice (Figure 4.15B). Heat map (Figure 4.15C) and bar charts (Figure 4.15D) demonstrating abundance of all significantly modulated metabolites of interest identified using IPA following TCDD treatment are shown.

4.4.5 ONTOLOGICAL ASSOCIATION OF DYSREGULATED SERUM METABOLITES WITH CELLULAR FUNCTIONALITY AND DISEASE PATHOLOGY

Next, we tried to correlate the changes in the metabolome composition following TCDD exposure in mice with diseases and disorders, molecular and cellular functions, and physiological system development and function, by using IPA software. The dysregulated metabolome profile within the serum of TCDD exposed mice was most heavily correlated with the diseases and disorders to include cancer, organismal injury

and abnormalities, developmental disorders, hereditary disorders and metabolic diseases (Figure 4.16A). The molecular and cellular functions associated with the dysregulated serum metabolite profile included alterations in: cellular growth and proliferation, cell cycle, protein synthesis, carbohydrate metabolism and molecular transport (Figure 4.16B). The top enriched physiological system development and function processes based on the content within the serum included: organismal development, endocrine system development and function, hematological system development and function, tissue development, and lymphoid structure and development (Figure 4.16C).

4.4.6 METAMAPP NETWORK VIEW OF SIGNIFICANTLY ALTERED CECAL CONTENT METABOLITES IN TCDD-TREATED MICE WHEN COMPARED TO THE VEHICLE CONTROL GROUP

To further identify the mechanisms behind these metabolic shifts in the cecal contents, metabolite enrichment based on structural homology was conducted using MetaMapp. MetaMapp analysis of the cecal content metabolites revealed that nucleotides, lipids, ethanolamine, indoles, steroids, dipeptides, and phenylalanine were selectively modulated following TCDD exposure (Figure 4.17).

4.4.7 TCDD EXPOSURE ALTERS CECAL METABOLOME THAT IS ASSOCIATED WITH ALTERED IMMUNE RESPONSE

IPA analysis was conducted to better understand the physiological importance of significantly altered metabolites within the cecal content. In the cecum, there were 2 metabolites that showed increased presence following TCDD exposure when compared to control group that either indirectly or directly showed associations with pro-inflammatory cytokines and NF-κB (Figure 4.18A). Heat map demonstrating metabolites

with significantly modulated abundance in VEH vs TCDD treated mice (Figure 4.18B). Heat map (Figure 4.18C) and bar charts (Figure 4.18D) demonstrating abundance of all significantly modulated metabolites of interest identified using IPA, as well as xanthosine which was identified independent of IPA has also been shown.

4.4.8 ONTOLOGICAL ASSOCIATION OF DYSREGULATED CECAL METABOLITES WITH CELLULAR FUNCTIONALITY AND DISEASE PATHOLOGY

The disparity in metabolites within the cecal content most heavily correlated with the diseases and disorders including cancer, organismal injury and abnormalities, tumor morphology, endocrine system disorders and metabolic disease (Figure 4.19A). The molecular and cellular functions associated with the dysregulated cecal content profile included altered abilities in: small molecule biochemistry, cell death and survival, cellular assembly and organization, cellular function and maintenance, and cell morphology (Figure 4.19B). The top enriched physiological system development and function processes based on the contents within the cecum included: Nervous system development and function, endocrine system development and function, hematological system development and function, immune cell trafficking and organismal development (Figure 4.19C).

4.5 DISCUSSION

The composition of circulating serum metabolites as well as within the cecal content, where a large portion of host-microbe interactions occur, provides novel insight into the physiology behind TCDD-mediated toxicity. This study demonstrates in an animal model that acute TCDD exposure significantly modulates the metabolomic profile

at these two sites. The differentially abundant metabolites present in the circulation and the GI tract reveal candidate pathways by which TCDD can potentially contribute towards toxicity including early development, and immunosuppression and cancer progression[235–237]. The significant change in the global composition of the serum metabolites and GI barrier site metabolites corroborates the previous conception that TCDD exposure drives metabolic imbalance within the host organism. Metabolic imbalance following TCDD exposure has been studied previously with the primary focus on membrane proteins involved in the degradation of adipose tissue, bile acid accumulation inducing hepatotoxicity, liver and skeletal muscle metabolism, and long term effects of TCDD exposure on surviving individuals[212,238,238,239]. These previous studies indicated the potential role of the metabolome in the pathology associated with TCDD exposure and intuitively suggested studying the acute effects of TCDD exposure within an animal model to better understand the immediate progression of TCDD-mediated toxicity.

Within the serum, we saw significant changes in various amino acid abundances, increases in various bioactive lipid concentrations and an upsurge in arachidonic acid-derived prostaglandins that signify organismal injury. Previous studies exploring circulating amino acid concentrations showed a significant increase associated with TCDD-mediated toxicity due to increased mobilization and reduced metabolism of amino acids in the liver[236]. This corresponded with significantly higher concentrations of L-phenylalanine, L-tyrosine, L-threonine, leucine, L-glutamate, N-acetyl glutamic acid, L-serine, methionine, L-lysine, and the proteogenic organic acid proline measured in this study. Additionally, previous findings suggested that TCDD exposure increases the

biosynthesis of sphingolipids in normal human epidermal keratinocytes[240]. Circulating metabolites associated with sphingolipid biosynthesis, specifically the ceramide pathway, were all elevated in mice exposed to TCDD, mirroring the process observed in the skin. These sphingolipids are protective molecules that mediate a wide variety of cellular functions that are associated with TCDD- induced toxicity including apoptosis, proliferation, inflammation, and necrosis[241,242]. Inflammation is also largely mediated by FAs and their products with omega-6 FAs associated with pro-inflammatory processes and omega-3 FAs associated with anti-inflammatory processes[243]. All four PUFAs were detected at higher concentrations in TCDD-exposed mice suggesting that inflammatory responses may be upregulated. AA, an omega-6 PUFA, is upregulated following injury or irritation and metabolized into eicosanoids, an important group of inflammatory mediators[244–246]. DHA, and omega-3 PUFA, is a precursor for the distinct family of SPMs called protectins as well as other SPMs such as resolvins and maresins[247,248]. ALA, an omega-3 PUFA, has been associated with reduction of pro-inflammatory gene expression such as IL-6, COX-2, and TNF-alpha[249]. Lastly, LA, an omega-6 PUFA, has been the topic of much controversy with several studies attributing inflammatory properties to it and others attributing no significant inflammatory properties. Additionally, increased uric acid in TCDD exposed mice could induce inflammation via NF-κB as observed in HepG2 cells[49].

The cecal metabolome exhibited substantially less differences as a whole between TCDD and VEH mice when compared to changes in the serum, however the changes observed indicated that TCDD exposure may still yield immediate changes in intestinal inflammation that modulate gut microbiota composition and metabolism, as has been

demonstrated with a variety of other AHR ligands[251]. Purine-mediated inflammatory responses have been extensively explored indicating an evolved extracellular role as danger signals released during events such as cell lysis, apoptosis, and degranulation[252]. Reductions in metabolites associated with lysine degradation, nicotinamide metabolism, and butanoate metabolism are all indicative of suppressed metabolism in the microbiome[253]. The variation in abundance of these metabolites provides context that aids in understanding the complex processes of inveterate immunosuppression, oncogenesis and congenital pathology observed following TCDD exposure. Within the cecal content, we saw much more narrow changes in the metabolome, however these changes correlated with the previously established immunosuppressive pathology following TCDD exposure.

NF-κB is a transcription factor vital for perpetuating innate and adaptive immunity by inducing expression of pro-inflammatory cytokines, enhancing immune cell fitness, and coercing differentiation of immune cells into activated pro-inflammatory subsets with potent effector functions. Exposure to dioxins such as TCDD has previously been shown to inhibit NF-κB expression in an AHR-dependent manner inducing sustained immunosuppression and immunotoxicity[254,255]. In the current study, we observed that the metabolomic profile following TCDD exposure may contribute to this immunotoxicity by increasing the relative abundance of NF-κB inhibitors, such as LA and oleoylethanolamide, in circulation[256–258]. It is noted however, that TCDD exposure results in the increased abundance of two NF-κB activating metabolites in arachidonic acid and uric acid[250,259]. At the site of injury following cell death, arachidonic acid is cleaved from the phospholipid membrane and enzymatically oxygenated via COX or

lipoxygenase pathways producing inflammatory mediator molecules [244]. The observed increase in the abundance of prostaglandin molecules and arachidonic acid correlates with a previously established increase in COX-1 activity and cell death following TCDD exposure[260]. The increased presence of the prostaglandin $F_{2\alpha}$, also referred to as "dinoprost", within the serum is a marker of injury and inflammation within the local host tissues[261]. This increase in arachidonic acid and dinoprost is likely due to organismal injury, apoptosis, and lesion formation following TCDD exposure and is likely being perpetuated by the previously established increases in COX-1 activity that follow [260,262]. Increases in uric acid content within the serum have already been shown in previous studies focusing on the metabolome of patients exposed to toxic AHR ligands with structural similarity to TCDD[263]. While uric acid also works as an activator of NF-κB in both mice and humans, it has been previously shown that reducing serum uric acid content with allopurinol results in a significant decrease in the anti-inflammatory cytokine TGF-β1[264,265]. These counteracting results make it hard to distinguish if uric acid in this case is contributing to inflammatory processes via NF-κB induction or alleviating inflammatory processes by maintaining or increasing TGF- β1 production. Collectively, however, these results suggest that the circulating metabolic profile within the serum content following TCDD exposure is likely contributing to the known immunomodulation by dioxins via an inhibition of NF-κB activity with some potential lingering NF-κB activation resulting from COX-1 activity at sites of cell damage and hyperuricemia.

ERK1/2 is a kinase enzyme that regulates a variety of cell activities including metabolism, proliferation and survival[266]. Previous research has demonstrated that

TCDD-mediated toxicity in the context of cancer and neuropathology are partially dependent on ERK1/2 signaling pathways[267–269]. Additionally, it has been shown that multiple inhibitors of ERK1/2 can reverse the observed effects of TCDD exposure by regulating the steady-state levels of the AHR and inhibiting cytochrome P450 family 1 subfamily member 1 activity[270]. These results collectively demonstrated that the observed changes in host physiology following TCDD exposure are at least partially dependent on downstream ERK1/2 signaling subsequently following AHR activation. Based on our findings which demonstrate that metabolites regulated following TCDD exposure directly interact with the ERK1/2, in combination with previous literature demonstrating AHR and ERK1/2 codependency, we suggest that TCDD-induced changes in the metabolome are contributing to systemic toxicity via activation of ERK1/2[271]. The amino acid L-phenylalanine, which is increased within the serum of TCDD-treated mice, has been shown to increase the activation of ERK1/2 via allosteric interactions with calcium ion sensing receptors[272]. Circulating levels of linolenic acid are increased following TCDD exposure, coinciding with vascular inflammation specific to endothelial cells via ERK1/2 signaling[273]. This correlates with previous studies which demonstrated that TCDD exposure worsens the incidence of atherosclerosis via the induction of vascular inflammation in a murine model[274]. Increased levels of circulating uric acid, as seen in the TCDD group, may result in nephropathy via ERK1/2 phosphorylation[275]. In one study, investigating hyperuricemia in rats, the pharmacological inhibition of ERK1/2 resulted in a significant reduction in the Smad3 dependent renal pathology[276]. Oleoylethanolamide is known to induce anti-inflammatory effects via ERK1/2 inhibition in a model of LPS-stimulated THP-1 cells in vitro[258], while within the hippocampi of rats

in a study focusing on alcohol abuse, oleoylethanolamide has been shown to selectively increase p-ERK1/2 levels relative to the vehicle alone[258,277]. These conflicting results due to the promiscuity of the ERK1/2 activation and inhibition following oleoylethanolamide supplementation make it difficult to deem in what manner and site the metabolite is enacting upon ERK1/2 in vivo, however its anti-inflammatory effects have been previously well established[278,279]. Collectively these results demonstrate that changes in the metabolome following TCDD exposure may drive the progression of renal pathology, inflammatory disorders, and atherosclerosis via ERK1/2 activation.

It has previously been established that exposure to dioxins which act via AHR activation results in wide spread changes in the gut microbiota composition that in turn results in lasting effects on host physiology, however the manner by which modulated gut microbiota composition can affect host immunity following TCDD exposure is not yet well described[280,281]. Mass spectrometry analysis reveals that within the cecal contents of TCDD exposed mice, there was an increase in the concentration of the anti-inflammatory molecule linoleoyl ethanolamide, which has previously been shown to limit production of pro-inflammatory cytokines and inhibit translocation of the pro-inflammatory transcription factor NF-κB[282]. TCDD exposure also decreased the abundance of ethylene glycol, a substance used to induce renal inflammation and activate the previously described transcription factor NF-κB[283–285]. The antiparallel increase of linoleoyl ethanolamide and decrease of ethylene glycol within the cecal contents 72h after TCDD exposure suggests that the metabolic dysbiosis occurring within the GI tract likely contributes to the immunosuppressive phenotype of TCDD in a manner dependent on NF-κB inhibition. Intestinal concentrations of the inflammation biomarker xanthosine, a

product of nucleobase deamination that arises from RNA damage at sites of inflammation, was shown to be significantly reduced within the cecal contents of TCDD exposed mice[286]. This decreased xanthosine abundance suggests that the acute exposure to TCDD results in suppression of pro-inflammatory processes within the GI tract under normal conditions. Collectively these results in the gut demonstrate that acute exposure of TCDD results in shifts in the cecal metabolome that suggests a localized inhibition of inflammatory processes.

4.5.3 CONCLUSIONS

Previous studies on TCDD toxicity have primarily focused on the long-term effects of exposure on metabolite abundance or the immediate effects of exposure on host immunity. To define the unknown role of host metabolism in AHR-mediated toxicity following TCDD exposure, we have applied mass spectrometry to measure the acute changes in serum and cecal metabolite abundance while demonstrating their contextual importance in pathologies that arise following TCDD exposure. Our work demonstrates that TCDD exposure results in significant modulations of the metabolomic profile of the serum and cecum contributing to previously established toxic side-effects. Specifically, TCDD exposure triggers an increase in anti-inflammatory metabolites inhibiting NF-κB activity and ERK1/2 activators.. Collectively, these results demonstrate that the changes in the metabolomic profile following TCDD exposure may play an important role in mediating TCDD toxicity by contributing to the immunomodulation, tissue damage and cell cycle regulation.

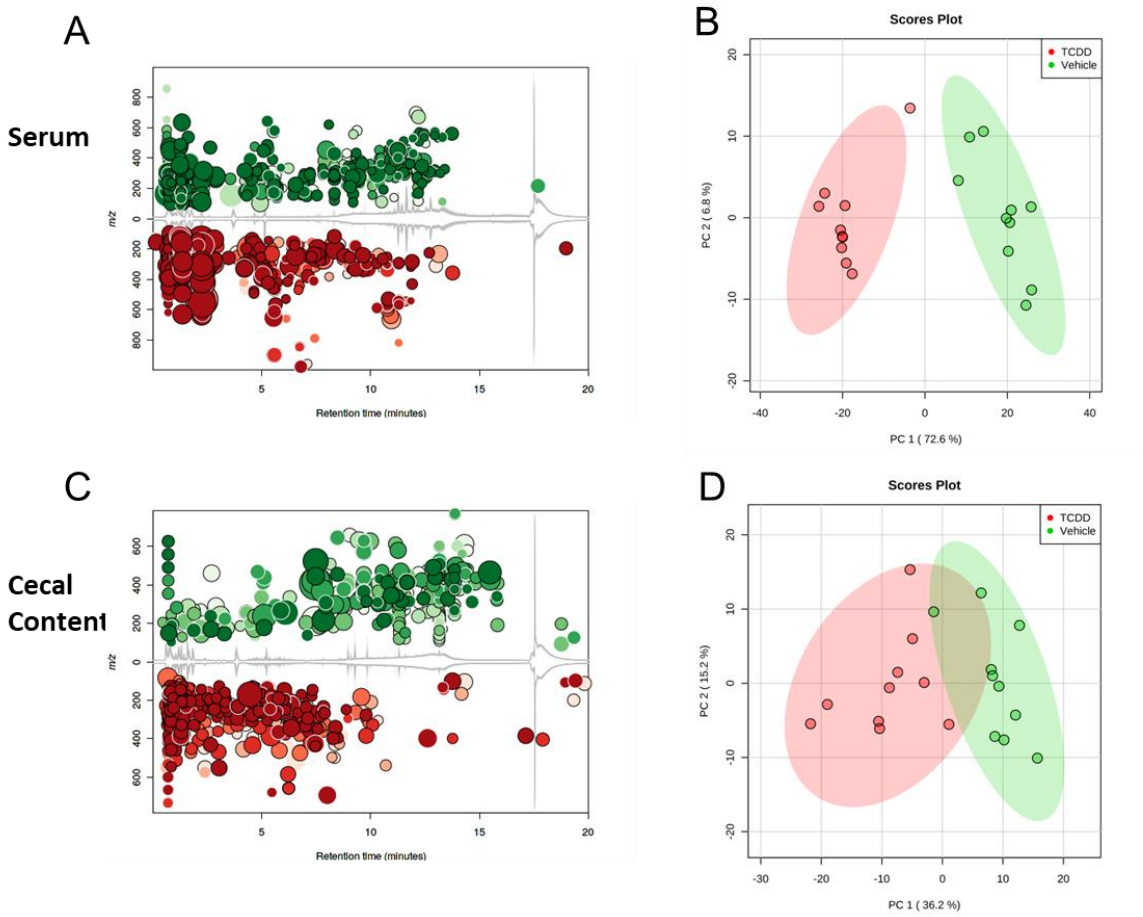

Figure 4.1 ***Characterization of Alterations in the Metabolic Profile Following Acute TCDD Exposure.*** Metabolomic global view of separation between TCDD vs VEH. TIC cloudplot of serum metabolites distinguishing 1212 metabolites significantly altered (p=< 0.01) between the TCDD (red) vs VEH (green) treated mice (A). Principal component analysis (PCA) plotting of serum metabolites with 95% confidence region highlighted (B). TIC cloudplot of cecal metabolites distinguishing 902 metabolites significantly regulated (p=< 0.01) between the TCDD (red) vs VEH (green) treated mice (C). Principal component analysis (PCA) plotting of cecal metabolites with 95% confidence region highlighted (D).

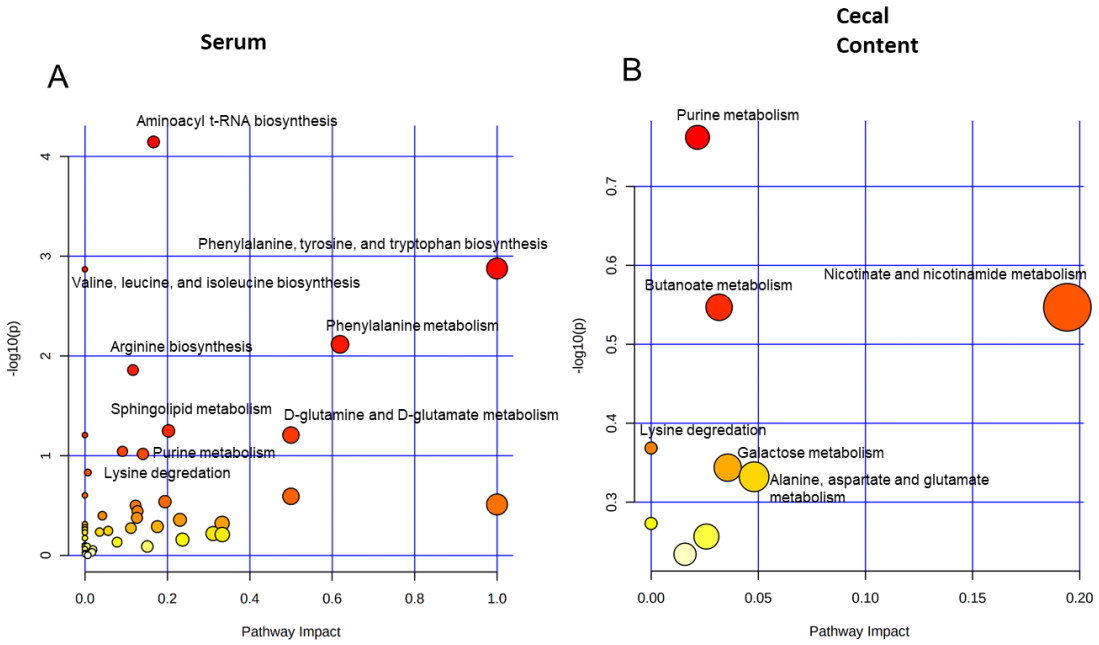

Figure 4.2 ***Pathway analysis based on over-representation analysis and pathway topology analysis reveals dysregulated upstream pathways of observed metabolites in acute TCDD exposure.*** Pathway analysis based on over-representation analysis (hypergeometric test) and pathway topology analysis (relative-betweenness centrality) reveals dysregulated upstream pathways of observed metabolites in acute TCDD exposure. MetaboAnalyst analysis revealed 40 unique metabolic pathways altered following TCDD exposure in the serum (A) and 9 unique metabolic pathways altered following TCDD exposure in the cecum (B). Analysis was performed in MetaboAnalyst, using “Mammals: Mus musculus (KEGG)” for pathway reference. (Larger dot size correlates to the relative Pathway Impact and intensity of the red hue correlates to the p value significance).

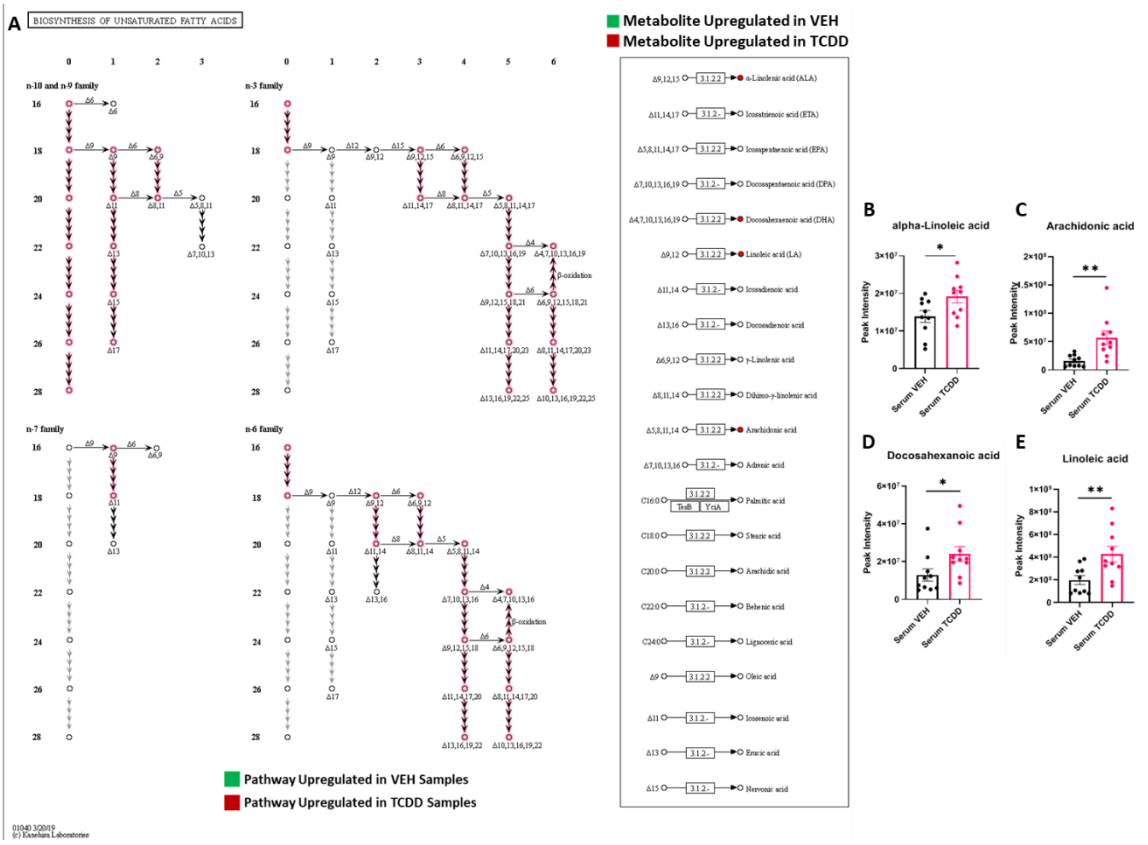

Figure 4.3 ***Biosynthesis of Unsaturated Fatty Acids in the Serum.*** (A) Biosynthesis of unsaturated fatty acid KEGG pathway illustrating metabolic networks including metabolites denoted by circles and associated enzymes denoted by squares. Significant metabolites are indicated by a solid node that correlates with upregulation in the TCDD (Red) or VEH (Green) exposed mice. Pathway sections and components highlighted by a red outline indicate likely enzymes and additional metabolites that may be involved in the difference of expression. (B-E) Bar charts demonstrating abundance of significantly modulated metabolites identified via the Biosynthesis of Unsaturated Fatty Acids KEGG pathway (Figure 4.3B $t(18)=2.877$, $P=0.03$: Figure 4.3C $t(18)=3.390$, $P=0.003$: Figure 4.3D $t(18)=2.206$, $P=0.046$: Figure 4.3E $t(18)=2.877$, $P=0.01$).

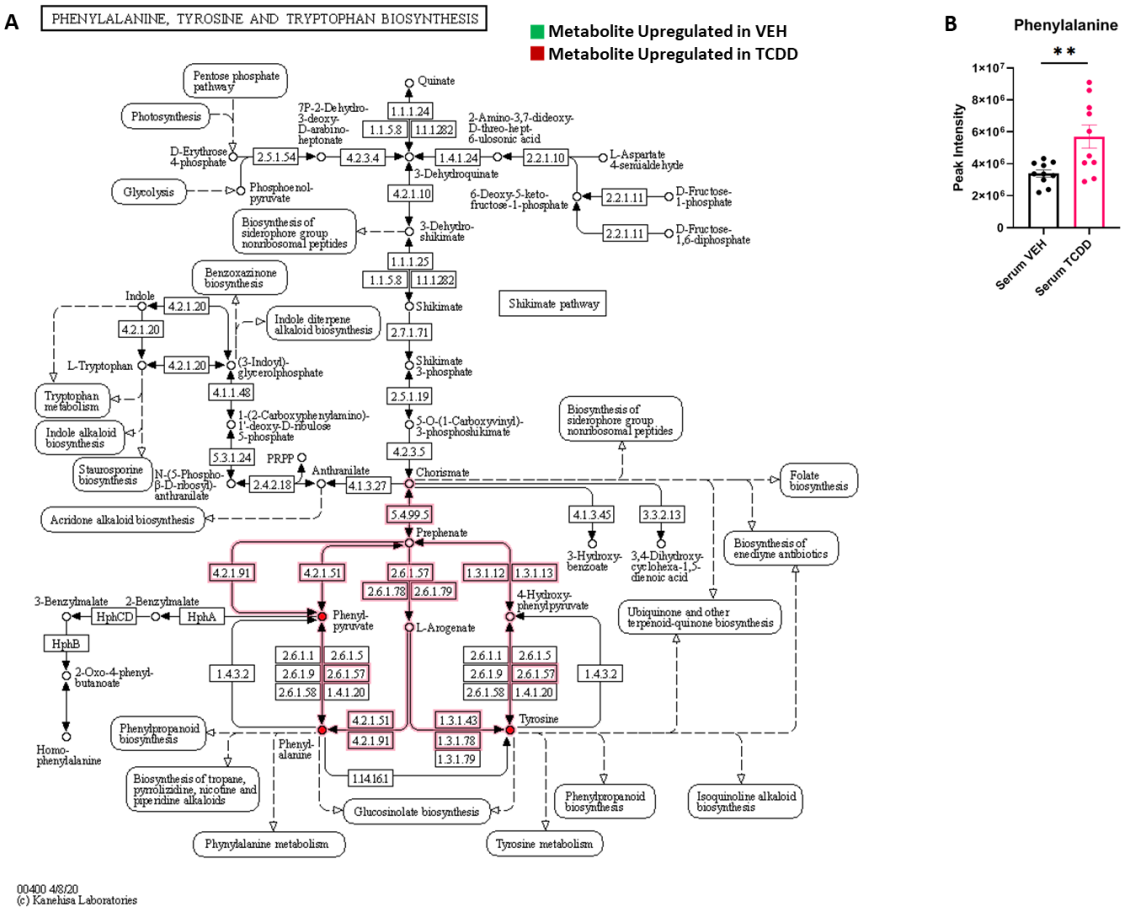

Figure 4.4 ***Phenylalanine, Tyrosine, and Tryptophan Biosynthesis in the Serum.*** (A) Purine metabolism KEGG pathway illustrating metabolic networks including metabolites denoted by circles and associated enzymes denoted by squares. Significant metabolites are indicated by a solid node that correlates with upregulation in the TCDD (Red) or VEH (Green) exposed mice. Pathway sections and components highlighted by a red outline indicate likely enzymes and additional metabolites that may be involved in the difference of expression. (B) Bar chart demonstrating abundance of significantly modulated metabolites identified via the Purine Biosynthesis KEGG pathway (Figure 4.4B $t(18)=3.04$, $P=0.007$).

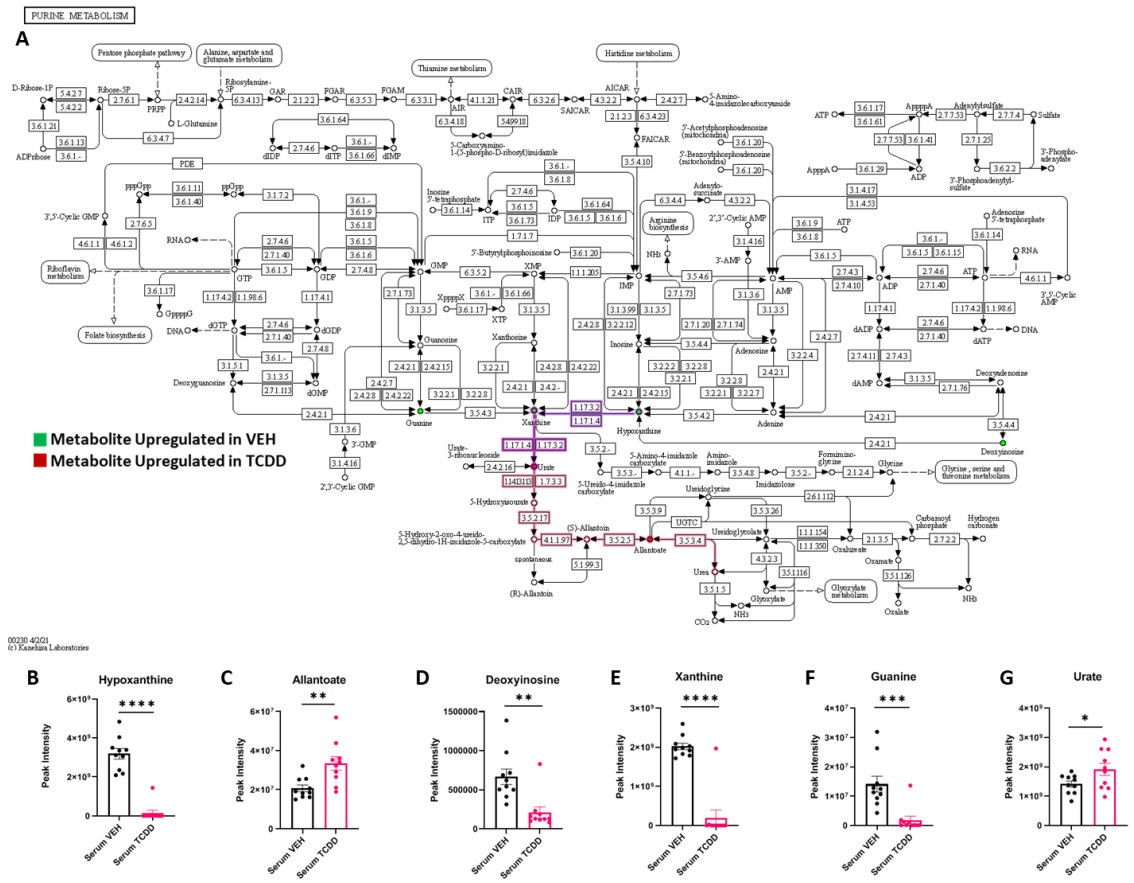

Figure 4.5 ***Purine Biosynthesis in the Serum.*** (A) Purine metabolism KEGG pathway illustrating metabolic networks including metabolites denoted by circles and associated enzymes denoted by squares. Significant metabolites are indicated by a solid node that correlates with upregulation in the TCDD (Red) or VEH (Green) exposed mice. Pathway sections and components highlighted by a red outline indicate likely enzymes and additional metabolites that may be involved in the difference of expression. (B-G) Bar charts demonstrating abundance of significantly modulated metabolites identified via the Purine Biosynthesis KEGG pathway (Figure 4.5B p t(18)=2.877, P<0.001: Figure 4.5C t(18)=3.276, P=0.004: Figure 4.5D t(18)=3.765, P=0.0014, Figure 4.5E t(18)=8.526, P<0.0001: Figure 4.5F t(18)=4.072, P<0.001, Figure 4.5G t(18)=2.127, P=0.047).

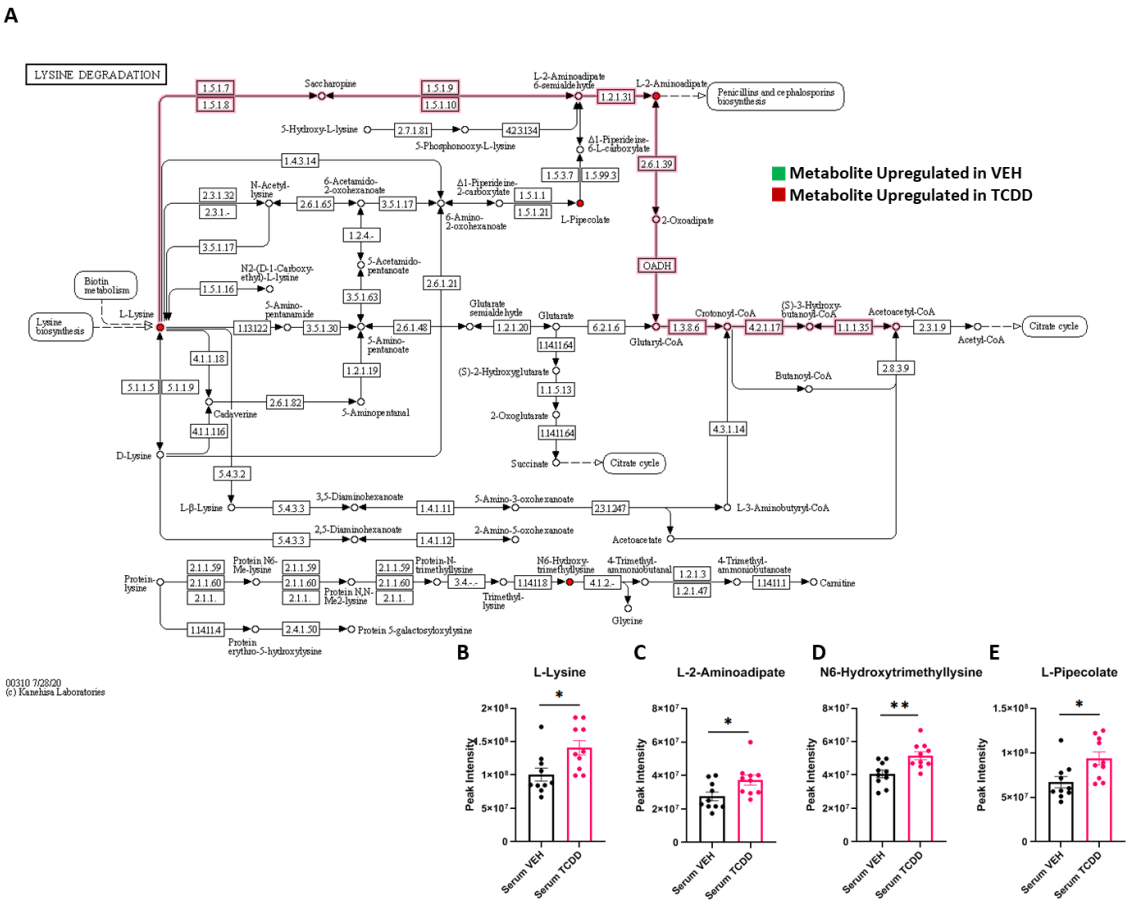

Figure 4.6 ***Lysine Degradation in the Serum.*** (A) Lysine degradation KEGG pathway illustrating metabolic networks including metabolites denoted by circles and associated enzymes denoted by squares. Significant metabolites are indicated by a solid node that correlates with upregulation in the TCDD (Red) or VEH (Green) exposed mice. Pathway sections and components highlighted by a red outline indicate likely enzymes and additional metabolites that may be involved in the difference of expression. (B-E) Bar charts demonstrating abundance of significantly modulated metabolites identified via the Lysine Degradation KEGG pathway (Figure 4.6B $t(18)=2.751$, $P=0.013$: Figure 4.6C $t(18)=2.112$, $P=0.0489$: Figure 4.6D $t(18)=2.925$, $P=0.009$: Figure 4.6E $t(18)=2.746$, $P=0.013$).

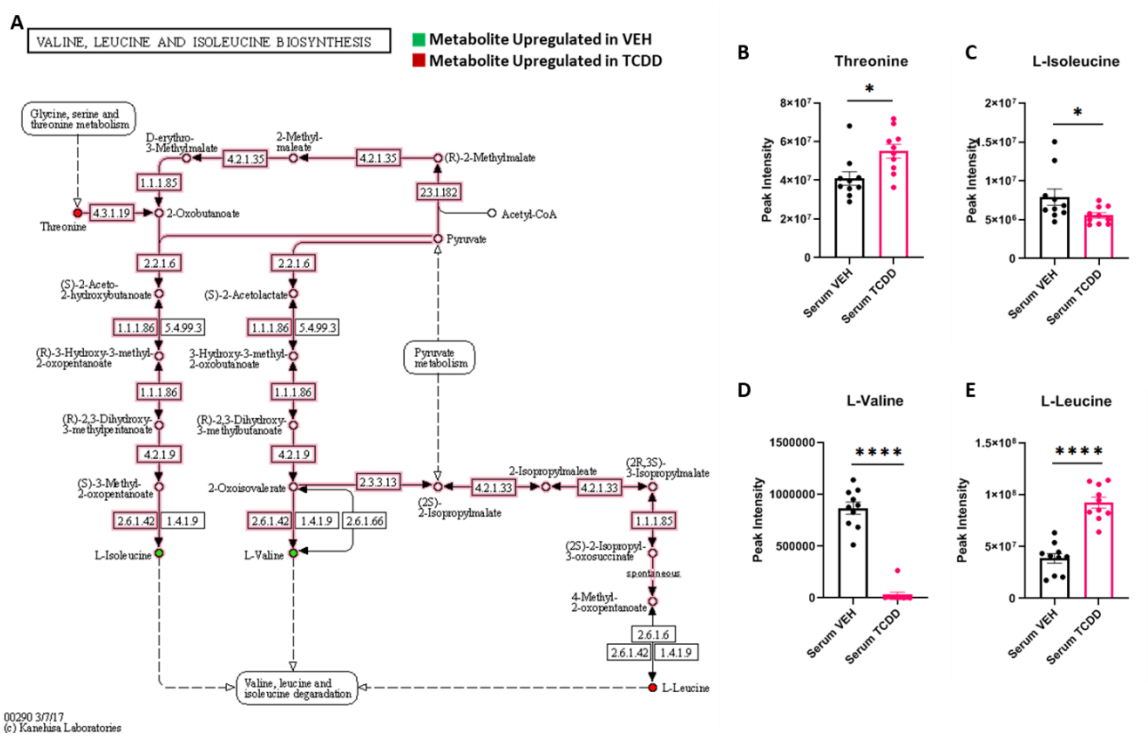

Figure 4.7 ***Valine, Leucine and Isoleucine Biosynthesis in the Serum.*** (A) Valine, leucine, and isoleucine biosynthesis KEGG pathway illustrating metabolic networks including metabolites denoted by circles and associated enzymes denoted by squares. Significant metabolites are indicated by a solid node that correlates with upregulation in the TCDD (Red) or VEH (Green) exposed mice. Pathway sections and components highlighted by a red outline indicate likely enzymes and additional metabolites that may be involved in the difference of expression. (B-E) Bar charts demonstrating abundance of significantly modulated metabolites identified via the Valine, Leucine and Isoleucine Biosynthesis KEGG pathway (Figure 4.7B $t(18)=2.848$, $P=0.017$: Figure 4.7C $t(18)=2.141$, $P=0.046$: Figure 4.7D $t(18)=12.90$, $P<0.001$: Figure 4.7E $t(18)=7.623$, $P<0.001$).

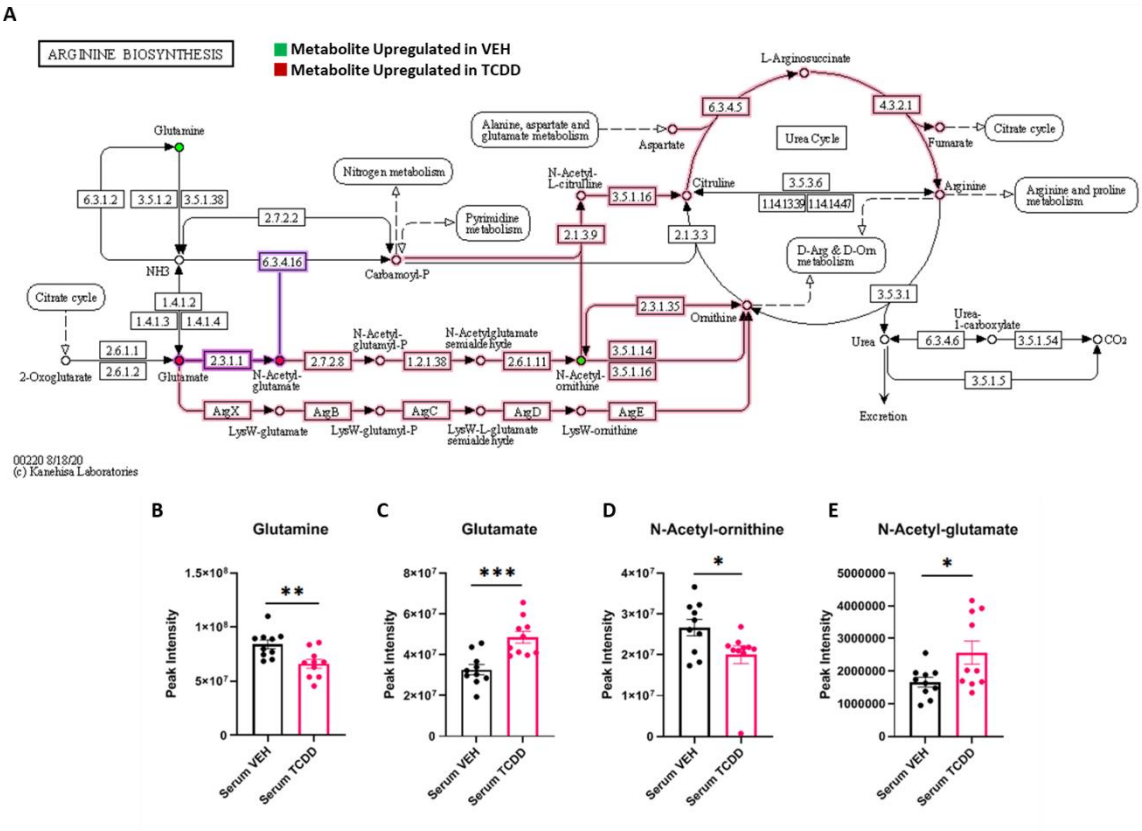

Figure 4.8 ***Arginine Biosynthesis in the Serum*** (A) Arginine biosynthesis KEGG pathway illustrating metabolic networks including metabolites denoted by circles and associated enzymes denoted by squares. Significant metabolites are indicated by a solid node that correlates with upregulation in the TCDD (Red) or VEH (Green) exposed mice. Pathway sections and components highlighted by a red outline indicate likely enzymes and additional metabolites that may be involved in the difference of expression. (B-E) Bar charts demonstrating abundance of significantly modulated metabolites identified via the Arginine Biosynthesis KEGG pathway (Figure 4.8B $t(18)=3.158$, $P=0.005$: Figure 4.8C $t(18)=4.165$, $P<0.001$: Figure 4.8D $t(18)=2.221$, $P=0.039$: Figure 4.8E $t(18)=2.363$, $P=0.029$).

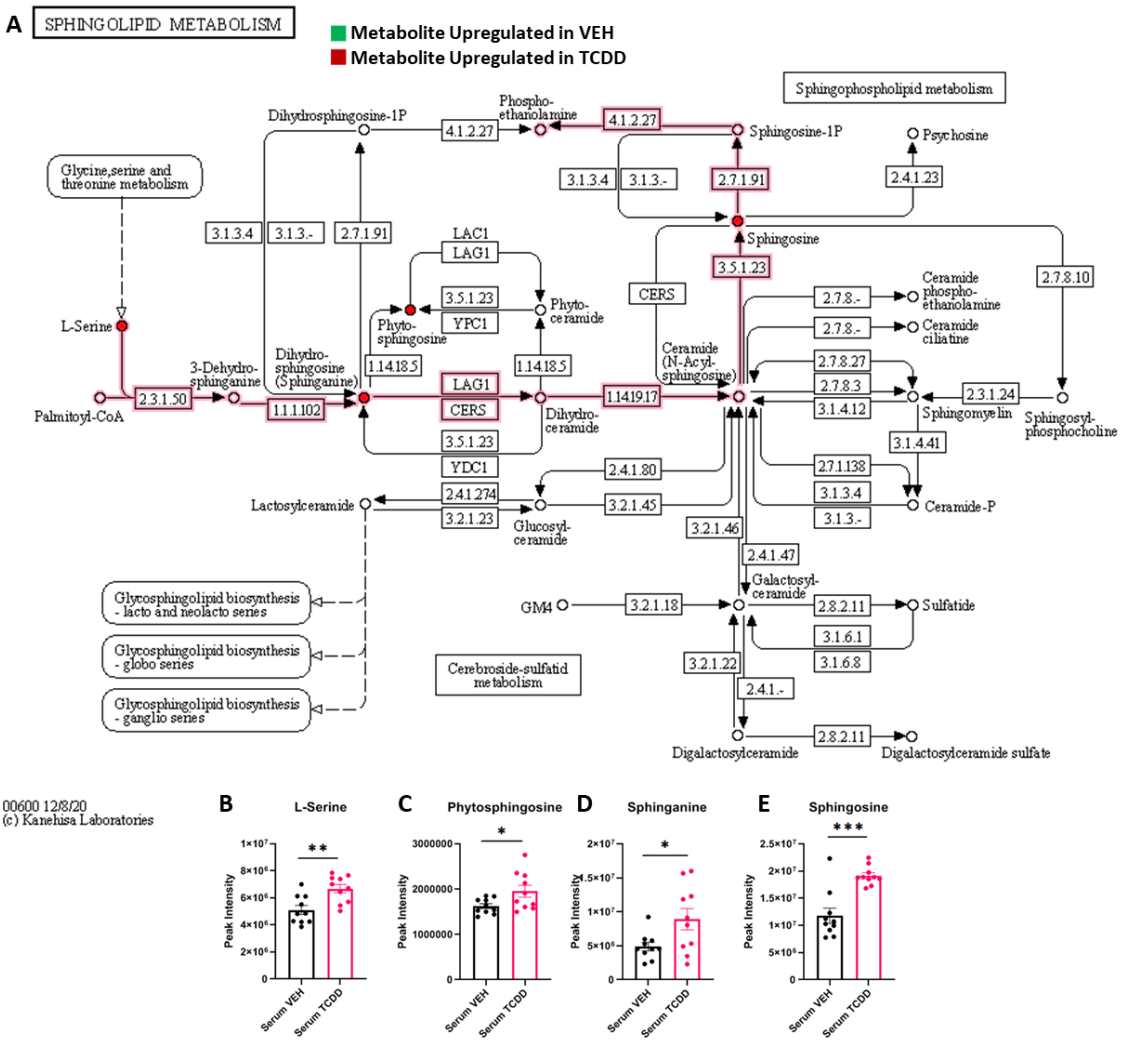

Figure 4.9 ***Sphingolipid Metabolism in the Serum*** (A) Sphingolipid metabolism KEGG pathway illustrating metabolic networks including metabolites denoted by circles and associated enzymes denoted by squares. Significant metabolites are indicated by a solid node that correlates with upregulation in the TCDD (Red) or VEH (Green) exposed mice. Pathway sections and components highlighted by a red outline indicate likely enzymes and additional metabolites that may be involved in the difference of expression. (B-E) Bar charts demonstrating abundance of significantly modulated metabolites identified via the Sphingolipid Metabolism KEGG pathway (Figure 4.9B $t(18)=3.455$, $P=0.0028$: Figure 4.9C $t(18)=2.308$, $P=0.0033$: Figure 4.9D $t(18)=2.392$, $P=0.027$: Figure 4.9E $t(18)=4.935$, $P<0.001$).

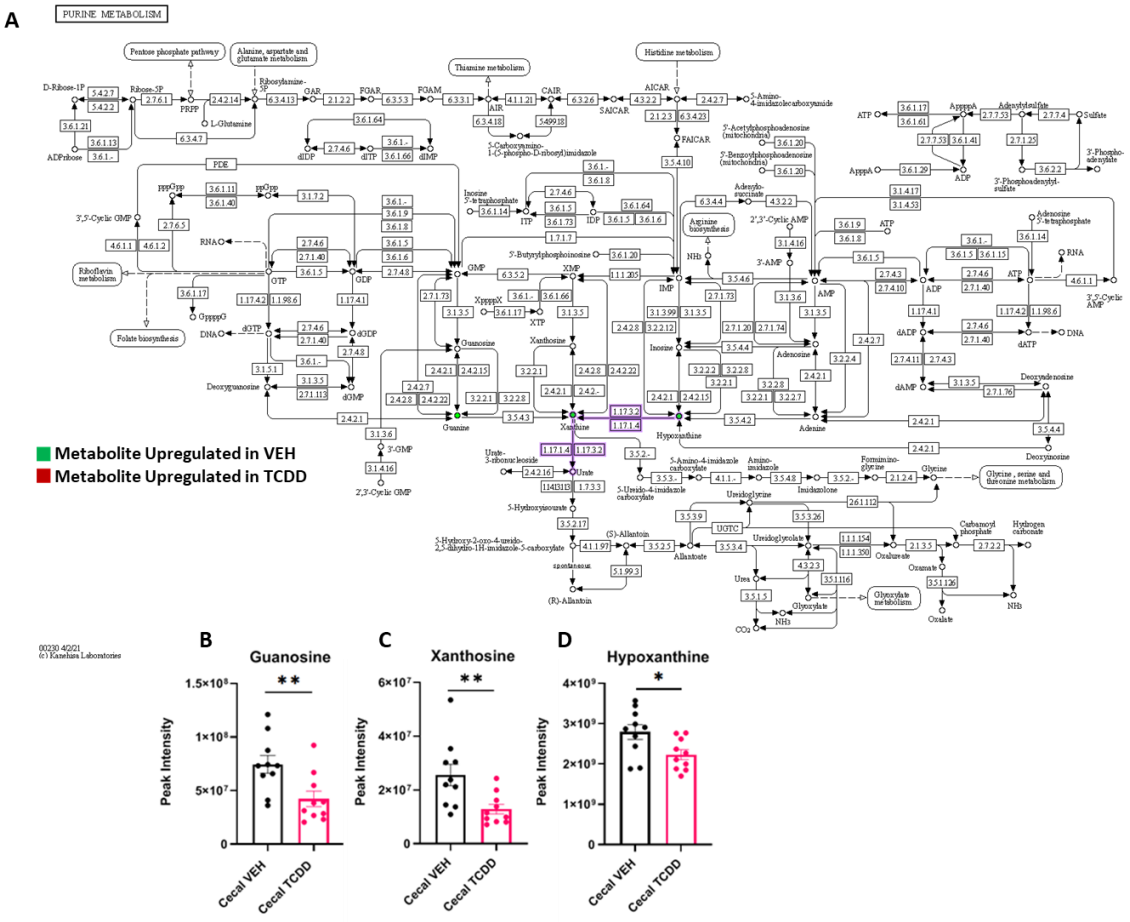

Figure 4.10 ***Purine Metabolism in the Cecal Contents*** (A) Purine metabolism KEGG pathway illustrating metabolic networks including metabolites denoted by circles and associated enzymes denoted by squares. Significant metabolites are indicated by a solid node that correlates with upregulation in the TCDD (Red) or VEH (Green) exposed mice. Pathway sections and components highlighted by a red outline indicate likely enzymes and additional metabolites that may be involved in the difference of expression. (B-E) Bar charts demonstrating abundance of significantly modulated metabolites identified via the Purine Metabolism KEGG pathway (Figure 4.10B $t(18)=2.922$, $P=0.009$: Figure 4.10C $t(18)=2.895$, $P=0.009$: Figure 4.10D $t(18)=2.499$, $P=0.02$).

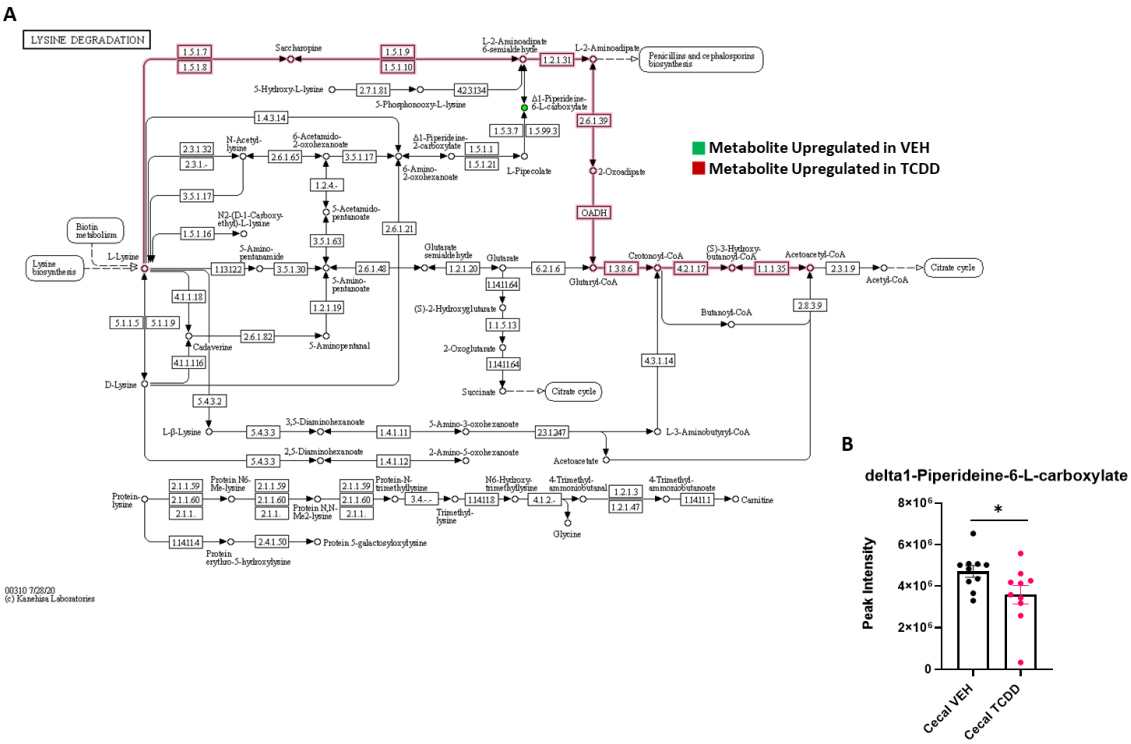

Figure 4.11 ***Lysine Degradation in the Cecal Contents*** (A) Lysine degradation KEGG pathway illustrating metabolic networks including metabolites denoted by circles and associated enzymes denoted by squares. Significant metabolites are indicated by a solid node that correlates with upregulation in the TCDD (Red) or VEH (Green) exposed mice. Pathway sections and components highlighted by a red outline indicate likely enzymes and additional metabolites that may be involved in the difference of expression. (B) Bar chart demonstrating abundance of delta1-Piperideine-6-L-carboxylate ($t(18)=2.122$, $P=0.048$

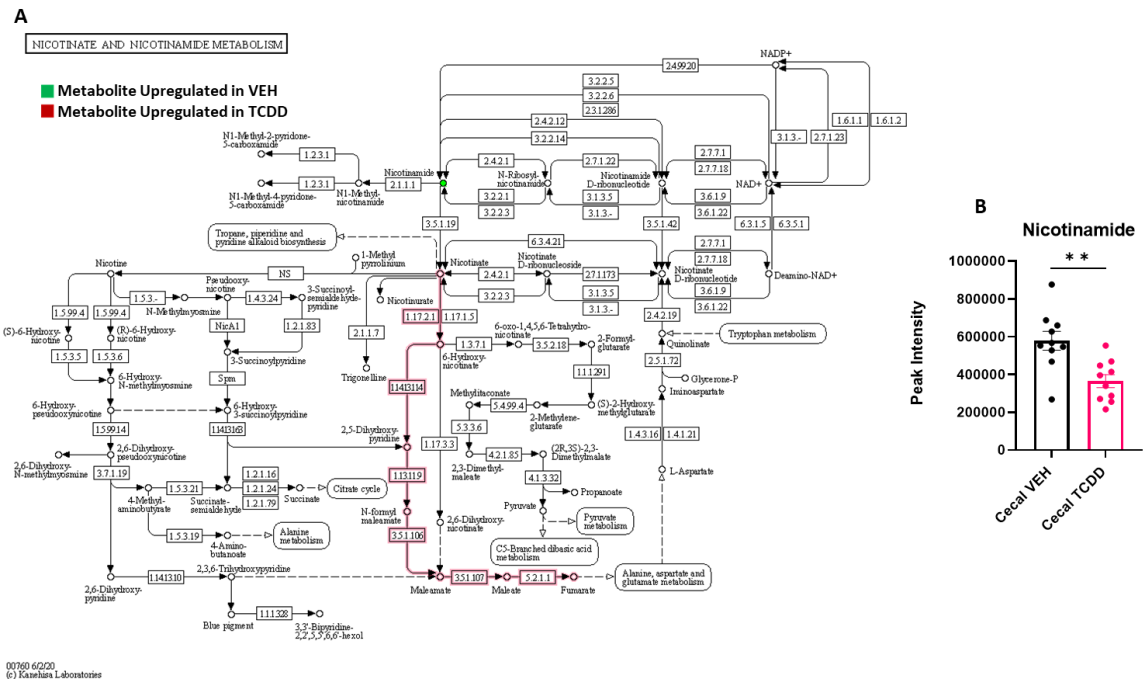

Figure 4.12 ***Nicotinate and Nicotinamide Metabolism in the Cecal Contents*** (A) Nicotinate and nicotinamide metabolism KEGG pathway illustrating metabolic networks including metabolites denoted by circles and associated enzymes denoted by squares. Significant metabolites are indicated by a solid node that correlates with upregulation in the TCDD (Red) or VEH (Green) exposed mice. Pathway sections and components highlighted by a red outline indicate likely enzymes and additional metabolites that may be involved in the difference of expression. (B) Bar chart demonstrating abundance of Nicotinamide ($t(18)=2.129$, $P=0.004$).

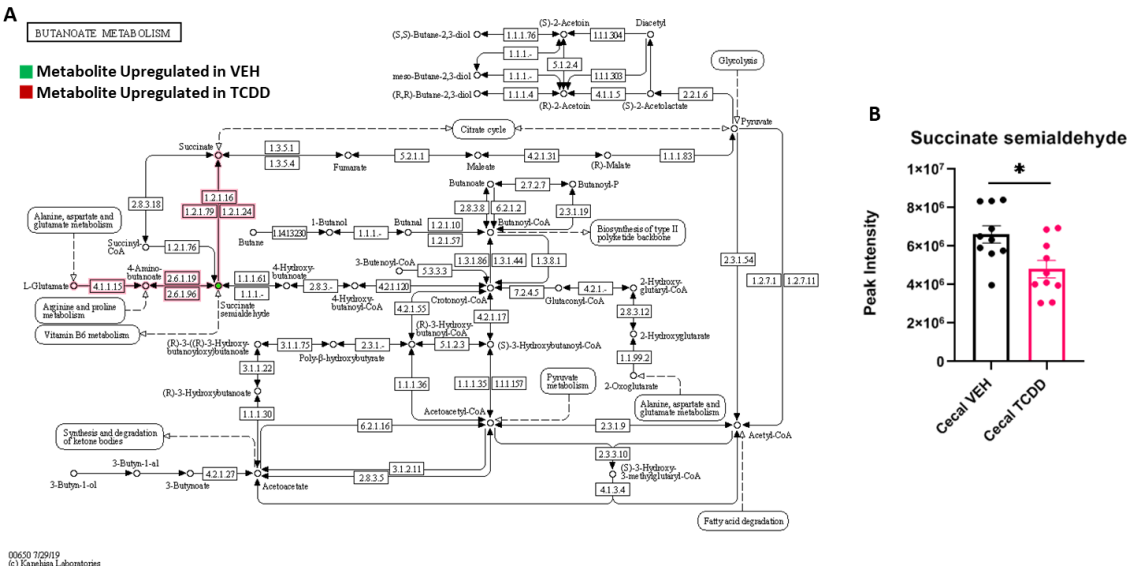

Figure 4.13 ***Butanoate Metabolism in the Cecal Contents*** (A) Butanoate metabolism KEGG pathway illustrating metabolic networks including metabolites denoted by circles and associated enzymes denoted by squares. Significant metabolites are indicated by a solid node that correlates with upregulation in the TCDD (Red) or VEH (Green) exposed mice. Pathway sections and components highlighted by a red outline indicate likely enzymes and additional metabolites that may be involved in the difference of expression. (B) Bar chart demonstrating abundance of Succinate Semialdehyde ($t(18)=2.823$, $P=0.01$).

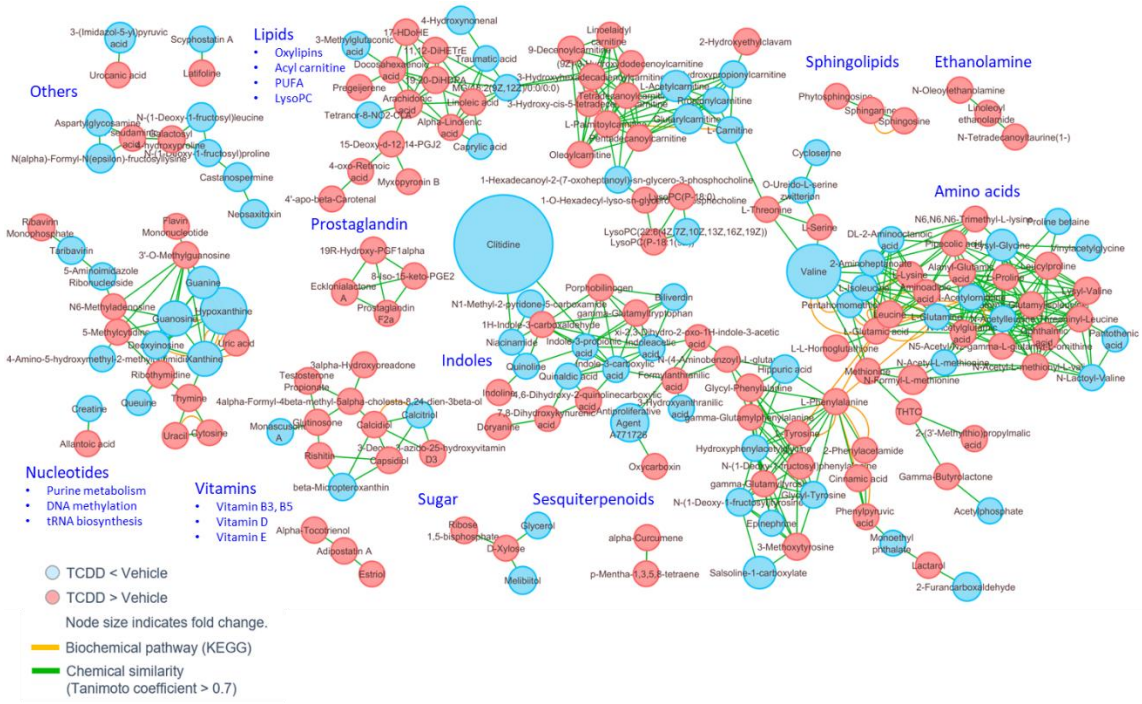

Figure 4.14 ***MetaMapp network view of significantly changed serum metabolites (p<0.05) in TCDD-treated mice as compared with the vehicle control group*.**
MetaMapp network view of significantly changed serum metabolites (p<0.05) in TCDD-treated mice as compared with the vehicle control group. The clustering is constructed based on biochemical relationships (KEGG) and chemical similarity (Tanimoto coefficient > 0.7).

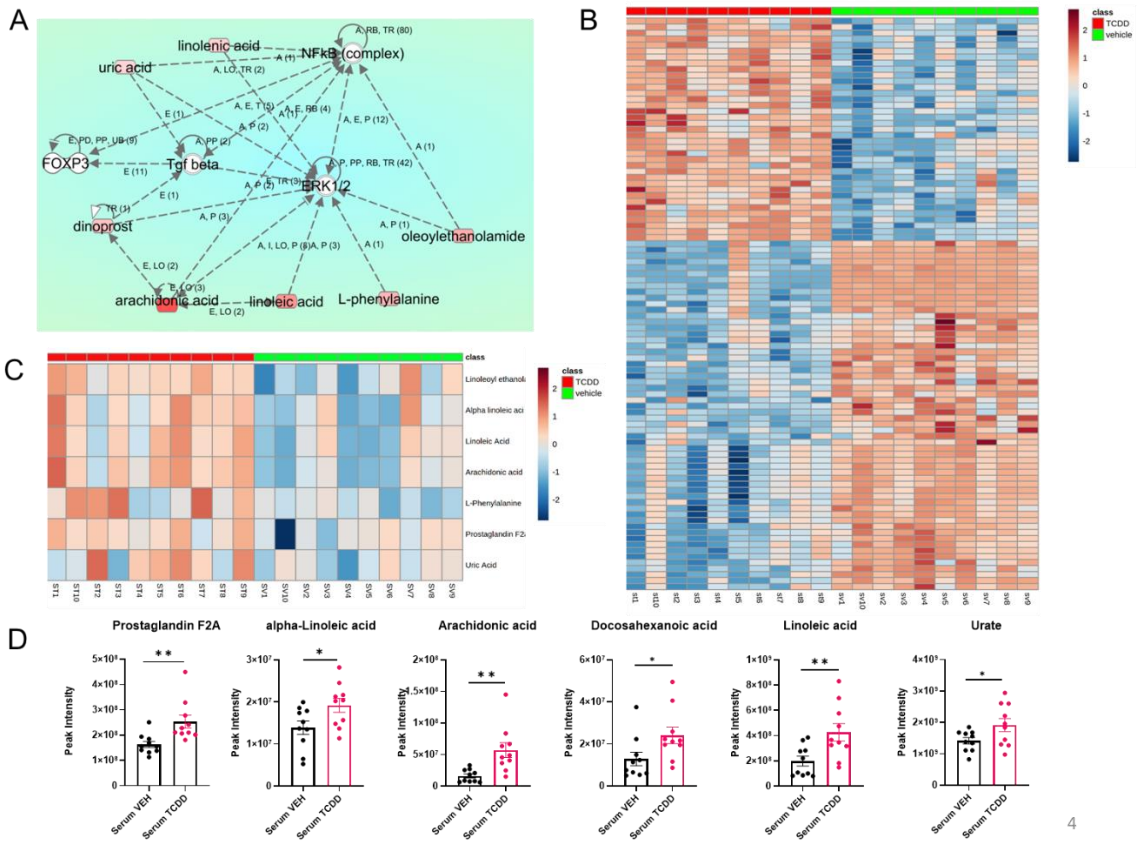

Figure 4.15 ***TCDD exposure significantly regulates the circulating metabolome in an immunosuppressive manner.*** TCDD exposure significantly regulates the circulating metabolome in an immunosuppressive manner. (A) Ingenuity pathway analysis of significantly modulated serum metabolites (Metabolites in green are higher in the VEH treated mice, while those in red are higher in the TCDD exposed). (B) Heat map displaying intensity of significantly different expressed individual metabolites within the serum of VEH and TCDD mice (n=10 per group). (C) Heat map displaying significantly modulates metabolites of interest within the serum of VEH and TCDD mice. (D) Peak intensities identified via GC-MS of metabolites of interest that are differentially abundant between the serum of VEH and TCDD mice (Prostaglandin F2A $t(18)=2.873$, $P=0.01$: Alpha-linolenic acid $t(18)=2.877$, $P=0.03$: Arachidonic Acid $t(18)=3.390$, $P=0.003$: Docosohexanoic Acid $t(18)=2.206$, $P=0.04$: Linoleic Acid $t(18)=2.877$, $P=0.01$: Urate $t(18)=2.127$, $P=0.047$).

A **Diseases and Disorders**

Name	p-value range	Number of molecules
Cancer	4.13E-02 – 1.52E-08	29
Organismal Injury and Abnormalities	4.33E-02 – 1.52E-08	44
Developmental Disorder	3.42E-02 – 4.01E-08	15
Hereditary Disorder	3.42E-02 – 4.01E-08	17
Metabolic Disease	3.42E-02 – 4.01E-08	15

B **Molecular and Cellular Functions**

Name	p-value range	Number of molecules
Cellular Growth and Proliferation	3.54E-02 – 3.90E-06	28
Cell Cycle	3.42E-02 – 4.46E-05	18
Protein Synthesis	4.12E-02 – 1.44E-04	13
Carbohydrate Metabolism	4.12E-02 – 2.21E-04	21
Molecular Transport	4.12E-02 – 2.21E-04	28

C **Physiological System Development and Function**

Name	p-value range	Number of molecules
Organismal Development	4.12E-02 – 9.76E-07	26
Endocrine System Development and Function	3.54E-02 – 4.94E-04	8
Hematological System Development and Function	4.20E-02 – 9.49E-04	21
Tissue Development	3.54E-02 – 9.49E-04	17
Lymphoid Tissue Structure and Development	3.54E-02 – 9.67E-04	12

Figure 4.16 ***Ontological Association of Dysregulated Serum Metabolites with Cellular Functionality and Disease Pathology*****.** Top enriched diseases and biological functions associated with dysregulated metabolomic profile within the serum following TCDD treatment using Ingenuity Pathway Analysis. The top 5 diseases and disorders (A), molecular and cellular functions (B) and physiological system development and function (C) associations are listed.

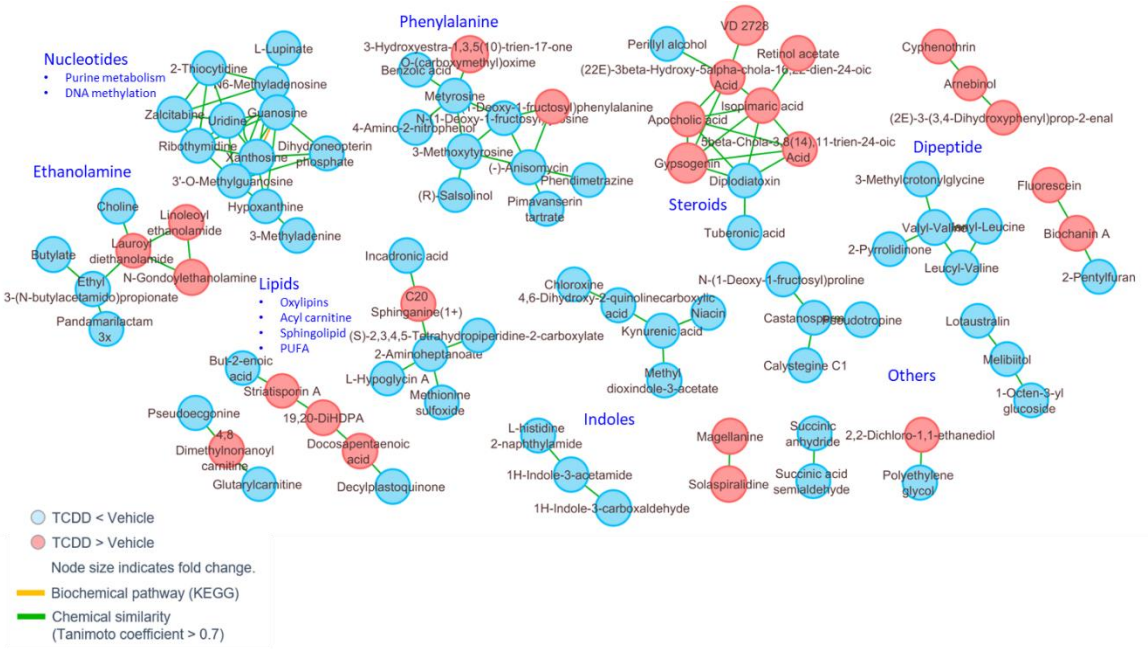

Figure 4.17 ***MetaMapp Network View of Significantly Changed Cecal Content Metabolites (p<0.05) in TCDD-treated Mice as Compared with the Vehicle Control Group*.** MetaMapp network view of significantly changed cecal content metabolites (p<0.05) in TCDD-treated mice as compared with the vehicle control group. The clustering is constructed based on biochemical relationships (KEGG) and chemical similarity (Tanimoto coefficient > 0.7).

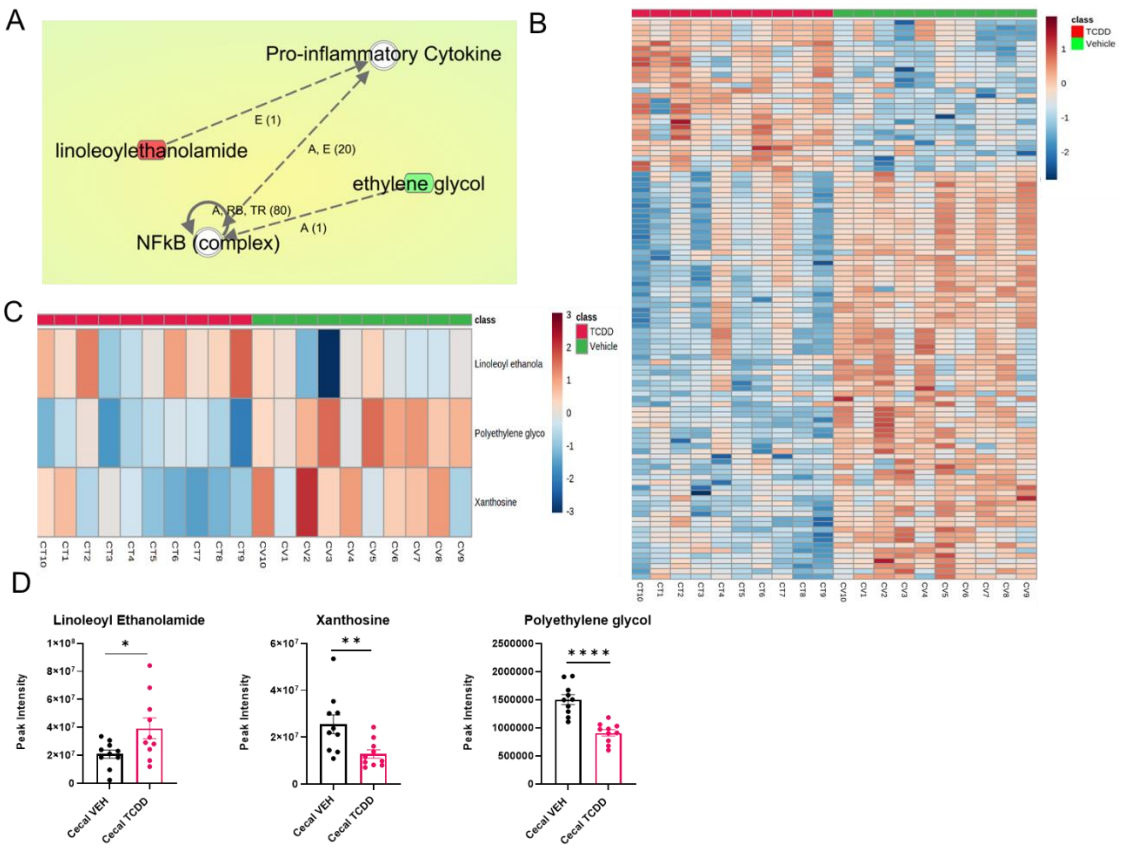

Figure 4.18 ***Pathway Analysis of Pathologically Relevant Metabolites in the Cecal Contents*****.** TCDD exposure promotes immunosuppression via modulations in the cecal metabolome. (A) Ingenuity pathway analysis of significantly modulated cecal metabolites (Metabolites in green are higher in the VEH treated mice, while those in red are higher in the TCDD exposed). (B) Heat map displaying abundance of individual metabolites within the cecal contents of VEH and TCDD mice. (C) Heat map displaying significantly modulates metabolites of interest within the cecal contents of VEH and TCDD mice. (D) Peak intensities identified via GC-MS of metabolites of interest that are differentially abundant between the cecal contents of VEH and TCDD mice (Linoleoyl Ethanolamide $t(18)=2.307$, $P=0.033$: Xanthosine $t(18)=2.895$, $P=0.009$: Polyetheylene Glycol $t(18)=5.705$, $P<0.0001$**).**

A **Diseases and Disorders**

Name	p-value range	Number of molecules
Cancer	4.73E-03 – 1.11E-03	3
Organismal Injury and Abnormalities	4.42E-02 – 1.11E-03	7
Tumor Morphology	4.73E-03 – 1.11E-03	3
Endocrine System Disorders	1.79E-02 – 5.56E-03	3
Metabolic Disease	3.55E-02 – 5.56E-03	4

B **Molecular and Cellular Functions**

Name	p-value range	Number of molecules
Small Molecule Biochemistry	4.42E-02 – 4.48E-04	6
Cell Death and Survival	3.55E-02 – 1.11E-03	4
Cellular Assembly and Organization	4.73E-03 – 4.73E-03	2
Cellular Function and Maintenance	2.67E-02 – 4.73E-03	3
Cell Morphology	2.67E-02 – 8.42E-03	2

C **Physiological System Development and Function**

Name	p-value range	Number of molecules
Nervous System Development and Function	4.42E-02 – 8.42E-03	5
Endocrine System Development and Function	2.67E-02 – 8.99E-03	2
Hematological System Development and Function	4.42E-02 – 8.99E-03	4
Immune Cell Trafficking	8.99E-03 – 8.99E-03	1
Organismal Development	2.33E-02 – 8.99E-03	4

Figure 4.19 ***Ontological Association of Dysregulated Cecal Metabolites with Cellular Functionality and Disease Pathology*****.** Top enriched diseases and biological functions associated with dysregulated metabolomic profile within the cecal content following TCDD treatment using Ingenuity Pathway Analysis. The top 5 diseases and disorders (A), molecular and cellular functions (B) and physiological system development and function (C) associations are listed.

CHAPTER 5

CONCLUSIONS AND SUMMARIES

The unregulated inflammatory processes that drive autoimmune disorders are a complicated result of dysregulated homeostasis between effector and regulatory components of the immune system. Despite the valiant efforts of the biomedical community to address these issues, there are no perfect solutions to combating the pathogenic inflammation that drives autoimmune disorders. Currently, the best hopes at combatting autoimmune disorders are to better understand how these pathogenic immunological processes initiate so that novel targeted therapeutics can be developed to prevent and treat chronic inflammation. While current market immunosuppressants are numerous, their side-effects and costs often outweigh their potential benefit.

In recent years, cannabinoid receptors and AHR have emerged as potential novel targets to suppress inflammation without overt toxic effects. Interestingly, while the endogenous ligands for these receptors play a critical role in regulating inflammation without mediating toxicity, some of the exogenous ligands can mediate significant toxicity. Thus, clearly additional studies are necessary to understand and identify new ligands that can suppress inflammation without causing toxicity.

To this end, in the current study, we investigated the effect of some AHR and Cannabinoid receptor ligands and demonstrated the manners by which 2 AHR ligands,

tryptamine and TCDD, can contribute to the anti-inflammatory processes associated with their consumption or exposure. Primarily, we demonstrated that tryptamine is innately able to inhibit the encephalitogenic capacity of the CD4+ T cells that drive demyelinating neuroinflammation by promoting their transition from a Th17 dominated pro-inflammatory landscape to an anti-inflammatory Treg dominated landscape. In the context of TCDD, we demonstrated that acute exposure to the contaminant yield shifts in the metabolome that contribute to the noted toxicity that follows exposure. These results further strengthen the pivotal role of the AHR in immunity, define how gut microorganisms can inhibit pathogenic neuroinflammation in a model of MS, and describe how acute exposure to toxic doses of dioxins can dysregulate inflammation.

Additionally, we demonstrated the benefit of orally consuming CBD, an active ingredient of Cannabis, during symptoms of autoimmune neuroinflammation and how locally within the CNS, CBD triggers a dramatic decrease in the inflammatory myeloid-derived immune processes. We further demonstrated that CBD is directly capable of inhibiting macrophage-mediated inflammation by inhibiting the cytokine IL-1β in a manner entirely independent of the classical cannabinoid receptors.

This work has provided novel insight to the molecular mechanisms that control inflammation under normal and encephalitogenic conditions and has demonstrated how exogenous compounds can exploit these systems to inhibit the pro-inflammatory processes that often go unregulated in autoimmune disorders.

REFERENCES

1. Dutta, R. & Trapp, B. D. Relapsing and progressive forms of multiple sclerosis: insights from pathology. *Curr Opin Neurol* **27**, 271–278 (2014).
2. Fletcher, J. M., Lalor, S. J., Sweeney, C. M., Tubridy, N. & Mills, K. H. G. T cells in multiple sclerosis and experimental autoimmune encephalomyelitis. *Clin Exp Immunol* **162**, 1–11 (2010).
3. Miller, S. D. & Karpus, W. J. Experimental autoimmune encephalomyelitis in the mouse. *Curr Protoc Immunol* **Chapter 15**, Unit 15.1 (2007).
4. Bittner, S., Afzali, A. M., Wiendl, H. & Meuth, S. G. Myelin oligodendrocyte glycoprotein (MOG35-55) induced experimental autoimmune encephalomyelitis (EAE) in C57BL/6 mice. *J Vis Exp* (2014) doi:10.3791/51275.
5. Constantinescu, C. S., Farooqi, N., O'Brien, K. & Gran, B. Experimental autoimmune encephalomyelitis (EAE) as a model for multiple sclerosis (MS). *Br. J. Pharmacol.* **164**, 1079–1106 (2011).
6. Lassmann, H. & Bradl, M. Multiple sclerosis: experimental models and reality. *Acta Neuropathol* **133**, 223–244 (2017).
7. Martins, T. B. *et al.* Analysis of proinflammatory and anti-inflammatory cytokine serum concentrations in patients with multiple sclerosis by using a multiplexed immunoassay. *Am J Clin Pathol* **136**, 696–704 (2011).
8. Khaibullin, T. *et al.* Elevated Levels of Proinflammatory Cytokines in Cerebrospinal Fluid of Multiple Sclerosis Patients. *Front Immunol* **8**, 531 (2017).

9. Escribano, B. M. *et al.* Dose-dependent S-allyl cysteine ameliorates multiple sclerosis disease-related pathology by reducing oxidative stress and biomarkers of dysbiosis in experimental autoimmune encephalomyelitis. *Eur J Pharmacol* **815**, 266–273 (2017).
10. Baecher-Allan, C. M. *et al.* CD2 Costimulation Reveals Defective Activity by Human CD4 $^{+}$ CD25 ^{hi} Regulatory Cells in Patients with Multiple Sclerosis. *J.I.* **186**, 3317–3326 (2011).
11. Vignali, D. A. A., Collison, L. W. & Workman, C. J. How regulatory T cells work. *Nat Rev Immunol* **8**, 523–532 (2008).
12. Kohm, A. P., Carpentier, P. A., Anger, H. A. & Miller, S. D. Cutting edge: CD4+CD25+ regulatory T cells suppress antigen-specific autoreactive immune responses and central nervous system inflammation during active experimental autoimmune encephalomyelitis. *J Immunol* **169**, 4712–4716 (2002).
13. Lozupone, C. A., Stombaugh, J. I., Gordon, J. I., Jansson, J. K. & Knight, R. Diversity, stability and resilience of the human gut microbiota. *Nature* **489**, 220–230 (2012).
14. Round, J. L. & Mazmanian, S. K. The gut microbiota shapes intestinal immune responses during health and disease. *Nat Rev Immunol* **9**, 313–323 (2009).
15. Moon, Y. Microbiome-Linked Crosstalk in the Gastrointestinal Exposome towards Host Health and Disease. *Pediatr Gastroenterol Hepatol Nutr* **19**, 221–228 (2016).
16. Ley, R. E., Peterson, D. A. & Gordon, J. I. Ecological and evolutionary forces shaping microbial diversity in the human intestine. *Cell* **124**, 837–848 (2006).
17. Belkaid, Y. & Hand, T. W. Role of the microbiota in immunity and inflammation. *Cell* **157**, 121–141 (2014).

18. Atarashi, K. *et al.* Treg induction by a rationally selected mixture of Clostridia strains from the human microbiota. *Nature* **500**, 232–236 (2013).
19. Krajmalnik-Brown, R., Ilhan, Z.-E., Kang, D.-W. & DiBaise, J. K. Effects of gut microbes on nutrient absorption and energy regulation. *Nutr Clin Pract* **27**, 201–214 (2012).
20. Secher, T. *et al.* Oral Administration of the Probiotic Strain Escherichia coli Nissle 1917 Reduces Susceptibility to Neuroinflammation and Repairs Experimental Autoimmune Encephalomyelitis-Induced Intestinal Barrier Dysfunction. *Front Immunol* **8**, 1096 (2017).
21. Forsberg, C. W. Sulfide Production from Cysteine by Desulfovibrio desulfuricans. *Appl Environ Microbiol* **39**, 453–455 (1980).
22. Tremlett, H. *et al.* Gut microbiota in early pediatric multiple sclerosis: a case-control study. *Eur J Neurol* **23**, 1308–1321 (2016).
23. Zhang, C. *et al.* Interactions between gut microbiota, host genetics and diet relevant to development of metabolic syndromes in mice. *ISME J* **4**, 232–241 (2010).
24. Lu, S. C. Glutathione synthesis. *Biochim Biophys Acta* **1830**, 3143–3153 (2013).
25. Choi, I.-Y. *et al.* In vivo evidence of oxidative stress in brains of patients with progressive multiple sclerosis. *Mult Scler* **24**, 1029–1038 (2018).
26. Sekhar, R. V. *et al.* Deficient synthesis of glutathione underlies oxidative stress in aging and can be corrected by dietary cysteine and glycine supplementation. *Am J Clin Nutr* **94**, 847–853 (2011).
27. Ortiz, G. G. *et al.* Immunology and oxidative stress in multiple sclerosis: clinical and basic approach. *Clin Dev Immunol* **2013**, 708659 (2013).

28. Van der Goes, A. *et al.* Reactive oxygen species enhance the migration of monocytes across the blood-brain barrier in vitro. *FASEB J* **15**, 1852–1854 (2001).
29. van der Goes, A. *et al.* Reactive oxygen species are required for the phagocytosis of myelin by macrophages. *J Neuroimmunol* **92**, 67–75 (1998).
30. Fischer, M. T. *et al.* NADPH oxidase expression in active multiple sclerosis lesions in relation to oxidative tissue damage and mitochondrial injury. *Brain* **135**, 886–899 (2012).
31. Jin, U.-H. *et al.* Microbiome-derived tryptophan metabolites and their aryl hydrocarbon receptor-dependent agonist and antagonist activities. *Mol. Pharmacol.* **85**, 777–788 (2014).
32. Li, G. & Young, K. D. Indole production by the tryptophanase TnaA in Escherichia coli is determined by the amount of exogenous tryptophan. *Microbiology (Reading)* **159**, 402–410 (2013).
33. Singh, N. P. *et al.* Dietary Indoles Suppress Delayed-Type Hypersensitivity by Inducing a Switch from Proinflammatory Th17 Cells to Anti-Inflammatory Regulatory T Cells through Regulation of MicroRNA. *J Immunol* **196**, 1108–1122 (2016).
34. Beischlag, T. V., Luis Morales, J., Hollingshead, B. D. & Perdew, G. H. The aryl hydrocarbon receptor complex and the control of gene expression. *Crit Rev Eukaryot Gene Expr* **18**, 207–250 (2008).
35. Denison, M. S., Soshilov, A. A., He, G., DeGroot, D. E. & Zhao, B. Exactly the same but different: promiscuity and diversity in the molecular mechanisms of action of the aryl hydrocarbon (dioxin) receptor. *Toxicol Sci* **124**, 1–22 (2011).

36. Singh, N. P. *et al.* Activation of Aryl Hydrocarbon Receptor (AhR) Leads to Reciprocal Epigenetic Regulation of FoxP3 and IL-17 Expression and Amelioration of Experimental Colitis. *PLoS ONE* **6**, e23522 (2011).
37. Nguyen, N. T., Hanieh, H., Nakahama, T. & Kishimoto, T. The roles of aryl hydrocarbon receptor in immune responses. *Int Immunol* **25**, 335–343 (2013).
38. Stevens, E. A., Mezrich, J. D. & Bradfield, C. A. The aryl hydrocarbon receptor: a perspective on potential roles in the immune system. *Immunology* **127**, 299–311 (2009).
39. Quintana, F. J. *et al.* Control of T(reg) and T(H)17 cell differentiation by the aryl hydrocarbon receptor. *Nature* **453**, 65–71 (2008).
40. Veldhoen, M. *et al.* The aryl hydrocarbon receptor links TH17-cell-mediated autoimmunity to environmental toxins. *Nature* **453**, 106–109 (2008).
41. Hwang, W.-B., Kim, D.-J., Oh, G.-S. & Park, J.-H. Aryl Hydrocarbon Receptor Ligands Indoxyl 3-sulfate and Indole-3-carbinol Inhibit FMS-like Tyrosine Kinase 3 Ligand-induced Bone Marrow-derived plasmacytoid Dendritic Cell Differentiation. *Immune Netw* **18**, e35 (2018).
42. Rothhammer, V. *et al.* Type I interferons and microbial metabolites of tryptophan modulate astrocyte activity and central nervous system inflammation via the aryl hydrocarbon receptor. *Nat Med* **22**, 586–597 (2016).
43. Duarte, J. H., Di Meglio, P., Hirota, K., Ahlfors, H. & Stockinger, B. Differential Influences of the Aryl Hydrocarbon Receptor on Th17 Mediated Responses in vitro and in vivo. *PLoS ONE* **8**, e79819 (2013).

44. Daly, C. & Rollins, B. J. Monocyte chemoattractant protein-1 (CCL2) in inflammatory disease and adaptive immunity: therapeutic opportunities and controversies. *Microcirculation* **10**, 247–257 (2003).
45. Galea, E. & Feinstein, D. L. Regulation of the expression of the inflammatory nitric oxide synthase (NOS2) by cyclic AMP. *FASEB J* **13**, 2125–2137 (1999).
46. Mizuno, M., Noto, D., Kaga, N., Chiba, A. & Miyake, S. The dual role of short fatty acid chains in the pathogenesis of autoimmune disease models. *PLoS ONE* **12**, e0173032 (2017).
47. Arpaia, N. *et al.* Metabolites produced by commensal bacteria promote peripheral regulatory T-cell generation. *Nature* **504**, 451–455 (2013).
48. Furusawa, Y. *et al.* Commensal microbe-derived butyrate induces the differentiation of colonic regulatory T cells. *Nature* **504**, 446–450 (2013).
49. Park, J. *et al.* Short-chain fatty acids induce both effector and regulatory T cells by suppression of histone deacetylases and regulation of the mTOR–S6K pathway. *Mucosal Immunol* **8**, 80–93 (2015).
50. Smith, P. M. *et al.* The microbial metabolites, short-chain fatty acids, regulate colonic Treg cell homeostasis. *Science* **341**, 569–573 (2013).
51. Aoyama, M., Kotani, J. & Usami, M. Butyrate and propionate induced activated or non-activated neutrophil apoptosis via HDAC inhibitor activity but without activating GPR-41/GPR-43 pathways. *Nutrition* **26**, 653–661 (2010).
52. Van den Abbeele, P. *et al.* Butyrate-producing Clostridium cluster XIVa species specifically colonize mucins in an in vitro gut model. *ISME J* **7**, 949–961 (2013).

53. Kim, C. H., Park, J. & Kim, M. Gut microbiota-derived short-chain Fatty acids, T cells, and inflammation. *Immune Netw* **14**, 277–288 (2014).

54. Miyake, S. *et al.* Dysbiosis in the Gut Microbiota of Patients with Multiple Sclerosis, with a Striking Depletion of Species Belonging to Clostridia XIVa and IV Clusters. *PLoS One* **10**, e0137429 (2015).

55. Chitrala, K. N. *et al.* CD44 deletion leading to attenuation of experimental autoimmune encephalomyelitis results from alterations in gut microbiome in mice. *Eur J Immunol* **47**, 1188–1199 (2017).

56. André, P., Laugerette, F. & Féart, C. Metabolic Endotoxemia: A Potential Underlying Mechanism of the Relationship between Dietary Fat Intake and Risk for Cognitive Impairments in Humans? *Nutrients* **11**, (2019).

57. Fawley, J. & Gourlay, D. M. Intestinal alkaline phosphatase: a summary of its role in clinical disease. *J Surg Res* **202**, 225–234 (2016).

58. Kaliannan, K., Wang, B., Li, X.-Y., Kim, K.-J. & Kang, J. X. A host-microbiome interaction mediates the opposing effects of omega-6 and omega-3 fatty acids on metabolic endotoxemia. *Sci Rep* **5**, 11276 (2015).

59. Bowling, A. C. Complementary and alternative medicine in multiple sclerosis. *Continuum (Minneap Minn)* **16**, 78–89 (2010).

60. Bates, D. *et al.* A double-blind controlled trial of long chain n-3 polyunsaturated fatty acids in the treatment of multiple sclerosis. *J Neurol Neurosurg Psychiatry* **52**, 18–22 (1989).

61. Nakatsuji, T. *et al.* Antimicrobial property of lauric acid against Propionibacterium acnes: its therapeutic potential for inflammatory acne vulgaris. *J Invest Dermatol* **129**, 2480–2488 (2009).
62. Rocha, D. M., Caldas, A. P., Oliveira, L. L., Bressan, J. & Hermsdorff, H. H. Saturated fatty acids trigger TLR4-mediated inflammatory response. *Atherosclerosis* **244**, 211–215 (2016).
63. Haghikia, A. *et al.* Dietary Fatty Acids Directly Impact Central Nervous System Autoimmunity via the Small Intestine. *Immunity* **43**, 817–829 (2015).
64. Banks, W. A. Characteristics of compounds that cross the blood-brain barrier. *BMC Neurol* **9 Suppl 1**, S3 (2009).
65. Banks, W. A., Kastin, A. J. & Broadwell, R. D. Passage of Cytokines across the Blood-Brain Barrier. *Neuroimmunomodulation* **2**, 241–248 (1995).
66. Pan, W. *et al.* Cytokine signaling modulates blood-brain barrier function. *Curr Pharm Des* **17**, 3729–3740 (2011).
67. Gutierrez, E. G., Banks, W. A. & Kastin, A. J. Murine tumor necrosis factor alpha is transported from blood to brain in the mouse. *J Neuroimmunol* **47**, 169–176 (1993).
68. Lexchin, J. L., Cude-Simpson, K. D. & Stancer, H. C. Brain and blood indole metabolites after peripheral administration of14C-5-HT in rat. *Neurochem Res* **2**, 39–50 (1977).
69. Kannan, R. *et al.* Evidence for carrier-mediated transport of glutathione across the blood-brain barrier in the rat. *J Clin Invest* **85**, 2009–2013 (1990).
70. Banks, W. A. & Robinson, S. M. Minimal penetration of lipopolysaccharide across the murine blood-brain barrier. *Brain Behav Immun* **24**, 102–109 (2010).

71. Braniste, V. *et al.* The gut microbiota influences blood-brain barrier permeability in mice. *Sci Transl Med* **6**, 263ra158 (2014).

72. Frost, G. *et al.* The short-chain fatty acid acetate reduces appetite via a central homeostatic mechanism. *Nat Commun* **5**, 3611 (2014).

73. Lafaye, G., Karila, L., Blecha, L. & Benyamina, A. Cannabis, cannabinoids, and health. *Dialogues Clin Neurosci* **19**, 309–316 (2017).

74. Volkow, N. D., Baler, R. D., Compton, W. M. & Weiss, S. R. B. Adverse health effects of marijuana use. *N Engl J Med* **370**, 2219–2227 (2014).

75. Nagarkatti, P., Pandey, R., Rieder, S. A., Hegde, V. L. & Nagarkatti, M. Cannabinoids as novel anti-inflammatory drugs. *Future Med Chem* **1**, 1333–1349 (2009).

76. Galiègue, S. *et al.* Expression of central and peripheral cannabinoid receptors in human immune tissues and leukocyte subpopulations. *Eur J Biochem* **232**, 54–61 (1995).

77. Pacher, P., Bátkai, S. & Kunos, G. The endocannabinoid system as an emerging target of pharmacotherapy. *Pharmacol Rev* **58**, 389–462 (2006).

78. Svizenska, I., Dubovy, P. & Sulcova, A. Cannabinoid receptors 1 and 2 (CB1 and CB2), their distribution, ligands and functional involvement in nervous system structures — A short review. *Pharmacology Biochemistry and Behavior* **90**, 501–511 (2008).

79. Basu, S. & Dittel, B. N. Unraveling the complexities of cannabinoid receptor 2 (CB2) immune regulation in health and disease. *Immunol Res* **51**, 26–38 (2011).

80. Nichols, J. M. & Kaplan, B. L. F. Immune Responses Regulated by Cannabidiol. *Cannabis Cannabinoid Res* **5**, 12–31 (2020).

81. Vučković, S., Srebro, D., Vujović, K. S., Vučetić, Č. & Prostran, M. Cannabinoids and Pain: New Insights From Old Molecules. *Front. Pharmacol.* **9**, 1259 (2018).

82. Zlebnik, N. E. & Cheer, J. F. Beyond the CB1 Receptor: Is Cannabidiol the Answer for Disorders of Motivation? *Annu Rev Neurosci* **39**, 1–17 (2016).

83. Maroon, J. & Bost, J. Review of the neurological benefits of phytocannabinoids. *Surg Neurol Int* **9**, 91 (2018).

84. Al-Ghezi, Z. Z., Busbee, P. B., Alghetaa, H., Nagarkatti, P. S. & Nagarkatti, M. Combination of cannabinoids, delta-9-tetrahydrocannabinol (THC) and cannabidiol (CBD), mitigates experimental autoimmune encephalomyelitis (EAE) by altering the gut microbiome. *Brain Behav Immun* **82**, 25–35 (2019).

85. Mohammed, A. *et al.* Δ9-Tetrahydrocannabinol Prevents Mortality from Acute Respiratory Distress Syndrome through the Induction of Apoptosis in Immune Cells, Leading to Cytokine Storm Suppression. *Int J Mol Sci* **21**, (2020).

86. Becker, W. *et al.* Cannabinoid Receptor Activation on Haematopoietic Cells and Enterocytes Protects against Colitis. *Journal of Crohn's and Colitis* jjaa253 (2020) doi:10.1093/ecco-jcc/jjaa253.

87. Becker, W. *et al.* Activation of Cannabinoid Receptor 2 Prevents Colitis-Associated Colon Cancer through Myeloid Cell De-activation Upstream of IL-22 Production. *iScience* **23**, 101504 (2020).

88. White, S. S. & Birnbaum, L. S. An Overview of the Effects of Dioxins and Dioxin-Like Compounds on Vertebrates, as Documented in Human and Ecological

Epidemiology. *Journal of Environmental Science and Health, Part C* **27**, 197–211 (2009).

89. Mimura, J. & Fujii-Kuriyama, Y. Functional role of AhR in the expression of toxic effects by TCDD. *Biochim Biophys Acta* **1619**, 263–268 (2003).
90. Sun, Y. V. Comparative analysis of dioxin response elements in human, mouse and rat genomic sequences. *Nucleic Acids Research* **32**, 4512–4523 (2004).
91. Birnbaum, L. S. Dioxin and the AH Receptor: Synergy of Discovery. *Curr Opin Toxicol* **2**, 120–123 (2017).
92. Pirkle, J. L. *et al.* Estimates of the half-life of 2,3,7,8-tetrachlorodibenzo-p-dioxin in Vietnam Veterans of Operation Ranch Hand. *J Toxicol Environ Health* **27**, 165–171 (1989).
93. Reich, D. S., Lucchinetti, C. F. & Calabresi, P. A. Multiple Sclerosis. *N Engl J Med* **378**, 169–180 (2018).
94. Dos Passos, G. R., Sato, D. K., Becker, J. & Fujihara, K. Th17 Cells Pathways in Multiple Sclerosis and Neuromyelitis Optica Spectrum Disorders: Pathophysiological and Therapeutic Implications. *Mediators Inflamm.* **2016**, 5314541 (2016).
95. Costantino, C. M., Baecher-Allan, C. & Hafler, D. A. Multiple sclerosis and regulatory T cells. *J. Clin. Immunol.* **28**, 697–706 (2008).
96. Li, Y.-F. *et al.* The proportion of peripheral regulatory T cells in patients with Multiple Sclerosis: A meta-analysis. *Mult Scler Relat Disord* **28**, 75–80 (2019).
97. Correale, J., Farez, M. F. & Gaitán, M. I. Environmental factors influencing multiple sclerosis in Latin America. *Mult Scler J Exp Transl Clin* **3**, 2055217317715049 (2017).

98. O'Gorman, C., Lucas, R. & Taylor, B. Environmental risk factors for multiple sclerosis: a review with a focus on molecular mechanisms. *Int J Mol Sci* **13**, 11718–11752 (2012).

99. Pandiyan, P. *et al.* Microbiome Dependent Regulation of Tregs and Th17 Cells in Mucosa. *Front. Immunol.* **10**, 426 (2019).

100. Dopkins, N., Nagarkatti, P. S. & Nagarkatti, M. The role of gut microbiome and associated metabolome in the regulation of neuroinflammation in multiple sclerosis and its implications in attenuating chronic inflammation in other inflammatory and autoimmune disorders. *Immunology* **154**, 178–185 (2018).

101. Castillo-Álvarez, F. & Marzo-Sola, M. E. Role of intestinal microbiota in the development of multiple sclerosis. *Neurología (English Edition)* **32**, 175–184 (2017).

102. Kirby, T. O. & Ochoa-Repáraz, J. The Gut Microbiome in Multiple Sclerosis: A Potential Therapeutic Avenue. *Med Sci (Basel)* **6**, (2018).

103. Dehner, C., Fine, R. & Kriegel, M. A. The microbiome in systemic autoimmune disease: mechanistic insights from recent studies. *Curr Opin Rheumatol* **31**, 201–207 (2019).

104. Ochoa-Repáraz, J. *et al.* A polysaccharide from the human commensal Bacteroides fragilis protects against CNS demyelinating disease. *Mucosal Immunol* **3**, 487–495 (2010).

105. Rothhammer, V. & Quintana, F. J. Environmental control of autoimmune inflammation in the central nervous system. *Curr. Opin. Immunol.* **43**, 46–53 (2016).

106. Vinolo, M. A. R., Rodrigues, H. G., Nachbar, R. T. & Curi, R. Regulation of Inflammation by Short Chain Fatty Acids. *Nutrients* **3**, 858–876 (2011).

107. Lee, Y. K., Menezes, J. S., Umesaki, Y. & Mazmanian, S. K. Proinflammatory T-cell responses to gut microbiota promote experimental autoimmune encephalomyelitis. *Proc. Natl. Acad. Sci. U.S.A.* **108 Suppl 1**, 4615–4622 (2011).

108. Opazo, M. C. *et al.* Intestinal Microbiota Influences Non-intestinal Related Autoimmune Diseases. *Front Microbiol* **9**, 432 (2018).

109. Saltzman, E. T., Palacios, T., Thomsen, M. & Vitetta, L. Intestinal Microbiome Shifts, Dysbiosis, Inflammation, and Non-alcoholic Fatty Liver Disease. *Front Microbiol* **9**, 61 (2018).

110. Li, B., Selmi, C., Tang, R., Gershwin, M. E. & Ma, X. The microbiome and autoimmunity: a paradigm from the gut-liver axis. *Cell. Mol. Immunol.* **15**, 595–609 (2018).

111. Williams, B. B. *et al.* Discovery and characterization of gut microbiota decarboxylases that can produce the neurotransmitter tryptamine. *Cell Host Microbe* **16**, 495–503 (2014).

112. Gao, J. *et al.* Impact of the Gut Microbiota on Intestinal Immunity Mediated by Tryptophan Metabolism. *Front Cell Infect Microbiol* **8**, 13 (2018).

113. Glatigny, S. & Bettelli, E. Experimental Autoimmune Encephalomyelitis (EAE) as Animal Models of Multiple Sclerosis (MS). *Cold Spring Harbor Perspectives in Medicine* **8**, a028977 (2018).

114. Mousseau, D. D. Tryptamine: a metabolite of tryptophan implicated in various neuropsychiatric disorders. *Metab Brain Dis* **8**, 1–44 (1993).

115. Nair, A. B. & Jacob, S. A simple practice guide for dose conversion between animals and human. *J Basic Clin Pharm* **7**, 27–31 (2016).

116. Wüst, N., Rauscher-Gabernig, E., Steinwider, J., Bauer, F. & Paulsen, P. Risk assessment of dietary exposure to tryptamine for the Austrian population. *Food Addit Contam Part A Chem Anal Control Expo Risk Assess* **34**, 404–420 (2017).

117. Pennartz, S., Reiss, S., Biloune, R., Hasselmann, D. & Bosio, A. Generation of single-cell suspensions from mouse neural tissue. *J Vis Exp* (2009) doi:10.3791/1267.

118. McPherson, R. C., Cambrook, H. E., O'Connor, R. A. & Anderton, S. M. Induction of Passive EAE Using Myelin-Reactive CD4+ T Cells. in *T-Helper Cells* (eds. Waisman, A. & Becher, B.) vol. 1193 187–198 (Springer New York, 2014).

119. Carriel, V., Campos, A., Alaminos, M., Raimondo, S. & Geuna, S. Staining Methods for Normal and Regenerative Myelin in the Nervous System. in *Histochemistry of Single Molecules* (eds. Pellicciari, C. & Biggiogera, M.) vol. 1560 207–218 (Springer New York, 2017).

120. Feldman, A. T. & Wolfe, D. Tissue Processing and Hematoxylin and Eosin Staining. in *Histopathology* (ed. Day, C. E.) vol. 1180 31–43 (Springer New York, 2014).

121. Weber, N. *et al.* Nephele: a cloud platform for simplified, standardized and reproducible microbiome data analysis. *Bioinformatics* **34**, 1411–1413 (2018).

122. Segata, N. *et al.* Metagenomic biomarker discovery and explanation. *Genome Biol.* **12**, R60 (2011).

123. Zhao, G., Nyman, M. & Jönsson, J. A. Rapid determination of short-chain fatty acids in colonic contents and faeces of humans and rats by acidified water-extraction and direct-injection gas chromatography. *Biomed. Chromatogr.* **20**, 674–682 (2006).

124. Busbee, P. B. *et al.* Indole-3-carbinol prevents colitis and associated microbial dysbiosis in an IL-22–dependent manner. *JCI Insight* **5**, (2020).

125. Lefever, D. E. *et al.* TCDD modulation of gut microbiome correlated with liver and immune toxicity in streptozotocin (STZ)-induced hyperglycemic mice. *Toxicology and Applied Pharmacology* **304**, 48–58 (2016).

126. Brawner, K. M. *et al.* Depletion of dietary aryl hydrocarbon receptor ligands alters microbiota composition and function. *Sci Rep* **9**, 14724 (2019).

127. Jangi, S. *et al.* Alterations of the human gut microbiome in multiple sclerosis. *Nat Commun* **7**, 12015 (2016).

128. Berer, K. *et al.* Gut microbiota from multiple sclerosis patients enables spontaneous autoimmune encephalomyelitis in mice. *Proceedings of the National Academy of Sciences* **114**, 10719–10724 (2017).

129. Cekanaviciute, E. *et al.* Gut bacteria from multiple sclerosis patients modulate human T cells and exacerbate symptoms in mouse models. *Proceedings of the National Academy of Sciences* **114**, 10713–10718 (2017).

130. Lee, N. & Kim, W.-U. Microbiota in T-cell homeostasis and inflammatory diseases. *Experimental & Molecular Medicine* **49**, e340–e340 (2017).

131. Shahi, S. K., Freedman, S. N. & Mangalam, A. K. Gut microbiome in multiple sclerosis: The players involved and the roles they play. *Gut Microbes* **8**, 607–615 (2017).

132. Chu, F. *et al.* Gut Microbiota in Multiple Sclerosis and Experimental Autoimmune Encephalomyelitis: Current Applications and Future Perspectives. *Mediators Inflamm.* **2018**, 8168717 (2018).

133. Rouse, M., Singh, N. P., Nagarkatti, P. S. & Nagarkatti, M. Indoles mitigate the development of experimental autoimmune encephalomyelitis by induction of reciprocal differentiation of regulatory T cells and Th17 cells. *Br. J. Pharmacol.* **169**, 1305–1321 (2013).

134. Ginwala, R. *et al.* Apigenin, a Natural Flavonoid, Attenuates EAE Severity Through the Modulation of Dendritic Cell and Other Immune Cell Functions. *J Neuroimmune Pharmacol* **11**, 36–47 (2016).

135. Rouse, M., Rao, R., Nagarkatti, M. & Nagarkatti, P. S. 3,3'-diindolylmethane ameliorates experimental autoimmune encephalomyelitis by promoting cell cycle arrest and apoptosis in activated T cells through microRNA signaling pathways. *J. Pharmacol. Exp. Ther.* **350**, 341–352 (2014).

136. Ye, J. *et al.* The Aryl Hydrocarbon Receptor Preferentially Marks and Promotes Gut Regulatory T Cells. *Cell Rep* **21**, 2277–2290 (2017).

137. Ji, J. & Qu, H. Cross-regulatory Circuit Between AHR and Microbiota. *Current Drug Metabolism* **20**, 4–8 (2019).

138. Wlodarska, M., Kostic, A. D. & Xavier, R. J. An integrative view of microbiome-host interactions in inflammatory bowel diseases. *Cell Host Microbe* **17**, 577–591 (2015).

139. Shi, Z. *et al.* Dysbiosis of gut microbiota in patients with neuromyelitis optica spectrum disorders: A cross sectional study. *Journal of Neuroimmunology* **339**, 577126 (2020).

140. Fan, P., Liu, P., Song, P., Chen, X. & Ma, X. Moderate dietary protein restriction alters the composition of gut microbiota and improves ileal barrier function in adult pig model. *Sci Rep* **7**, 43412 (2017).

141. Leng, Y. *et al.* Effects of acute intra-abdominal hypertension on multiple intestinal barrier functions in rats. *Sci Rep* **6**, 22814 (2016).

142. Yu, L. C.-H. Microbiota dysbiosis and barrier dysfunction in inflammatory bowel disease and colorectal cancers: exploring a common ground hypothesis. *Journal of Biomedical Science* **25**, (2018).

143. Paun, A. & Danska, J. S. Immuno-ecology: how the microbiome regulates tolerance and autoimmunity. *Current Opinion in Immunology* **37**, 34–39 (2015).

144. Goldenberg, M. M. Multiple sclerosis review. *P T* **37**, 175–184 (2012).

145. Huang, W.-J., Chen, W.-W. & Zhang, X. Multiple sclerosis: Pathology, diagnosis and treatments. *Exp Ther Med* **13**, 3163–3166 (2017).

146. Hartung, D. M., Bourdette, D. N., Ahmed, S. M. & Whitham, R. H. The cost of multiple sclerosis drugs in the US and the pharmaceutical industry: Too big to fail? *Neurology* **84**, 2185–2192 (2015).

147. Dargahi, N. *et al.* Multiple Sclerosis: Immunopathology and Treatment Update. *Brain Sci* **7**, (2017).

148. Ahmed, W. & Katz, S. Therapeutic Use of Cannabis in Inflammatory Bowel Disease. *Gastroenterol Hepatol (N Y)* **12**, 668–679 (2016).

149. Mohammed, A. *et al.* Protective effects of Δ9 -tetrahydrocannabinol against enterotoxin-induced acute respiratory distress syndrome are mediated by modulation of microbiota. *Br J Pharmacol* **177**, 5078–5095 (2020).

150. Rodríguez Mesa, X. M. *et al.* Therapeutic Prospects of Cannabinoids in the Immunomodulation of Prevalent Autoimmune Diseases. *Cannabis Cannabinoid Res* (2021) doi:10.1089/can.2020.0183.

151. Vermersch, P. Sativex ® (tetrahydrocannabinol + cannabidiol), an endocannabinoid system modulator: basic features and main clinical data. *Expert Review of Neurotherapeutics* **11**, 15–19 (2011).

152. Al-Ghezi, Z. Z., Miranda, K., Nagarkatti, M. & Nagarkatti, P. S. Combination of Cannabinoids, Δ9- Tetrahydrocannabinol and Cannabidiol, Ameliorates Experimental Multiple Sclerosis by Suppressing Neuroinflammation Through Regulation of miRNA-Mediated Signaling Pathways. *Front Immunol* **10**, 1921 (2019).

153. Singh, N. P., Hegde, V. L., Hofseth, L. J., Nagarkatti, M. & Nagarkatti, P. Resveratrol (trans-3,5,4'-trihydroxystilbene) ameliorates experimental allergic encephalomyelitis, primarily via induction of apoptosis in T cells involving activation of aryl hydrocarbon receptor and estrogen receptor. *Mol. Pharmacol.* **72**, 1508–1521 (2007).

154. Rouse, M., Singh, N. P., Nagarkatti, P. S. & Nagarkatti, M. Indoles mitigate the development of experimental autoimmune encephalomyelitis by induction of reciprocal differentiation of regulatory T cells and Th17 cells. *Br. J. Pharmacol.* **169**, 1305–1321 (2013).

155. Dopkins, N. *et al.* Tryptamine Attenuates Experimental Multiple Sclerosis Through Activation of Aryl Hydrocarbon Receptor. *Front Pharmacol* **11**, 619265 (2020).

156. Bolyen, E. *et al.* Reproducible, interactive, scalable and extensible microbiome data science using QIIME 2. *Nat Biotechnol* **37**, 852–857 (2019).

157. Weber, N. *et al.* Nephele: a cloud platform for simplified, standardized and reproducible microbiome data analysis. *Bioinformatics* **34**, 1411–1413 (2018).

158. Wickham, H. *ggplot2: elegant graphics for data analysis*. (Springer, 2016).

159. Paradis, E., Claude, J. & Strimmer, K. APE: Analyses of Phylogenetics and Evolution in R language. *Bioinformatics* **20**, 289–290 (2004).

160. McMurdie, P. J. & Holmes, S. phyloseq: An R Package for Reproducible Interactive Analysis and Graphics of Microbiome Census Data. *PLoS ONE* **8**, e61217 (2013).

161. Gérikas Ribeiro, C. *et al.* Pico and nanoplankton abundance and carbon stocks along the Brazilian Bight. *PeerJ* **4**, e2587 (2016).

162. Butler, A., Hoffman, P., Smibert, P., Papalexi, E. & Satija, R. Integrating single-cell transcriptomic data across different conditions, technologies, and species. *Nat. Biotechnol.* **36**, 411–420 (2018).

163. Stuart, T. *et al.* Comprehensive Integration of Single-Cell Data. *Cell* **177**, 1888-1902.e21 (2019).

164. Miranda, K. *et al.* MicroRNA-30 modulates metabolic inflammation by regulating Notch signaling in adipose tissue macrophages. *Int J Obes (Lond)* **42**, 1140–1150 (2018).

165. Li, H.-D. *et al.* Wogonin attenuates inflammation by activating PPAR-γ in alcoholic liver disease. *International Immunopharmacology* **50**, 95–106 (2017).

166. Elliott, D. M., Singh, N., Nagarkatti, M. & Nagarkatti, P. S. Cannabidiol Attenuates Experimental Autoimmune Encephalomyelitis Model of Multiple Sclerosis Through Induction of Myeloid-Derived Suppressor Cells. *Front Immunol* **9**, 1782 (2018).

167. Yang, X., Bam, M., Nagarkatti, P. S. & Nagarkatti, M. Cannabidiol Regulates Gene Expression in Encephalitogenic T cells Using Histone Methylation and noncoding RNA during Experimental Autoimmune Encephalomyelitis. *Sci Rep* **9**, 15780 (2019).

168. Corey-Bloom, J. *et al.* Smoked cannabis for spasticity in multiple sclerosis: a randomized, placebo-controlled trial. *CMAJ* **184**, 1143–1150 (2012).

169. Paré, A. *et al.* IL-1β enables CNS access to CCR2 ^{hi} monocytes and the generation of pathogenic cells through GM-CSF released by CNS endothelial cells. *Proc Natl Acad Sci USA* **115**, E1194–E1203 (2018).

170. Elliott, D. M., Singh, N., Nagarkatti, M. & Nagarkatti, P. S. Cannabidiol Attenuates Experimental Autoimmune Encephalomyelitis Model of Multiple Sclerosis Through Induction of Myeloid-Derived Suppressor Cells. *Front Immunol* **9**, 1782 (2018).

171. Boziki, M. K. *et al.* Microbiome in Multiple Sclerosis; Where Are We, What We Know and Do Not Know. *Brain Sci* **10**, (2020).

172. Mestre, L., Carrillo-Salinas, F. J., Mecha, M., Feliú, A. & Guaza, C. Gut microbiota, cannabinoid system and neuroimmune interactions: New perspectives in multiple sclerosis. *Biochemical Pharmacology* **157**, 51–66 (2018).

173. Kadowaki, A. & Quintana, F. J. The Gut-CNS Axis in Multiple Sclerosis. *Trends Neurosci* **43**, 622–634 (2020).

174. Zhu, S. *et al.* The progress of gut microbiome research related to brain disorders. *J Neuroinflammation* **17**, 25 (2020).

175. Lublin, F. *et al.* Oral fingolimod in primary progressive multiple sclerosis (INFORMS): a phase 3, randomised, double-blind, placebo-controlled trial. *Lancet* **387**, 1075–1084 (2016).

176. Waldman, A. *et al.* Multiple sclerosis in children: an update on clinical diagnosis, therapeutic strategies, and research. *Lancet Neurol* **13**, 936–948 (2014).

177. Paolicelli, D., Manni, A., Iaffaldano, A. & Trojano, M. Efficacy and Safety of Oral Therapies for Relapsing-Remitting Multiple Sclerosis. *CNS Drugs* (2020) doi:10.1007/s40263-019-00691-7.

178. Aranami, T. & Yamamura, T. Th17 Cells and Autoimmune Encephalomyelitis (EAE/MS). *Allergology International* **57**, 115–120 (2008).

179. Fletcher, J. M., Lalor, S. J., Sweeney, C. M., Tubridy, N. & Mills, K. H. G. T cells in multiple sclerosis and experimental autoimmune encephalomyelitis. *Clin. Exp. Immunol.* **162**, 1–11 (2010).

180. Herz, J., Filiano, A. J., Smith, A., Yogev, N. & Kipnis, J. Myeloid Cells in the Central Nervous System. *Immunity* **46**, 943–956 (2017).

181. Ghasemi, N., Razavi, S. & Nikzad, E. Multiple Sclerosis: Pathogenesis, Symptoms, Diagnoses and Cell-Based Therapy. *Cell J* **19**, 1–10 (2017).

182. Bruni, N. *et al.* Cannabinoid Delivery Systems for Pain and Inflammation Treatment. *Molecules* **23**, (2018).

183. Bellnier, T., Brown, G. W. & Ortega, T. R. Preliminary evaluation of the efficacy, safety, and costs associated with the treatment of chronic pain with medical cannabis. *Ment Health Clin* **8**, 110–115 (2018).

184. Paré, A. *et al.* IL-1β enables CNS access to CCR2 ^{hi} monocytes and the generation of pathogenic cells through GM-CSF released by CNS endothelial cells. *Proc Natl Acad Sci USA* **115**, E1194–E1203 (2018).

185. Zhu, B. *et al.* CD11b+Ly-6C(hi) suppressive monocytes in experimental autoimmune encephalomyelitis. *J. Immunol.* **179**, 5228–5237 (2007).

186. Crook, K. R. & Liu, P. Role of myeloid-derived suppressor cells in autoimmune disease. *World J Immunol* **4**, 26–33 (2014).

187. Ioannou, M. *et al.* Crucial Role of Granulocytic Myeloid-Derived Suppressor Cells in the Regulation of Central Nervous System Autoimmune Disease. *The Journal of Immunology* **188**, 1136–1146 (2012).

188. Hegde, V. L., Nagarkatti, P. S. & Nagarkatti, M. Role of myeloid-derived suppressor cells in amelioration of experimental autoimmune hepatitis following activation of TRPV1 receptors by cannabidiol. *PLoS One* **6**, e18281 (2011).

189. Leweke, F. M. *et al.* Cannabidiol enhances anandamide signaling and alleviates psychotic symptoms of schizophrenia. *Transl Psychiatry* **2**, e94 (2012).

190. Varga, T., Czimmerer, Z. & Nagy, L. PPARs are a unique set of fatty acid regulated transcription factors controlling both lipid metabolism and inflammation. *Biochimica et Biophysica Acta (BBA) - Molecular Basis of Disease* **1812**, 1007–1022 (2011).

191. Wahli, W. & Michalik, L. PPARs at the crossroads of lipid signaling and inflammation. *Trends in Endocrinology & Metabolism* **23**, 351–363 (2012).

192. O'Sullivan, S. E. An update on PPAR activation by cannabinoids. *Br J Pharmacol* **173**, 1899–1910 (2016).

193. Zizzo, G. & Cohen, P. L. The PPAR-γ antagonist GW9662 elicits differentiation of M2c-like cells and upregulation of the MerTK/Gas6 axis: a key role for PPAR-γ in human macrophage polarization. *J Inflamm* **12**, 36 (2015).

194. Heming, M. *et al.* Peroxisome Proliferator-Activated Receptor-γ Modulates the Response of Macrophages to Lipopolysaccharide and Glucocorticoids. *Front Immunol* **9**, 893 (2018).

195. Ding, J. *et al.* Pore-forming activity and structural autoinhibition of the gasdermin family. *Nature* **535**, 111–116 (2016).

196. Broz, P., Pelegrín, P. & Shao, F. The gasdermins, a protein family executing cell death and inflammation. *Nat. Rev. Immunol.* (2019) doi:10.1038/s41577-019-0228-2.

197. Erben, U. *et al.* A guide to histomorphological evaluation of intestinal inflammation in mouse models. *Int J Clin Exp Pathol* **7**, 4557–4576 (2014).

198. Greenson, J. K., Stern, R. A., Carpenter, S. L. & Barnett, J. L. The clinical significance of focal active colitis. *Hum Pathol* **28**, 729–733 (1997).

199. Nouri, M., Bredberg, A., Weström, B. & Lavasani, S. Intestinal barrier dysfunction develops at the onset of experimental autoimmune encephalomyelitis, and can be induced by adoptive transfer of auto-reactive T cells. *PLoS One* **9**, e106335 (2014).

200. Miyauchi, E. *et al.* Gut microorganisms act together to exacerbate inflammation in spinal cords. *Nature* **585**, 102–106 (2020).

201. Fournier, B. M. & Parkos, C. A. The role of neutrophils during intestinal inflammation. *Mucosal Immunol* **5**, 354–366 (2012).

202. Institute of Medicine (US) Committee to Review the Health Effects in Vietnam Veterans of Exposure to Herbicides. *Veterans and Agent Orange: Health Effects of Herbicides Used in Vietnam*. (National Academies Press (US), 1994).

203. Safe, S. *et al.* 2,3,7,8-Tetrachlorodibenzo-p-dioxin (TCDD) and Related Compounds as Antioestrogens: Characterization and Mechanism of Action. *Pharmacology & Toxicology* **69**, 400–409 (1991).

204. Mandal, P. K. Dioxin: a review of its environmental effects and its aryl hydrocarbon receptor biology. *Journal of Comparative Physiology B* **175**, 221–230 (2005).

205. Kerkvliet, N. I. Recent advances in understanding the mechanisms of TCDD immunotoxicity. *International Immunopharmacology* **2**, 277–291 (2002).

206. Xu, J. *et al.* Association between dioxin and cancer incidence and mortality: a meta-analysis. *Scientific Reports* **6**, (2016).

207. Antkiewicz, D. S., Burns, C. G., Carney, S. A., Peterson, R. E. & Heideman, W. Heart Malformation Is an Early Response to TCDD in Embryonic Zebrafish. *Toxicological Sciences* **84**, 368–377 (2005).

208. Suskind, R. R. Chloracne, 'the hallmark of dioxin intoxication'. *Scand J Work Environ Health* **11**, 165–171 (1985).

209. Birnbaum, L. S. The mechanism of dioxin toxicity: relationship to risk assessment. *Environmental Health Perspectives* **102**, 157–167 (1994).

210. Singh, N. P., Singh, U. P., Guan, H., Nagarkatti, P. & Nagarkatti, M. Prenatal Exposure to TCDD Triggers Significant Modulation of microRNA Expression Profile in the Thymus That Affects Consequent Gene Expression. *PLoS ONE* **7**, e45054 (2012).

211. Okino, S. T. & Whitlock, J. P. Dioxin induces localized, graded changes in chromatin structure: implications for Cyp1A1 gene transcription. *Mol. Cell. Biol.* **15**, 3714–3721 (1995).

212. Fader, K. A. *et al.* 2,3,7,8-Tetrachlorodibenzo-p-dioxin (TCDD)-elicited effects on bile acid homeostasis: Alterations in biosynthesis, enterohepatic circulation, and microbial metabolism. *Scientific Reports* **7**, (2017).

213. Harrill, J. A. *et al.* Aryl hydrocarbon receptor knockout rats are insensitive to the pathological effects of repeated oral exposure to 2,3,7,8-tetrachlorodibenzo- *p* -dioxin: AHR-KO rats are insensitive to pathological effects of TCDD. *J. Appl. Toxicol.* **36**, 802–814 (2016).

214. Fernandez-Salguero, P. M., Hilbert, D. M., Rudikoff, S., Ward, J. M. & Gonzalez, F. J. Aryl-hydrocarbon receptor-deficient mice are resistant to 2,3,7,8-tetrachlorodibenzo-p-dioxin-induced toxicity. *Toxicol. Appl. Pharmacol.* **140**, 173–179 (1996).

215. Denison, M. S., Soshilov, A. A., He, G., DeGroot, D. E. & Zhao, B. Exactly the Same but Different: Promiscuity and Diversity in the Molecular Mechanisms of

Action of the Aryl Hydrocarbon (Dioxin) Receptor. *Toxicological Sciences* **124**, 1–22 (2011).

216. Marlowe, J. L. & Puga, A. Aryl hydrocarbon receptor, cell cycle regulation, toxicity, and tumorigenesis. *J. Cell. Biochem.* **96**, 1174–1184 (2005).

217. Barhoover, M. A., Hall, J. M., Greenlee, W. F. & Thomas, R. S. Aryl Hydrocarbon Receptor Regulates Cell Cycle Progression in Human Breast Cancer Cells via a Functional Interaction with Cyclin-Dependent Kinase 4. *Mol Pharmacol* **77**, 195–201 (2010).

218. Hwang, H. J. *et al.* Mitochondrial-targeted aryl hydrocarbon receptor and the impact of 2,3,7,8-tetrachlorodibenzo-p-dioxin on cellular respiration and the mitochondrial proteome. *Toxicology and Applied Pharmacology* **304**, 121–132 (2016).

219. Pryputniewicz, S. J., Nagarkatti, M. & Nagarkatti, P. S. Differential induction of apoptosis in activated and resting T cells by 2,3,7,8-tetrachlorodibenzo-p-dioxin (TCDD) and its repercussion on T cell responsiveness1. *Toxicology* **129**, 211–226 (1998).

220. Prasad Singh, N., Nagarkatti, M. & Nagarkatti, P. From Suppressor T cells to Regulatory T cells: How the Journey That Began with the Discovery of the Toxic Effects of TCDD Led to Better Understanding of the Role of AhR in Immunoregulation. *Int J Mol Sci* **21**, E7849 (2020).

221. Nichols, R. G. *et al.* Metatranscriptomic Analysis of the Mouse Gut Microbiome Response to the Persistent Organic Pollutant 2,3,7,8-Tetrachlorodibenzofuran. *Metabolites* **10**, 1 (2019).

222. Busbee, P. B. *et al.* Indole-3-carbinol prevents colitis and associated microbial dysbiosis in an IL-22-dependent manner. *JCI Insight* **5**, (2020).

223. Belton, K. R. *et al.* Metabolomics Reveals Aryl Hydrocarbon Receptor Activation Induces Liver and Mammary Gland Metabolic Dysfunction in Lactating Mice. *J. Proteome Res.* **17**, 1375–1382 (2018).

224. Matsubara, T. *et al.* Metabolomics identifies an inflammatory cascade involved in dioxin- and diet-induced steatohepatitis. *Cell Metab.* **16**, 634–644 (2012).

225. Marshall, N. B. & Kerkvliet, N. I. Dioxin and immune regulation: Emerging role of aryl hydrocarbon receptor in the generation of regulatory T cells. *Annals of the New York Academy of Sciences* **1183**, 25–37 (2010).

226. Gao, B., Bian, X., Mahbub, R. & Lu, K. Sex-Specific Effects of Organophosphate Diazinon on the Gut Microbiome and Its Metabolic Functions. *Environ. Health Perspect.* **125**, 198–206 (2017).

227. Lu, K. *et al.* Arsenic exposure perturbs the gut microbiome and its metabolic profile in mice: an integrated metagenomics and metabolomics analysis. *Environ. Health Perspect.* **122**, 284–291 (2014).

228. Gowda, H. *et al.* Interactive XCMS Online: simplifying advanced metabolomic data processing and subsequent statistical analyses. *Anal. Chem.* **86**, 6931–6939 (2014).

229. Tautenhahn, R., Patti, G. J., Rinehart, D. & Siuzdak, G. XCMS Online: a web-based platform to process untargeted metabolomic data. *Anal. Chem.* **84**, 5035–5039 (2012).

230. Patti, G. J. *et al.* A view from above: cloud plots to visualize global metabolomic data. *Anal. Chem.* **85**, 798–804 (2013).

231. Pang, Z. *et al.* MetaboAnalyst 5.0: narrowing the gap between raw spectra and functional insights. *Nucleic Acids Research* gkab382 (2021) doi:10.1093/nar/gkab382.

232. Xia, J., Psychogios, N., Young, N. & Wishart, D. S. MetaboAnalyst: a web server for metabolomic data analysis and interpretation. *Nucleic Acids Res* **37**, W652-660 (2009).

233. Barupal, D. K. *et al.* MetaMapp: mapping and visualizing metabolomic data by integrating information from biochemical pathways and chemical and mass spectral similarity. *BMC Bioinformatics* **13**, 99 (2012).

234. Krämer, A., Green, J., Pollard, J. & Tugendreich, S. Causal analysis approaches in Ingenuity Pathway Analysis. *Bioinformatics* **30**, 523–530 (2014).

235. Ahmed, R. G. Perinatal TCDD exposure alters developmental neuroendocrine system. *Food and Chemical Toxicology* **49**, 1276–1284 (2011).

236. Miettinen, H. M. *et al.* The Effect of Perinatal TCDD Exposure on Caries Susceptibility in Rats. *Toxicological Sciences* **91**, 568–575 (2006).

237. Tran, N. N. *et al.* Impacts of Perinatal Dioxin Exposure on Motor Coordination and Higher Cognitive Development in Vietnamese Preschool Children: A Five-Year Follow-Up. *PLOS ONE* **11**, e0147655 (2016).

238. Enan, E., Liu, P. C. & Matsumura, F. 2,3,7,8-Tetrachlorodibenzo-p-dioxin causes reduction of glucose transporting activities in the plasma membranes of adipose tissue and pancreas from the guinea pig. *J. Biol. Chem.* **267**, 19785–19791 (1992).

239. Lin, S., Yang, Z., Liu, H. & Cai, Z. Metabolomic analysis of liver and skeletal muscle tissues in C57BL/6J and DBA/2J mice exposed to 2,3,7,8-tetrachlorodibenzo-p-dioxin. *Molecular BioSystems* **7**, 1956 (2011).

240. Kennedy, L. H. *et al.* 2,3,7,8-Tetrachlorodibenzo-p-dioxin-mediated production of reactive oxygen species is an essential step in the mechanism of action to accelerate human keratinocyte differentiation. *Toxicol Sci* **132**, 235–249 (2013).

241. Hannun, Y. A. & Obeid, L. M. The Ceramide-centric universe of lipid-mediated cell regulation: stress encounters of the lipid kind. *J Biol Chem* **277**, 25847–25850 (2002).

242. Lavieu, G. *et al.* Regulation of Autophagy by Sphingosine Kinase 1 and Its Role in Cell Survival during Nutrient Starvation. *Journal of Biological Chemistry* **281**, 8518–8527 (2006).

243. Calder, P. C. Polyunsaturated fatty acids, inflammatory processes and inflammatory bowel diseases. *Mol Nutr Food Res* **52**, 885–897 (2008).

244. Higgins, A. J. & Lees, P. The acute inflammatory process, arachidonic acid metabolism and the mode of action of anti-inflammatory drugs. *Equine Veterinary Journal* **16**, 163–175 (1984).

245. Rutting, S. *et al.* Dietary ω-6 polyunsaturated fatty acid arachidonic acid increases inflammation, but inhibits ECM protein expression in COPD. *Respir Res* **19**, 211 (2018).

246. Sztolsztener, K., Chabowski, A., Harasim-Symbor, E., Bielawiec, P. & Konstantynowicz-Nowicka, K. Arachidonic Acid as an Early Indicator of

Inflammation during Non-Alcoholic Fatty Liver Disease Development. *Biomolecules* **10**, (2020).

247. Levy, B. D. & Serhan, C. N. Resolution and Regulation of Inflammation. in *Pathobiology of Human Disease* 332–348 (Elsevier, 2014). doi:10.1016/B978-0-12-386456-7.01811-6.

248. Souza, P. R. & Norling, L. V. Implications for eicosapentaenoic acid- and docosahexaenoic acid-derived resolvins as therapeutics for arthritis. *Eur J Pharmacol* **785**, 165–173 (2016).

249. Reifen, R., Karlinsky, A., Stark, A. H., Berkovich, Z. & Nyska, A. α-Linolenic acid (ALA) is an anti-inflammatory agent in inflammatory bowel disease. *J Nutr Biochem* **26**, 1632–1640 (2015).

250. Spiga, R. *et al.* Uric Acid Is Associated With Inflammatory Biomarkers and Induces Inflammation Via Activating the NF-κB Signaling Pathway in HepG2 Cells. *Arteriosclerosis, Thrombosis, and Vascular Biology* **37**, 1241–1249 (2017).

251. Dong, F. & Perdew, G. H. The aryl hydrocarbon receptor as a mediator of host-microbiota interplay. *Gut Microbes* **12**, 1859812 (2020).

252. Linden, J., Koch-Nolte, F. & Dahl, G. Purine Release, Metabolism, and Signaling in the Inflammatory Response. *Annu Rev Immunol* **37**, 325–347 (2019).

253. Tian, Y. *et al.* Metabolic impact of persistent organic pollutants on gut microbiota. *Gut Microbes* **12**, 1–16 (2020).

254. Tian, Y., Ke, S., Denison, Michael. S., Rabson, A. B. & Gallo, M. A. Ah Receptor and NF-κB Interactions, a Potential Mechanism for Dioxin Toxicity. *Journal of Biological Chemistry* **274**, 510–515 (1999).

255. Tian, Y., Rabson, A. B. & Gallo, M. A. Ah receptor and NF-kappaB interactions: mechanisms and physiological implications. *Chem. Biol. Interact.* **141**, 97–115 (2002).

256. Song, J., Jing, Z., Hu, W., Yu, J. & Cui, X. α-Linolenic Acid Inhibits Receptor Activator of NF-κB Ligand Induced (RANKL-Induced) Osteoclastogenesis and Prevents Inflammatory Bone Loss via Downregulation of Nuclear Factor-KappaB-Inducible Nitric Oxide Synthases (NF-κB-iNOS) Signaling Pathways. *Med. Sci. Monit.* **23**, 5056–5069 (2017).

257. Fan, A. *et al.* Atheroprotective effect of oleoylethanolamide (OEA) targeting oxidized LDL. *PLoS ONE* **9**, e85337 (2014).

258. Yang, L. *et al.* Oleoylethanolamide exerts anti-inflammatory effects on LPS-induced THP-1 cells by enhancing PPARα signaling and inhibiting the NF-κB and ERK1/2/AP-1/STAT3 pathways. *Sci Rep* **6**, 34611 (2016).

259. Camandola, S. *et al.* Nuclear Factor kB Is Activated by Arachidonic Acid but Not by Eicosapentaenoic Acid. *Biochemical and Biophysical Research Communications* **229**, 643–647 (1996).

260. Crofford, L. J. COX-1 and COX-2 tissue expression: implications and predictions. *J Rheumatol Suppl* **49**, 15–19 (1997).

261. Ricciotti, E. & FitzGerald, G. A. Prostaglandins and inflammation. *Arterioscler. Thromb. Vasc. Biol.* **31**, 986–1000 (2011).

262. Mbonye, U. R. *et al.* The 19-amino Acid Cassette of Cyclooxygenase-2 Mediates Entry of the Protein into the Endoplasmic Reticulum-associated Degradation System. *Journal of Biological Chemistry* **281**, 35770–35778 (2006).

263. Imamura, T. *et al.* Cutaneous symptoms such as acneform eruption and pigmentation are closely associated with blood levels of 2,3,4,7,8-penta-chlorodibenzofurans in Yusho patients, using data mining analysis. *BMC Res Notes* **2**, 27 (2009).

264. Kim, S.-M. *et al.* Reducing Serum Uric Acid Attenuates TGF-β_1-Induced Profibrogenic Progression in Type 2 Diabetic Nephropathy. *Nephron Experimental Nephrology* **121**, e109–e121 (2013).

265. Lu, W. *et al.* Uric Acid Produces an Inflammatory Response through Activation of NF-κB in the Hypothalamus: Implications for the Pathogenesis of Metabolic Disorders. *Sci Rep* **5**, 12144 (2015).

266. Roskoski, R. ERK1/2 MAP kinases: Structure, function, and regulation. *Pharmacological Research* **66**, 105–143 (2012).

267. Xu, G. *et al.* Role of mitogen-activated protein kinase cascades in 2,3,7,8-tetrachlorodibenzo- *p* -dioxin-induced apoptosis in neuronal pheochromocytoma cells. *Human & Experimental Toxicology* **32**, 1278–1291 (2013).

268. Chen, R.-J. *et al.* TCDD Promotes Lung Tumors via Attenuation of Apoptosis through Activation of the Akt and ERK1/2 Signaling Pathways. *PLoS ONE* **9**, e99586 (2014).

269. Davis, J. W., Lauer, F. T., Burdick, A. D., Hudson, L. G. & Burchiel, S. W. Prevention of apoptosis by 2,3,7,8-tetrachlorodibenzo-p-dioxin (TCDD) in the MCF-10A cell line: correlation with increased transforming growth factor alpha production. *Cancer Res.* **61**, 3314–3320 (2001).

270. Chen, S., Operaña, T., Bonzo, J., Nguyen, N. & Bonferonni, R. H. ERK Kinase Inhibition Stabilizes the Aryl Hydrocarbon Receptor: IMPLICATIONS FOR TRANSCRIPTIONAL ACTIVATION AND PROTEIN DEGRADATION. *Journal of Biological Chemistry* **280**, 4350–4359 (2005).

271. Puga, A., Ma, C. & Marlowe, J. L. The aryl hydrocarbon receptor cross-talks with multiple signal transduction pathways. *Biochem. Pharmacol.* **77**, 713–722 (2009).

272. Lee, H. J. *et al.* Allosteric activation of the extracellular Ca $^{2+}$ -sensing receptor by L-amino acids enhances ERK1/2 phosphorylation. *Biochemical Journal* **404**, 141–149 (2007).

273. Hennig, B. *et al.* Linoleic acid induces proinflammatory events in vascular endothelial cells via activation of PI3K/Akt and ERK1/2 signaling. *The Journal of Nutritional Biochemistry* **17**, 766–772 (2006).

274. Wu, D. *et al.* Activation of aryl hydrocarbon receptor induces vascular inflammation and promotes atherosclerosis in apolipoprotein E-/- mice. *Arterioscler. Thromb. Vasc. Biol.* **31**, 1260–1267 (2011).

275. Tao, M. *et al.* Blockade of ERK1/2 by U0126 alleviates uric acid-induced EMT and tubular cell injury in rats with hyperuricemic nephropathy. *Am. J. Physiol. Renal Physiol.* **316**, F660–F673 (2019).

276. Liu, N. *et al.* Pharmacologic targeting ERK1/2 attenuates the development and progression of hyperuricemic nephropathy in rats. *Oncotarget* **8**, (2017).

277. Silva-Peña, D. *et al.* Oleoylethanolamide Modulates BDNF-ERK Signaling and Neurogenesis in the Hippocampi of Rats Exposed to Δ9-THC and Ethanol Binge Drinking During Adolescence. *Front Mol Neurosci* **12**, 96 (2019).

278. Payahoo, L., Khajebishak, Y., Asghari Jafarabadi, M. & Ostadrahimi, A. Oleoylethanolamide Supplementation Reduces Inflammation and Oxidative Stress in Obese People: A Clinical Trial. *Adv Pharm Bull* **8**, 479–487 (2018).

279. Sayd, A. *et al.* Systemic administration of oleoylethanolamide protects from neuroinflammation and anhedonia induced by LPS in rats. *Int. J. Neuropsychopharmacol.* **18**, (2014).

280. Lefever, D. E. *et al.* TCDD modulation of gut microbiome correlated with liver and immune toxicity in streptozotocin (STZ)-induced hyperglycemic mice. *Toxicology and Applied Pharmacology* **304**, 48–58 (2016).

281. Zhang, L. *et al.* Persistent Organic Pollutants Modify Gut Microbiota-Host Metabolic Homeostasis in Mice Through Aryl Hydrocarbon Receptor Activation. *Environ. Health Perspect.* **123**, 679–688 (2015).

282. Ishida, T. *et al.* Linoleoyl ethanolamide reduces lipopolysaccharide-induced inflammation in macrophages and ameliorates 2,4-dinitrofluorobenzene-induced contact dermatitis in mice. *Eur. J. Pharmacol.* **699**, 6–13 (2013).

283. Aslan, Z. & Aksoy, L. Anti-inflammatory effects of royal jelly on ethylene glycol induced renal inflammation in rats. *Int Braz J Urol* **41**, 1008–1013 (2015).

284. Ilbey, Y. O. *et al.* Pyrrolidine dithiocarbamate treatment prevents ethylene glycol-induced urolithiasis through inhibition of NF-kappaB and p38-MAPK signaling pathways in rat kidney. *Arch Ital Urol Androl* **82**, 87–94 (2010).

285. Kim, M. J., Rehman, S. U., Amin, F. U. & Kim, M. O. Enhanced neuroprotection of anthocyanin-loaded PEG-gold nanoparticles against Aβ1-42-induced

neuroinflammation and neurodegeneration via the NF-KB /JNK/GSK3β signaling pathway. *Nanomedicine* **13**, 2533–2544 (2017).

286. Prestwich, E. G. *et al.* Increased levels of inosine in a mouse model of inflammation. *Chem. Res. Toxicol.* **26**, 538–546 (2013).

APPENDIX A

IMMUNOLOGY PERMISSIONS TO REPRINT:

BELOW IS THE PERMISSIONS GRANTED FROM *IMMUNOLOGY* TO

REPRINT THE WORKS IN CHAPTER 1 OF THIS DISSERTATION

Jun 14, 2021 This Agreement between University of South Carolina -- Nicholas Dopkins and John Wiley and Sons consists of your license details and the terms and conditions provided by John Wiley and Sons and Copyright Clearance Center.
License Number 5087680889810
License date Jun 14, 2021
Licensed Content Publisher John Wiley and Sons
Licensed Content Publication Immunology
Licensed Content Title The role of gut microbiome and associated metabolome in the regulation of neuroinflammation in multiple sclerosis and its implications in attenuating chronic inflammation in other inflammatory and autoimmune disorders.
Licensed Content Author Nicholas Dopkins, Prakash S. Nagarkatti, Mitzi Nagarkatti
Licensed Content Date Feb 27, 2018
Licensed Content Volume 154
Licensed Content Issue 2
Licensed Content Pages 8
Type of use Dissertation/Thesis
Requestor type Author of this Wiley article Format Electronic
Portion Full article
Institution name University of South Carolina
Expected presentation date July 2021
Requestor Location University of South Carolina

APPENDIX B

FRONTIERS IN PHARMACOLOGY PERMISSIONS TO REPRINT: BELOW IS THE PERMISSIONS GRANTED FROM *FRONTIERS IN PHARMACOLOGY* TO REPRINT THE WORKS IN CHAPTER 2 OF THIS DISSERTATION